UNIVERSIDADE FEDERAL DO RIO GRANDE DO SUL
PROGRAMA DE PÓS GRADUAÇÃO EM SENSORIAMENTO REMOTO

Recuperação de Temperatura de Superfície Terrestre da radiância termal coletada pelo sensor TIRS/Landsat 8: Aplicações de medidas de campo e laboratório

Pâmela Suélen Käfer

PORTO ALEGRE
2019

UNIVERSIDADE FEDERAL DO RIO GRANDE DO SUL
PROGRAMA DE PÓS GRADUAÇÃO EM SENSORIAMENTO REMOTO

Recuperação de Temperatura de Superfície Terrestre da radiância termal coletada pelo sensor TIRS/Landsat 8: Aplicações de medidas de campo e laboratório

Dissertação de Mestrado apresentada ao Programa de Pós-Graduação em Sensoriamento Remoto para obtenção do Título de Mestre em Sensoriamento Remoto.
Área de Concentração: Sensoriamento Remoto Aplicado.

Pâmela Suélen Käfer
Orientadora: Silvia Beatriz Alves Rolim

PORTO ALEGRE
2019

FOLHA DE APROVAÇÃO

Pâmela Suélen Käfer

Recuperação de Temperatura de Superfície Terrestre da radiância termal coletada pelo sensor TIRS/Landsat 8: Aplicações de medidas de campo e laboratório

BANCA EXAMINADORA

_____

Profa. Dra. Denise Cybis Fontana

_____

Prof. Dr. Jean Marcel de Almeida Espinoza

_____

Profa. Dra. María Luján Iglesias

APROVADO EM: ____DE_____DE 2019.

“When I was a child, when I was an adolescent, books saved me from despair: that convinced me that culture was the highest of values[...].”

— Simone de Beauvoir, The Woman Destroyed

AGRADECIMENTOS

Aos meus pais, Ivete e Lauri por sempre acreditarem no meu potencial e auxiliarem de todas as formas possíveis.

Ao Jaydson Gomes, pelo apoio, paciência e amor.

À Prof. Dr. Silvia Rolim, pela orientação, críticas, sugestões construtivas e apoio essencial para a realização desta pesquisa. Além disso, pela amizade, incentivo e grande confiança depositada.

Aos colegas, pela amizade e discussões. Em especial aos colegas de laboratório María Lujan, Nájila, Luíza, Lucas, Suzi e Kaiser pela parceria e por estarem sempre dispostos a ajudar.

Aos amigos do peito que são herança da graduação, Franciel, Franciele e Vanessa.

À Universidade Federal do Rio Grande do Sul e ao Centro Estadual de Pesquisas em Sensoriamento Remoto e Meteorologia, pela estrutura disponibilizada para o desenvolvimento desta dissertação, pelos auxílios financeiros disponíveis para a realização dos trabalhos de campo e auxílios para participação de eventos que muito engrandeceram meu aprendizado.

À Coordenação de Aperfeiçoamento de Pessoal de Nível Superior (CAPES), pela bolsa de estudos concedida em nível de pós-graduação.

RESUMO

A temperatura da superfície terrestre (*Land surface temperature* - LST) é um importante parâmetro na investigação de mudanças ambientais e climáticas em várias escalas. Entretanto, estimar esse parâmetro da radiação emitida na região do infravermelho termal (TIR) é uma tarefa difícil, pois as radiações medidas pelos sensores dos satélites são fortemente afetadas por efeitos atmosféricos. Todos métodos de recuperação de LST requerem validação com medidas de campo. Porém, a validação deste tipo de dado é um desafio, visto que a LST muda rapidamente no tempo e as medidas devem ser realizadas em conjunto com a passagem do sensor. Além disso, a maioria das metodologias são desenvolvidas e testadas com foco no hemisfério norte. Tendo em vista que maneiras operacionais de se obter LST devem ser constantemente investigadas, o objetivo desta pesquisa foi estudar o efeito do uso de medidas de emissividade de laboratório tomadas com base em temperaturas na determinação da LST a partir de dados de sensoriamento remoto orbital. Ademais, pretendeu-se realizar uma análise comparativa entre os algoritmos *single-channel* mais recentes existentes na literatura, aplicados à banda 10 (10,6-11,19 μm) do Landsat 8 TIRS. Os algoritmos considerados foram: *Single-Channel Generalizado* (SCG), *Improved Single-Channel* (ISC) e *Improved Mono-Window* (IMW). Um campo de dunas costeiras foi escolhido como área de estudo. Dois conjuntos de medidas de emissividade de laboratório foram construídos com amostras de campo em diferentes temperaturas com uso de um *Fourier Transform Infrared* (FT-IR). Dados de emissividade e temperatura foram obtidos na área de estudo concomitamente com a passagem do sensor. A equação de transferência radiativa (*Radiative Transfer Equation* - RTE) com parâmetros de perfis atmosféricos globais foi testada como forma de validação de dados. Uma variação de aproximadamente 2% na emissividade em relação à temperatura foi observada, podendo ser negligenciada. O FT-IR apresenta limitações quanto ao período para adquirir estabilidade, porém respeitando esta limitação e realizando abordagem correta de calibração, medidas laboratoriais podem atingir ótima acurácia e substituir a validação de campo. Bibliotecas espectrais disponíveis de emissividade demonstraram ser também uma alternativa válida. Todos métodos *single-channel* avaliados são adequados para obter LST; no entanto, o ISC forneceu resultados superiores em todas as análises, produzindo maior R^2 (0,99978) e menor RMSE (0.019) em relação aos demais.

ABSTRACT

Land surface temperature (LST) is an important parameter in the investigation of environmental and climatic changes at various scales. However, estimating this parameter from the radiation emitted in the thermal infrared (TIR) region is a difficult task because the radiation measured by the satellite sensors is strongly affected by atmospheric effects. All LST retrieval methods require validation with field measurements. Nonetheless, the validation of this type of data is a challenge because the LST changes rapidly in time and the measurements must be performed togheter with the sensor overpass. In addition, most methodologies are developed and tested focusing on the Northern Hemisphere. Considering that operational ways of obtaining LST should be constantly investigated, the aim of this paper was to study the effect of the use of temperature-based laboratory measurements in the determination of the emissivity and LST retrieval from orbital remote sensing data. Moreover, it was intended to perform a comparative analysis among the most recent single-channel algorithms available on the literature, applied to band 10 (10.6-11.19 μm) of the Landsat 8 TIRS. The algorithms considered were: Single-channel generalized (SC), Improved Single-channel (ISC) and Improved Mono-window (IMW). A field of coastal dunes was chosen as study area. Two sets of laboratory emissivity measurements were performed with field samples at different temperatures using a Fourier Transform Infrared (FT-IR). Emissivity and temperature data were obtained in the study area concomitantly with the satellite overpass. The Radiative Transfer Equation (RTE) with parameters of global atmospheric profiles was tested as a method of validation. A variation of approximately 2% in the emissivity in relation to the temperature was observed, which could be neglected. The FT-IR presents limitations on the period to acquire stability, however as long as this limitation is respected and the calibration approach correctly carried out, laboratory measurements can achieve optimum accuracy and replace field validation. Available spectral libraries of emissivity have also proved to be a good alternative. All evaluated single-channel methods are suitable for obtaining LST; however, ISC provided superior results in all analyzes, producing higher R^2 (0.99978) and lower RMSE (0.019) relative to the other algorithms tested.

LISTA DE FIGURAS

Figura 1. Janelas atmosféricas e bandas de absorção ao longo do espectro eletromagnético. (Fonte: JENSEN, 2009). 23
Figura 2. Função resposta espectral (SRF) das bandas do TIR do sensor TIRS a bordo do satélite Landsat 8. (Dados adaptados de USGS, 2018). 34
Figura 3. Localização da área de estudo no Brasil e no Rio Grande do Sul. Uma composição colorida falsa-cor RGB654 é representada na imagem. 36
Figura 4. Fluxograma ilustrando as principais etapas do estudo. 38

ARTIGO 1

Fig. 1. Study area location in Southern Brazil. Dune field mask shown by the red line (Landsat 8 OLI - color composite RGB: 432).....41
Fig. 2. Main steps of the study. 41
Fig. 3. Relative spectral response function of Landsat 8 TIRS bands. (Data adapted from USGS, 2018). 42
Fig. 4. Emissivity curves of quartz sand sample for five different temperatures (K). (a) refers to the set of measurements performed at the first half hour of the instrument turned on, (b) refers to measurements performed at the time after the second calibration. 45
Fig. 5. Quartz emissivity versus temperature at the band 10 Landsat 8 (10.6-11.19 μm) measured at laboratory. The SRF was applied to the data. 45
Fig. 6. Comparison between emissivities in-situ and from laboratory. Both curves chosen to perform the comparison were measured at 313 K of temperature. 46
Fig. 7. LST in-situ and retrieved by TIRS sensor for the study area at the time of the Landsat 8 overpass. 46

ARTIGO 2

Figure 1. Location of the study site in Southern Brazil. 56

Figure 2. LST measures in situ by FT-IR spectrometer at the time of the Landsat 8 overpass and retrieved by the algorithms. ISC is the improved single-channel, SC is the single-channel, and IMW is the improved mono-window.....67
Figure 3. Box plot of the three LST retrieval methods (ISC, SC, IMW) and RTE using Landsat 8 band 10 with the parameters L↓, L↑ and τ generated by ACPC.....71

LISTA DE TABELAS

Tabela 1. Emissividade média em canais específicos de sensores remotos para diferentes tipos de superfícies terrestres existentes na natureza. 32
Tabela 2. Especificações do FT-IR model 102F. 33

ARTIGO 1

TABLE I Landsat 8 OLI/TIRS image information. 41
TABLE II Emissivity of quartz and vegetation for Landsat 8 band 10. The SRF was applied to the quartz values 43
TABLE III Parameters used in the LST determination by single-channel algorithms and results of the LSTs retrieved 46

ARTIGO 2

Table 1. Comparison of a pure pixel of SiO_2 among the LST retrieval methods applied in the March, 14 Landsat TIRS band 10 image and the FT-IR field data. An average of the $\varepsilon_{in\ situ}$ measured is assumed in the $NDVI^{THM}$ and applied for all the methods 66
Table 2. Comparison of the Coefficient of determination (R^2) and the root mean square error (RMSE) for all scenes evaluated 68
Table 3. Comparison among the LSTs retrieved by the methods and the ACPC results 69

LISTA DE ABREVIATURAS E SIGLAS

ACPC	Calculatora de parâmetros de correção atmosférica
AF	Função atmosférica
ANOVA	Análise de variância
ASTER	Advanced Spaceborne Thermal Emission and Reflection Radiometer
AVHRR	Advanced Very High Resolution Radiometer
CAPES	Coordenação de Aperfeiçoamento de Pessoal de Nível Superior
CBEM	Método de classificação semi-empírico
DN	Número digital
ENVI	Environment for Visualizing Images
ETM+	Enhanced Thematic Mapper
FT-IR	Fourier Transform Infrared spectrometer
IMW	Improved mono-window
INMET	Instituto Nacional de Meteorologia
ISC	Improved single-channel
JHU	Johns Hopkings University
LSE	Emissividade da superfície Terrestre
LST	Temperatura da superfície terrestre
MATLAB	MATrix LABoratory
MODIS	Moderate-Resolution Imaging Spectroradiometer
MODTRAN	MODerate resolution atmospheric TRANsmission
MW	Mono-window
NCEP	Centro Nacional de Predição Ambiental
NDVI	Índice de vegetação por diferença normalizada
$NDVI^{THM}$	Método do NDVI threshold
NIR	Região do infravermelho próximo
OLI	Operational Land Imager
PV	Proporção de cobertura vegetal no pixel
R^2	Coeficiente de determinação
RED	Região do vermelho
RMSE	Raiz do erro quadrático médio
RTE	Equação de transferência radiativa

SC	Single-channel
SCG	Single-channel generalizado
SRF	Função resposta espectral
SW	Split-window
SWIR	Região do infravermelho de ondas curtas
Ta	Temperatura média atmosférica
TIR	Região do Infravermelho Termal
TIRS	Thermal Infrared Sensor
TM	Thematic Mapper
To	Temperatura do ar próxima da superfície
TOA	Radiância de topo da atmosfera
USGS	United States Geological Survey
w	Conteúdo de vapor água

LISTA DE EQUAÇÕES

Equação de Planck.....23
Equação de Transferência Radiativa 24

ARTIGO 1

Sample Spectral Emissivity 42
Planck’s Function 42
Soil emissivity.....43
Vegetation emissivity.....43
Pixel-mixing emissivity 43
Vegetation proportion..... 43
Geometrical distribution of the natural surfaces and the internal reflections 43
Convertion from DN to radiance.....43
Convertion from DN to brightness temperature.....43
Generalized single-channel and Improved single-channel methods 44
γ variable based on the Planck’s function 44
δ variable based on the Planck’s function 44
Atmospheric Function 1 for SC method…….....44
Atmospheric Function 2 for SC method 44
Atmospheric Function 3 for SC method..... 44
Atmospheric Function 1 for ISC method..... ..44
Atmospheric Function 2 for ISC method..... 44
Atmospheric Function 3 for ISC method…….. 44
Mean atmospheric temperature equation for mid-latitude summer 44
Water vapor content.....44
Partial pressure of water vapor.....44

ARTIGO 2

Sample Spectral Emissivity 57
Planck's Function 57
Sensor Spectral Response Function 58
Radiative Transfer Equation..... 58
Convertion from DN to brightness temperature 59
Generalized single-channel and Improved single-channel methods 59
γ and δ variables calculation..... 59
Atmospheric Function 1 for SC method..... 60
Atmospheric Function 2 for SC method.....60
Atmospheric Function 3 for SC method.....60
Atmospheric Function 1 for ISC method.....60
Atmospheric Function 2 for ISC method.....60
Atmospheric Function 3 for ISC method.....60
Mono-window method 61
C10.....61
D10..... 61
Mean atmospheric temperature equation for mid-latitude summer 61
Transmitance..... 62
Water vapor content 62
Partial pressure of water vapor.....62
Normalized Difference Vegetation Index 63
Vegetation proportion..... 63
Pixel-mixing emissivity.....63
Geometrical distribution of the natural surfaces and the internal reflections 63

Sumário

1. INTRODUÇÃO 17
1.1 Objetivo 21
1.2 Objetivos específicos 21
2. REFERENCIAL TEÓRICO 22
2.1 Sensoriamento remoto 22
2.1.1 Princípios Físicos do sensoriamento remoto 22
2.1.2 Sensoriamento remoto no infravermelho termal (TIR) 23
2.2 Temperatura da superfície terrestre (LST) 25
2.2.1 Algoritmos single-channel 26
2.3 Emissividade da superfície terrestre (LSE) 28
2.3.1 Emissividade do quartzo 29
2.3.2 Emissividade da vegetação 30
2.3.3 Biblioteca espectral 31
2.4 Dados de satélite 33
2.4.1 Landsat 33
2.4.2 Stray Light 34
3. MATERIAL E MÉTODOS 35
3.1 Área de estudo 35
3.2 Material 37
3.3 Procedimentos metodológicos 37
4. RESULTADOS E DISCUSSÃO 39
4.1 ARTIGO 1 - Land Surface Temperature Retrieval by LANDSAT 8 Thermal Band: Applications of Laboratory and Field Measurements 39
Introduction 40
Methodology 41
Results 44
Discussion 46
Conclusions 47
Acknowledgment 47
References 48
4.2 ARTIGO 2 - Towards single-channel methods for land surface temperature retrieval from Landsat 8 thermal band in Southern Brazil 50

Introduction *51*
Material and Methods *55*
Results and discussion *65*
Conclusions *71*
Acknowledgment *72*
Conflicts of Interest *72*
References *72*
5. CONSIDERAÇÕES FINAIS 77
6. REFERÊNCIAS 81
7. APÊNDICES 92
7.1 Proximal Remote Sensing: Potential And Limitations of FT-IR Spectrometer for Validation of Satellite Measurements 93
7.2 Land Surface Temperature Retrieval from Landsat-8 Data: a Comparison Using a Quartz Spectral Library Based on Temperatures 97

1. INTRODUÇÃO

A temperatura da superfície terrestre (*Land surface temperature* - LST) é um parâmetro essencial na investigação de processos ambientais em diversas escalas, visto que desempenha um importante papel em uma ampla variedade de estudos científicos, incluindo diversas áreas como climatologia, hidrologia, ecologia, biogeologia, e estudos de mudanças globais (ZHANG e HE, 2013; YU et al., 2014; WENG et al., 2014). Tal parâmetro também está envolvido em muitos outros processos da superfície terrestre, como evapotranspiração, saldo de radiação e modelagem de temperatura do ar (CRISTÓBAL et al., 2009), e pode ser utilizado como um indicador para quantificar alterações nas características físicas da cobertura da terra (SOBRINO e RAISSOUNI, 2000). Além disso, uma descrição quantitativa precisa do ambiente térmico é valiosa, especialmente no contexto do aquecimento global (CHEN et al., 2016).

O sensoriamento remoto na região do Infravermelho Termal (*Thermal Infrared* - TIR) é reconhecido como uma maneira útil de obter informações quantitativas e qualitativas sobre a LST (ZHANG et al., 2016; TARDY et al., 2016). Nesse sentido, a determinação da LST a partir de dados de sensoriamento remoto é influenciada principalmente pela atmosfera e pela emissividade da superfície terrestre (*Land surface emissivity* - LSE), sendo esta última uma propriedade intrínseca de materiais naturais (LI et al., 2013a). É necessário que a LSE seja conhecida para se determinar a LST. Contudo, esta variável é considerada crítica, sendo um erro de 2,5% no cálculo da LSE capaz de produzir erros de até 2 K na recuperação da LST (TAN et al., 2017).

A série de satélites Landsat tem sido um dos principais fatores que contribuem para o desenvolvimento de pesquisas científicas em sistemas terrestres de escala global. Ela representa a mais completa sequência contínua de dados de sensoriamento remoto no TIR, que remonta a 1982 (ROSAS et al., 2017; MALAKAR et al., 2018). Durante grande parte desse período (1982-atual), os dados Landsat do TIR eram fornecidos através de uma única banda nesta região espectral (*broadband*) (ROSAS et al., 2017). O lançamento do satélite Landsat-8 OLI/TIRS (Operational Land Imager/Thermal Infrared Sensor) garantiu a continuidade dos dados Landsat de sensoriamento remoto, representando avanços, entre eles, na janela do TIR. O sensor

TIRS coleta dados em duas bandas espectrais localizadas na janela atmosférica entre 10 e 12 µm (IRONS, DWYER e BARSI, 2012).

Apesar da inovação para duas bandas na região espectral do TIR, o Landsat 8 apresentou por um longo período de tempo sérios problemas de calibração causados por *stray light* (BARSI et al., 2014; JIMÉNEZ-MUÑOZ et al., 2014; YU et al., 2014; MONTANARO et al., 2014; WANG et al., 2015; CRISTÓBAL et al., 2018) relatados desde o seu lançamento em 2013. Nesta perspectiva, houve inúmeras tentativas de correção e alguns avanços na resolução do problema, que atingia especialmente a banda 11 do sensor TIRS. Entretanto, somente final de 2017, a questão foi completamente corrigida (GERACE e MONTANARO, 2017). Como resultado, os pesquisadores mantiveram o foco no desenvolvimento e melhoria das técnicas de canal único (*single-channel*) para uso com a banda 10 (10,6-11,19 µm) do Landsat 8 (JIMÉNEZ-MUÑOZ et al., 2014, WANG et al., 2015, ZHANG et al., 2016, CRISTÓBAL et al. 2018). Desse modo, diversas metodologias precisas foram desenvolvidas ou refinadas nos últimos anos e têm demonstrado grande potencial na recuperação de LST por sensoriamento remoto.

De uma forma geral, os métodos de obtenção de LST podem ser agrupados a grosso modo em três categorias, de acordo com Li et al. (2013) e Du et al. (2015): (i) métodos de canal único (*single-channel*), (ii) métodos multicanais e (iii) métodos multitempo. Os métodos single-channel, abordados nesta pesquisa, utilizam a radiância medida pelo sensor do satélite em uma banda específica, escolhida dentro de uma janela atmosférica, e requerem dados de entrada de perfis atmosféricos, que são obtidos a partir de radiossondagens *in situ* (SOBRINO et al., 2004). A LST é então recuperada a partir da radiância medida pelo sensor, considerando que a LSE é conhecida previamente (HOOK et al., 1992; LI et al., 2013b). No entanto, dados de radiossondagem dificilmente estão disponíveis para locais específicos, ou coincidem com o horário de passagem do satélite (LI et al., 2013b).

As técnicas single-channel são, de modo geral, mais sensíveis a incertezas nos parâmetros de entrada (ver seção 2.2.1), dificultando as correções atmosféricas (CRISTÓBAL et al., 2018). Como os dados de radiossondagem estão geralmente indisponíveis para certos locais, é possível utilizar a ferramenta online *Atmospheric Correction Parameter Calculator* (ACPC), disponível gratuitamente para toda a série Landsat (https://atmcorr.gsfc.nasa.gov/), e atualizada para o Landsat 8. Esta ferramenta permite gerar perfis verticais interpolados por meio de dados de reanálise

do Centro Nacional de Predição Ambiental (NCEP) (BARSI et al., 2005). Entretanto, é importante considerar que uma única radiossondagem atmosférica pode não ser representativa das condições atmosféricas em toda a imagem do Landsat, que possui cerca de 180 x 185 km (CRISTÓBAL et al., 2018). Para reduzir a dependência desses dados e recuperar a LST de uma única banda de forma regional e precisa, alguns métodos foram propostos nas últimas décadas (QIN et al., 2001; JIMÉNEZ-MUÑOZ et al., 2003; JIMÉNEZ-MUÑOZ et al., 2009; CRISTÓBAL et al., 2009; JIMÉNEZ-MUÑOZ et al., 2014; WANG et al., 2015; CRISTÓBAL et al., 2018).

Os dois principais métodos single-channel da literatura foram originalmente desenvolvidos por Qin et al. (2001) e Jiménez-Muñoz et al. (2003), denominados de *Mono-window* (MW) e *Single-channel Generalizado* (SCG), respectivamente. Ambos os métodos são baseados na Equação de Transferência Radiativa (*Radiative Transfer Equation* - RTE) e foram desenvolvidos para evitar a dependência da radiossondagem. O SCG tem melhor desempenho quando comparado ao algoritmo MW (Sobrino et al., 2004; Copertino et al., 2012). O algoritmo MN foi estendido para Landsat 8 e melhorado no trabalho de Wang et al. (2015), sendo chamado de *Improved Mono-window* (IMW). Já o SCG, foi estendido para Landsat 8 em Jiménez-Muñoz et al. (2014) (denominado de SC) e melhorado por Cristóbal et al. (2018) com a inserção de outro parâmetro no modelo, sendo sua nova versão denominada de *Improved Single-channel* (ISC). Neste contexto, os algoritmos IMN e ISC de Wang et al. (2015), e Cristóbal et al. (2018), bem como a inversão da RTE com parâmetros obtidos a partir da calculadora ACPC, podem ser considerados os métodos single-channel mais recentes existentes na literatura para determinar a LST de dados Landsat.

Conforme mencionado, a aplicação de algoritmos single-channel exige o conhecimento a priori da LSE (SOBRINO et al., 2004), e raramente se obtém esta variável com a acurácia necessária (LI et al., 2013b). Nas interações atmosféricas, erros na recuperação da LST são fortemente dependentes da acurácia da LSE (LI et al., 2007). Além disso, Chen et al. (2016) relataram que os erros na determinação da LST da banda 10 do Landsat 8 têm mostrado ser mais sensíveis às incertezas na LSE do que as bandas Landsat dos sensores anteriores, o que segundo os autores é uma característica da própria banda termal do sensor. Nesse contexto, há diversas metodologias para determinar a LSE e algumas delas utilizam índices de vegetação, como o *Normalized Difference Vegetation Index* (NDVI) (VAN DE GRIEND e Owe,

1993; VALOR e CASSELES, 1996; SOBRINO e RAISSOUNI, 2000; SOBRINO et al., 2008) devido à relação existente entre NDVI e as emissividades de materiais terrestres.

O método do NDVI Threshold ($NDVI^{THM}$) (SOBRINO et al., 2008) é amplamente utilizado pela comunidade científica para determinar a LSE, pois, além de sua simplicidade, nenhuma correção atmosférica precisa é exigida nas bandas do visível que compõem o cálculo do NDVI (LI et al., 2013a). Este método considera que a superfície é composta por solo e vegetação, e para sua aplicação, são necessários valores predeterminados de emissividade desses alvos. Desta maneira, um valor típico para a vegetação é geralmente atribuído, uma vez que esta é considerada um *grey body* (HULLEY e HOOK, 2011). Contudo, a escolha de um valor típico para o solo é a questão crítica deste método, devido à alta variabilidade de seus valores de emissividade (SOBRINO et al., 2004). De modo geral, os valores de emissividade utilizados na aplicação da metodologia sempre são obtidos de bibliotecas espectrais disponíveis. Porém, estas bibliotecas dificilmente contêm informações de temperatura dos alvos.

Considerando que as dunas costeiras são comportas em sua maioria por quartzo (SiO_2) (PITTIGLIANNI e ROLIM, 2017) e que este mineral apresenta uma assinatura espectral característica na região do TIR (SALISBURY e D'ARIA, 1992), é possível partir do princípio de que, enquanto a emissividade é um parâmetro na derivação da LST, ela mesma varia com a temperatura. Portanto, uma calibração correta da emissividade baseada na temperatura pode ser requerida para uma estimativa da LST mais precisa. A recuperação de LST por dados de sensoriamento remoto requer validação com medições de campo, mas na maioria dos lugares não há dados de campo de LST disponíveis (COPERTINO et al., 2012; MATTAR et al., 2018), o que torna a validação um desafio.

Para realizar medições de campo de LST no Sul do Brasil especificamente, os pesquisadores precisam organizar campanhas de campo, em dias previamente programados (com condições atmosféricas claras). Ademais, as estações meteorológicas comuns fornecem apenas as variáveis de radiação, umidade relativa do ar, temperatura do ar, precipitação e velocidade do vento. Assim, é preferível que as metodologias para recuperar LST a partir de dados de satélite dependam apenas desses parâmetros, a fim de ser o mais operacional possível para essas regiões.

Considerando que a maioria das metodologias são desenvolvidas e testadas com foco no hemisfério norte, maneiras operacionais e precisas de obter LST devem ser constantemente investigadas para a realidade do hemisfério sul.

1.1 Objetivo

O objetivo desta pesquisa é estudar o efeito do uso de medidas de laboratório baseadas em temperaturas na determinação da LSE e recuperação da LST a partir de dados de sensoriamento remoto orbital. Além disso, pretendeu-se realizar uma análise comparativa entre os algoritmos single-channel mais recentes existentes na literatura (SC, ISC e IMW), aplicados à banda 10 do Landsat 8 TIRS.

1.2 Objetivos específicos

- ✓ Analisar a relação entre a emissividade e a temperatura do quartzo, em laboratório, no comprimento de onda específico da banda 10 (10,6-11,19 μm) do Landsat 8.
- ✓ Avaliar o o efeito do uso de medidas de emissividade de quartzo, realizadas em laboratório e baseadas em temperaturas, na atribuição da emissividade no método do $NDVI^{THM}$.
- ✓ Analisar as particularidades do Fourier Transform Infrared (FT-IR) na obtenção de emissividade e temperatura em campo e em laboratório.
- ✓ Constatar se a utilização de medidas baseadas em temperaturas é capaz de contribuir para uma maior precisão da LST.
- ✓ Testar dados de emissividade de bibliotecas espectrais disponíveis e amplamente utilizadas pela comunidade científica para este fim.
- ✓ Comparar os métodos *single-channel* mais precisos e atuais existentes na literatura para a recuperação da LST e constatar a melhor metodologia para o sul do Brasil.

2. REFERENCIAL TEÓRICO

2.1 Sensoriamento remoto

O sensoriamento remoto é definido por alguns autores como sendo uma tenologia para obtenção de imagens e outros dados da superfície terrestre através da captação e do registro da energia refletida ou emitida, sem contato físico entre o sensor e a superfície (NOVO, 2010; JENSEN, 2009).

2.1.1 Princípios Físicos do sensoriamento remoto

Todo corpo com temperatura acima de zero absoluto (0 K) radia energia e pode ser considerado como uma fonte de energia eletromagnética (LI et al., 2013b). Nesta perspectiva, o Sol e a Terra são as duas principais fontes naturais de energia eletromagnética utilizadas no sensoriamento remoto da superfície terrestre (JENSEN, 2009). Segundo a Teoria ondulatória, esta energia se transmite de um lugar ao outro seguindo um modelo harmônico e contínuo, composto por duas ortogonais entre si: elétrica e magnética, que permitem a propagação da energia eletromagnética no vácuo (RONDÓN, 2017).

As características deste fluxo de energia podem ser descritas por dois elementos: o comprimento de onda (λ) e a frequência (ƒ). O comprimento de onda faz referência à distância entre dois picos sucessivos de uma onda, já a frequência designa o número de ciclos passando por um ponto fixo numa unidade de tempo. Os dois elementos estão inversamente relacionados. A ordenação da energia eletromagnética de maneira contínua em função de seu comprimento de onda ou de frequência é denominada de espectro eletromagnético. O mesmo apresenta subdivisões conforme o tipo de processo físico que dá origem à energia eletromagnética, a interação que ocorre entre a radiação e o objeto sobre o qual esta incide e à transparência da atmosfera em relação à radiação eletromagnética (RONDÓN, 2017).

No espectro eletromagnético, os comprimentos de onda em que a energia é capaz de atravessar a atmosfera são denominados de janelas atmosféricas. Em outras palaveas, são as regiões espectrais em que a radiação é menos afetada pela

atmosfera (GRONDONA et al. 2015). Já aqueles comprimentos de onda em que há interação da energia com a atmosfera (absorção por gases, entre outros) são chamados de bandas de absorção. Na Figura 1 podem ser observadas as janelas atmosféricas, bem como as bandas de absorção presentes no espectro eletromagnético (JENSEN, 2009).

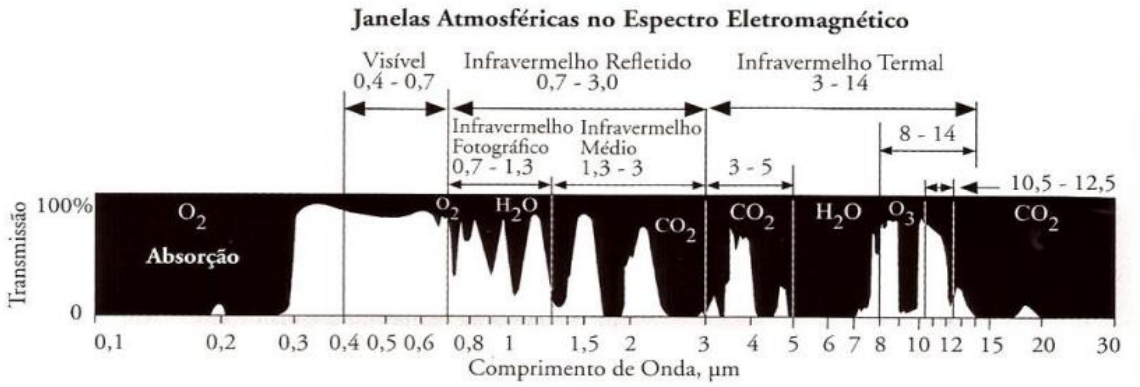

Figura 1. Janelas atmosféricas e bandas de absorção ao longo do espectro eletromagnético. (Fonte: JENSEN, 2009).

2.1.2 Sensoriamento remoto no infravermelho termal (TIR)

Nas faixas de comprimentos de onda em que ocorrem as bandas de absorção (Figura 1), não há possibilidade de registros de alvos terrestres por sistemas sensores passivos (NOVO, 2010). Deste modo, na região do TIR do espectro eletromagnético existem duas faixas de comprimentos de onda para as quais a atmosfera é mais transparente: 3 a 5 µm e 8 a 14 µm. Em estudos de sensoriamento remoto, o intervalo de comprimento de onda de 3 a 5 µm é utilizado para o monitoramento de alvos quentes, como queimadas e atividades geotermais. Já o intervalo entre 8 e 14 µm corresponde a estudos da vegetação, solo e rocha (JENSEN, 2009).

Dado que todos os objetos que apresentam temperaturas superiores a zero absoluto emitem radiação (LI et al., 2013b), a quantidade de radiação de um corpo negro em equilíbrio térmico em um determinado comprimento de onda λ e em uma determinada temperatura *T* é descrita pela lei de Planck:

$$B_\lambda(T) = \frac{C_1}{\lambda^5[exp\left(\frac{C_2}{\lambda T}\right)-1]} \quad (1)$$

Onde *Bλ(T)* é a radiância espectral em $Wm^{-2}\mu m^{-1}sr^{-1}$ de um corpo negro a uma temperatura *T* em Kelvin (K) e λ (μm), *C1* e *C2* são constantes físicas (*C1* = 1,191 × 10^8 $W\mu m^4$ sr^{-1} m^{-2}, *C2* = 1,439 × 10^4 μm·K). Como a maioria dos objetos naturais não são corpos negros, a emissividade (ε), que é definida como a relação entre a radiância de um objeto e a de um corpo negro à uma mesma temperatura, deve ser levada em consideração (LI et al., 2013b).

Assumindo-se a superfície como um emissor/reflector lambertiano, a equação de transferência radiativa (RTE) para uma banda específica na região do TIR pode ser expressa por meio da seguinte equação simplificada:

$$L_{sensor,\lambda} = \left[\varepsilon_\lambda B_\lambda(T_s) + (1-\varepsilon_\lambda)L^{\downarrow}_{atm,\lambda}\right]\tau_\lambda + L^{\uparrow}_{atm,\lambda} \quad (2)$$

Onde L_{sensor} é a radiância de topo da atmosfera (TOA) medida pelo sensor, $B_\lambda(T_s)$ é a radiância do corpo negro dada pela lei de Planck e T_s é a LST, $L^{\downarrow}_{atm}$ é a radiância atmosférica *donwelling*, τ é a transmitância atmosférica total entre a superfície e o sensor, $L^{\uparrow}_{atm}$ é a radiância atmosférica *upwelling*. Os parâmetros $L^{\downarrow}_{atm}$, τ e $L^{\uparrow}_{atm}$ podem ser calculados por meio de dados de radiossondagem *in situ.* Desta maneira, a LST é encontrada (Equação 2) por meio da inversão da lei de Planck (Equação 1).

De modo geral, na região espectral do TIR, os dados de sensoriamento remoto compreendem a radiação proveniente de comprimentos de ondas entre 3,5-20 μm. No entanto, ao se trabalhar com imagens orbitais a maioria das aplicações faz uso do intervalo compreendido entre 8-14 μm devido às janelas atmosféricas (GRONDONA, 2013). Na realidade, a maior parte da superfície da Terra se comporta entre um lambertiano e um reflector especular. Como a atmosfera não é completamente transparente mesmo nas janelas atmosféricas, a radiância da superfície da Terra é influenciada pela composição e estrutura térmica da atmosfera (DASH et al., 2002; TANG e LI, 2014).

A obtenção da LST por sensoriamento remoto é baseada na função de Planck (Equação 1) (DASH et al., 2002). Entretanto, estimar esse parâmetro da radiação emitida no TIR é uma tarefa difícil de ser executada com grande precisão, uma vez que as radiações medidas pelos sensores dos satélites dependem não apenas dos parâmetros da superfície (temperatura e emissividade), mas também dos efeitos atmosféricos (COLL et al., 1994; LI et al., 2013b). Os principais constituintes

atmosféricos que interagem com a energia eletromagnética são: o vapor de água (H_2O), o oxigênio (O_2), o ozônio (O_3), e o dióxido de carbono (CO_2). Dentre as citadas, o vapor de água, que para fins de cálculo foi denominado de *w*, é a molécula absorvedora que mais influencia negativamente na degradação de informações em dados TIR.

2.2 Temperatura da superfície terrestre (LST)

O sensoriamento remoto no TIR fornece uma oportunidade para obter informações sobre a LST nas escalas regional e global, uma vez que a maior parte da energia detectada pelo sensor nesta região espectral é emitida diretamente pela superfície terrestre. Nesse sentido, muitos esforços têm sido dedicados a estabelecer métodos para recuperar a LST a partir de dados de sensoriamento remoto, e avanços significativos foram feitos na última década.

Diversos algoritmos foram propostos considerando as características de vários sensores a bordo de diferentes satélites e utilizando diferentes pressupostos e aproximações para a RTE (Equação 2) e LSE (BECKER e LI, 1990b; GILLESPIE et al., 1998; HOOK et al., 1992; JIMÉNEZ-MUÑOZ e SOBRINO, 2003; KEALY e HOOK, 1993; KERR et al., 1992; POZO VAZQUEZ et al., 1997; PRICE, 1983; QIN et al., 2001; SUSSKIND et al., 1984; TONOOKA, 2001; WAN e DOZIER, 1996; WAN e LI, 1997).

Como mencionado anteriormente, esses algoritmos podem ser agrupados em três categorias conforme Du et al., (2015): (i) algoritmos de canal único ou *single-channel* (JIMÉNEZ-MUÑOZ e SOBRINO, 2003), (ii) métodos multicanais, como por exemplo, os algoritmos *split-window* (SW) e os métodos de separação de temperatura e emissividade (GILLESPIE et al., 1998) e (iii) métodos multi-tempo, como por exemplo, o método de índices espectrais independentes de temperatura (BECKER e LI 1990b), o método de duas temperaturas (WATSON et al., 1992) e o método físico dia/noite (WAN e LI, 1997).

Sendo a atmosfera um dos principais problemas no sensoriamento remoto no TIR para obter estimativas confiáveis da LST a partir de medições por satélite, os efeitos atmosféricos, angulares e de emissividade devem ser compensados. Devido à sua simplicidade e precisão, técnicas SW são mais populares, pois utilizam duas bandas TIR (entre 10 e 12 μm) e partem do pressuposto de que a atenuação da

radiância para a absorção atmosférica é proporcional à diferença de radiância das medições simultâneas em dois comprimentos de onda diferentes, cada uma delas sujeita a diferentes quantidades de absorção atmosférica (JIMÉNEZ-MUÑOZ et al., 2014). No entanto, os métodos single-channel podem se mostrar mais precisos, desde que disponham de dados suficientes sobre o estado da atmosfera (DASH et al., 2002) e metodologias robustas.

2.2.1 Algoritmos single-channel

Os métodos single-channel de obtenção de LST, foco desta pesquisa, utilizam a radiância medida pelo sensor do satélite em uma única banda, escolhida dentro de uma janela atmosférica, e corrigem a atenuação atmosférica residual da radiância e da emissividade. Um código de transferência radiativa, que requer dados de entrada de perfis atmosféricos, obtidos por radiossondagens, é usado para gerar os parâmetros radiância downwelling ($L\downarrow$), radiância upwelling ($L\uparrow$) e transmitância atmosférica (τ). A LST é então recuperada da radiância medida pelo sensor, pela inversão da RTE (Equação 2), desde que a LSE seja conhecida ou estimada anteriormente (LI et al., 2013b). A fim de simplificar o processo de correção atmosférica pela RTE diminuindo a dependência de dados de perfis atmosféricos, alguns algoritmos single-channel de recuperação LST foram desenvolvidos para as séries Landsat (TM e ETM+) (QIN et al., 2001; JIMÉNEZ-MUÑOZ et al., 2003; JIMÉNEZ-MUÑOZ et al., 2009; CRISTÓBAL et al., 2009; WANG et al., 2015; CRISTÓBAL et al., 2018).

Entre os métodos desenvolvidos mais significativos está o amplamente utilizado algoritmo *Mono-window* (MW) (QIN et al., 2001) que requer três parâmetros essenciais para a recuperação da LST: a LSE, a τ, e a temperatura média atmosférica (*Ta*). O método para determinar τ foi dado no mesmo trabalho através da simulação das condições atmosféricas com o programa LOWTRAN 7. Uma abordagem prática para estimar a temperatura média atmosférica de dados meteorológicos locais também foi proposta quando os dados do perfil atmosférico *in situ* não estivessem disponíveis. Entretanto, uma das principais limitações deste algoritmo era que o conteúdo de vapor de água (*w*) devia estar entre 0-3 $g \cdot cm^{-2}$, o que limitava a recuperação da LST além desses valores (CRISTÓBAL et al., 2009).

Nesse contexto, Wang et al., (2015) desenvolveram um algoritmo aprimorado (IMW) baseado em Qin et al., (2001), que foi capaz de fornecer resultados satisfatórios mesmo em atmosferas com *w* maior que 3 $g \cdot cm^{-2}$. Em seguida, validaram os resultados com dados simulados considerando várias situações de sete atmosferas e concluíram que, mesmo com erros moderados no *w* e nas estimativas de LSE, o algoritmo pode ter uma precisão de aproximadamente 1,4 K para a recuperação da LST. Os autores constataram, ainda, que os resultados do novo algoritmo eram mais precisos quando comparados ao método SCG, amplamente utilizado e proposto por Jiménez-Muñoz e Sobrino (2003).

O algoritmo SCG (JIMÉNEZ-MUÑOZ e SOBRINO, 2003) é dependente apenas da LSE e *w* para a recuperação da LST. Uma vez que os dados de entrada são minimizados para apenas *w*, um erro na sua estimativa pode aumentar o erro na determinação da LST. O SCG foi inicialmente desenvolvido para dados Landsat 5, mas foi estendido para dados Landsat 4 e Landsat 7 (JIMÉNEZ-MUÑOZ et al., 2009) e Landsat 8 (JIMÉNEZ-MUÑOZ et al., 2014). Neste último trabalho, os autores relatam que a banda 10 foi utilizada em função de estar localizada em uma região de baixa absorção atmosférica, (altos valores de τ), além do fato de problema de calibração da banda 11 já ser conhecido na época.

A validação do método com dados simulados exibia resultados de raiz do erro médio quadrático (RMSE) menores do que 1,5 K somente para valores de *w* abaixo de 3 $g.cm^{-2}$, que aumentavam conforme o *w* na atmosfera também aumentava. Esse problema havia sido resolvido adicionando-se a *Ta* também como dado de entrada ao modelo no trabalho de Cristóbal et al. (2009), mas até o trabalho de Cristóbal et al. (2018), ainda não haviam coeficientes disponíveis para aplicar o modelo com uso de dados Landsat 8. Em Cristóbal et al. (2018) os autores provaram que, com a inserção do parâmetro *Ta* no algoritmo, ele foi capaz de diminuir o RMSE de 1,5 para 1 K. O estudo foi conduzido utilizando-se uma base de dados robusta e global de perfis atmosféricos (MATTAR et al., 2014) sendo passível de aplicação em qualquer local da Terra. Ademais, foram conduzidas validações em quatro áreas de estudo. Porém, é de grande importância mencionar que no trabalho de Cristóbal et al. (2018), as únicas coberturas da terra consideradas para validação terrestre foram vegetação e neve, o que evidencia a necessidade de estudos também em outros tipos de cobertura.

2.3 Emissividade da superfície terrestre (LSE)

Conforme já dito anteriormente, a LSE é pré-requisito para recuperar a LST a partir de métodos *single-channel* (YU et al., 2014; CHEN et al., 2016). Diferentes abordagens têm sido utilizadas nas últimas décadas para estimar a LSE para diversos sensores, os quais foram revistos e discutidos em detalhes nos trabalhos de Dash et al. (2002) e Li et al. (2013). Esses métodos são geralmente categorizados em três grupos: os métodos semi-empíricos; os métodos multicanais de separação de temperatura/emissividade; e os métodos baseados em física. Para sensores que apresentam apenas uma banda na região do TIR do espectro, apenas os semi-empíricos são aplicáveis (CHEN et al., 2016). Os mesmos se referem à estimativa da LSE com base em uma classificação semi-empírica (CBEM), ou na relação estatística entre o índice de vegetação de diferença normalizada (NDVI) e a emissividade na banda do infravermelho termal.

Na aplicação do CBEM, a LSE pode ser obtida a partir de uma classificação da cobertura do solo, na qual os valores de emissividade para cada classe são assumidos (SNYDER et al., 1998). Este tipo de abordagem é exercido para os produtos MODIS LST e emissividade, por exemplo. Porém, ao aplicar este método perde-se em operacionalidade, visto que necessita de um bom conhecimento da área de estudo e medidas de emissividade *in situ* de todos os alvos das superfícies que compõem as diferentes classes (SOBRINO et al., 2004), assim, os usuários são aconselhados a ter cautela em suas aplicações (ROZENSTEIN et al., 2014). Além disso, como a cobertura tende a mudar com o tempo, são desejados bons conhecimentos do local de estudo e medições de LSE *in situ* em diferentes períodos (ROZENSTEIN et al., 2014). Assim, se as condições necessárias para a classificação não forem cumpridas, é indicado o uso do índice de vegetação NDVI (GRIEND e OWE, 1993; VALOR e CASELLES, 1996; SOBRINO e RAISSOUNI, 2000; SOBRINO et al., 2008).

Diversas abordagens têm utilizado esse índice para predizer a LSE devido a uma relação significativa entre o NDVI (ROUSE, 1973) e as emissividades de materiais terrestres (VAN DE GRIEND e OWE, 1993). Valor e Caselles (1996) propuseram um modelo teórico que relaciona a emissividade com o NDVI. Sobrino e Raissouni (2000) introduziram o método do $NDVI^{THM}$ e aplicaram a dados Advanced Very High Resolution Radiometer (AVHRR) em uma área de estudo localizada em Marrocos.

Uma comparação foi feita entre os métodos do $NDVI^{THM}$, TISI (BECKER e LI., 1995) e DNM aplicada a dados AVHRR na Península Ibérica por Sobrino et al., (2001), tendo o método do $NDVI^{THM}$ propiciado resultados semelhantes aos demais métodos. O $NDVI^{THM}$ também foi aplicado a dados MODIS na Península Ibérica por Sobrino et al. (2003) e foi comparado ao algoritmo MODIS DNM por Momeni e Saradjian (2007). A conclusão deste último estudo é que o $NDVI^{THM}$ fornece resultados similares que os derivados do algoritmo MODIS DNM e, além disso, é de maior facilidade de implementação (SOBRINO et al., 2008). A aplicação do método a dados Landsat 5 TM foi feita por Sobrino et al. (2004), aplicadas a área de Requena-Utiel (Valência, Espanha), e os resultados foram comparados com medidas *in situ* usando o *Box-Method*. O RMSE obtido foi inferior a 0,01.

Sobrino et al. (2008) pontuou que as principais vantagens da utilização desse método são: (1) Não é necessária uma correção atmosférica precisa ao utilizar um NDVI escalado para estimar a proporção de cobertura vegetal no pixel (PV); (2) Pode ser aplicado a sensores com apenas uma banda na região do TIR ou mesmo a sensores sem bandas TIR; (3) mapas de emissividade de maior resolução podem ser obtidos para sensores nos quais as bandas do vermelho (RED) e infravermelho próximo (NIR) possuem maior resolução espacial do que as bandas TIR.

Ainda segundo Sobrino et al. (2008), os problemas envolvidos na aplicação do método do $NDVI^{THM}$ são principalmente quanto ao conhecimento das emissividades do solo, que possui alta variação em seus valores de emissividade e, também, que não pode ser aplicado a certas superfícies como água, neve e gelo. Alguns problemas também foram encontrados nas aplicações para mapeamento mineral com dados de resolução espacial muito elevados, uma vez que o método pressupõe que a superfície é composta de solo e vegetação. Também é recomendável recalcular os limiares do NDVI utilizando o histograma para locais com vegetação muito densa, nesse caso, valores de NDVI mais altos para a vegetação são encontrados. Porém, valores globais de 0,2 para o solo e 0,5 para a vegetação podem ser escolhidos (SOBRINO e RAISSOUNI, 2000).

2.3.1 Emissividade do quartzo

O quartzo (SiO_2) é o principal constituinte mineral da maioria dos solos da Terra. Este mineral não possui feições espectrais típicas dentro do intervalo espectral do infravermelho próximo ao infravermelho médio (VNIR-SWIR) (HUNT e SALISBURY, 1970; EISELE et al., 2015). Além disso, frequentemente as partículas de quartzo se apresentam revestidas com óxidos de ferro e/ou oxihidróxidos (hematita e goethita), que revelam um forte contraste espectral no VNIR e, portanto, geralmente obscurecem quaisquer outras características espectrais potenciais nessa região do espectro.

O comportamento dos minerais, em geral, no TIR apresenta particularidades, principalmente em relação aos silicatos, visto que suas principais feições de absorção ocorrem na faixa centrada em 10µm (SALISBURY e D'ARIA, 1992). Estas feições estão relacionadas às diferenças nas ligações Si-O destes minerais (HOOK et al., 2005). Os minerais silicatados, como o quartzo, apresentam feições de absorção típicas no TIR (VICENTE e SOUZA FILHO, 2010). Nesse sentido, a utilização dos dados de emissividade pode conter informações valiosas para monitoramento do estado e das mudanças no ambiente (HULLEY et al., 2014).

A feição *reststrahlen* é uma dessas feições de absorção típica do mineral de quartzo em que ocorre mínima absorção e mínima emissão, e é verificada em aproximadamente 8,2-9,3µm. Desse modo, estas feições já diagnosticadas permitem que o quartzo seja estudado de forma precisa por sensoriamento remoto no TIR, especialmente dentro da janela atmosférica entre 8 e 14 µm. Já os espectros de matéria vegetal, por exemplo, são distintos e têm consistentemente alta emissividade espectralmente plana nesta região (HULLEY et al. 2014), sendo possível evidenciar esta distinção entre tipos superfícies. Os resultados de diversos estudos indicam que o uso do sensoriamento remoto no TIR em estudos geológicos é promissor (CUDAHY et al., 2012; NOTESCO et al., 2014; EISELE, et al., 2015).

2.3.2 Emissividade da vegetação

De acordo com Li et al. (2013), a vegetação sadia exibe baixo contraste espectral na região do TIR, especialmente as coníferas, que apresentam uma emissividade quase uniforme, com exceção de uma pequena feição reststrahlen entre de 3,43-3,51 µm, associada com as bandas de vibração hidrogênio-carbono. O

mesmo autor, comenta que há uma diferença quanto à vegetação senescente, onde a emissividade é evidentemente reduzida.

Ribeiro da Luz e Crowley (2007) descobriram que algumas informações espectrais úteis associadas aos constituintes químicos da folha e aos aspectos estruturais podem ser detectáveis a partir dos comportamentos espectrais da emissividade. No entanto, a medição remota das características sutis de emissividade da vegetação continua a ser um grande desafio técnico.

2.3.3 Biblioteca espectral

Ao se utilizarem os métodos de estimativa de LSE semi-empíricos descritos anteriormente, os valores representativos de emissividade atribuídos são, na prática, baseados em bibliotecas espectrais. As bibliotecas espectrais tratam-se de bancos de dados que armazenam uma quantidade de espectros que podem ser obtidos em medidas em campo ou laboratório. Nesta perspectiva, uma das bibliotecas espectrais mais utilizadas como parte de estudos de sensoriamento remoto é a biblioteca espectral ASTER <http://speclib.jpl.nasa.gov> que possui mais 2300 espectros de materiais naturais e artificiais (BALDRIDGE et al., 2009). A biblioteca inclui espectros de rochas, minerais, solos lunares, solos terrestres, materiais artificiais, meteoritos, vegetação, neve, gelo, cobrindo desde a região do visível até a região do TIR.

Outra biblioteca espectral amplamente utilizada é a MODIS UCSB Emissivity Library < https://icess.eri.ucsb.edu/modis/EMIS/html/em.html>, que é uma coleção de medidas de emissividade de materiais naturais e artificiais. Esta biblioteca é um recurso espectral para o cálculo da emissividade da superfície para recuperação de LST de dados MODIS, contando com espectros de água, gelo, neve, solo, minerais, vegetação, e uma grande variedade de materiais antropogênicos.

Na Tabela 1 são exibidos os valores de emissividade de diversos alvos da superfície terrestre para bandas específicas de sensores remotos. No contexto do uso de bibliotecas espectrais de emissividade em conjunto com imagens de sensoriamento remoto, a função resposta espectral (SRF) dos sensores deve ser levada em consideração (HULLEY e HOOK, 2009). Esta função varia entre sensores e, também, entre bandas de um mesmo sensor, podendo ser uma potencial fonte de incertezas na recuperação da LSE caso não seja considerada (CHEN et al., 2016).

Tabela 1. Emissividade média em bandas específicas de sensores remotos para diferentes tipos de superfícies terrestres existentes na natureza.

Tipo de superfície	Emissividade	Banda/Sensor
Lavoura	0.971	10 TIRS/Landsat 8
Floresta	0.995	10 TIRS/Landsat 8
Pastagem	0.970	10 TIRS/Landsat 8
Arbustos	0.969	10 TIRS/Landsat 8
Grama	0.982	10 TIRS/Landsat 8
Solo	0.928	6 TM/Landsat 5
Concreto	0.937	6 TM/Landsat 5
Asfalto	0.942	6 TM/Landsat 5
Áreas úmidas	0.992	10 TIRS/Landsat 8
Corpos d'água	0.992	10 TIRS/Landsat 8
Tundra	0.980	10 TIRS/Landsat 8
Impermeável	0.973	10 TIRS/Landsat 8
Terras áridas	0.969	10 TIRS/Landsat 8
Neve e gelo	0.992	10 TIRS/Landsat 8
Areia	0.951	10 TIRS/Landsat 8

Fonte: Adaptado de Mallick et al. (2012), Du et al. (2015) e Mattar et al. (2018)

Teoricamente, é sabido que a emissividade de um alvo varia conforme sua temperatura e comprimento de onda (OLSEN, 2007). Entretanto, na maior parte dos estudos que envolvem bibliotecas espectrais para estimativa de LSE, dificilmente os bancos de dados contêm informações emissivas dos alvos em diferentes temperaturas. Isso provavelmente está relacionado com o termo *T* da função Planck que, segundo alguns estudos, dependendo do material considerado, pode ser retirado do processo de ponderação pela SRF sem apresentar um erro significativo, já que a dependência da temperatura da emissividade pode ser pequena para alguns materiais da superfície (WILBER et al., 1999; WAN e DOZIER, 1996; DASH et al., 2002).

No entanto, no caso do quartzo se tem possibilidade de estas variações da emissividade com sua temperatura serem mais significativas (HULLEY e HOOK, 2009), o que justifica a importância de investigar estes efeitos. O radiômetro *Fourier*

Transform Infrared (FT-IR) modelo 102F, utilizado nesta pesquisa, é um equipamento projetado e fabricado pela D&P instruments (SIMSBURY, CT, EUA) que é capaz de medir a radiância total, incluindo a radiância emitida pela amostra e a radiância do ambiente refletida pela amostra (ZHANG et al. 2016). Suas principais especificações estão listadas na Tabela 2.

Tabela 2. Especificações do FT-IR model 102F.

Name	Características
Intervalo espectral	2 a 16 micrômetros
Resolução espectral	4 cm^{-1}, 8 cm^{-1} e 16 cm^{-1} (ajustável), 2 cm^{-1} podem ser escolhidos
Precisão espectral	±1 cm^{-1} abrange todo o intervalo espectral
Velocidade de digitalização	1 digitalização/s, resolução de 4 cm^{-1}
Frequência de amostragem	5 kHz
Largura de banda de sinal	2 kHz

Fonte: Adaptado de Zhang et al. (2016).

2.4 Dados de satélite

2.4.1 Landsat

O projeto Landsat fornece uma oportunidade particular para a recuperação LST, pois apresenta um período de registro de dados relativamente longo (YU et al., 2014) (1984-atual) de imagens TIR em resolução espacial média adequada para diferentes estudos ambientais (JIMÉNEZ-MUÑOZ et al., 2009). Os dados do TIR eram inicialmente coletados através da banda 6 dos sensores Thematic Mapper-TM (plataformas Landsat 4 e Landsat 5) e Enhanced Thematic Mapper-ETM+ (plataforma Landsat 7).

Devido à sua resolução espacial e disponibilidade de imagens, os dados TIR da série Landsat foram amplamente aplicados para recuperação LST para estudos como estimativa do balanço de energia, monitoramento da umidade superficial e da evapotranspiração, monitoramento de ilhas de calor urbano, e simulação de processo biogeoquímicos, exigindo a LST como parâmetro de entrada (WANG et al., 2015).

O interesse nos dados Landsat TIR aumentou nos últimos anos, o que incentivou o surgimento de diferentes publicações relacionadas a essa questão. O satélite Landsat 8 foi lançado em fevereiro de 2013 como continuidade da série de satélites Landsat. Este satélite possui dois sensores, o *Operational Land Imager* (OLI) e o *Thermal Infrared Sensor* (TIRS).

O OLI coleta dados em uma resolução espacial de 30 m com oito bandas localizadas no RED, NIR, e infravermelho de ondas curtas (SWIR) do espectro eletromagnético, além de uma banda pancromática adicional com resolução espacial de 15 m. O sensor TIRS (Figura 2) mede a radiância na resolução espacial de 100 m usando duas bandas com intervalos de comprimento de onda de 10,60-11,19 μm (banda 10) e 11,50-12,51 μm (banda 11) (IRONS et al. 2012), e os dados são reamostrados para 30 m para coincidir com as bandas multiespectrais OLI. Sua resolução radiométrica é de 16 bits e seu período de revisita é de 16 dias.

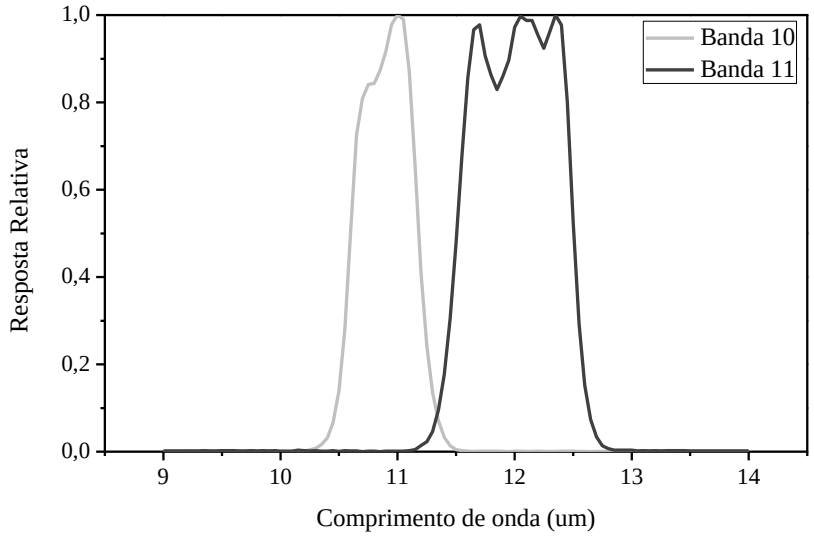

Figura 2. Função resposta espectral (SRF) das bandas do TIR do sensor TIRS a bordo do satélite Landsat 8. (Fonte: Adaptado de USGS, 2018).

2.4.2 Stray Light

Após o lançamento do Landsat 8 no início de 2013, foram realizados procedimentos para caracterizar o desempenho do instrumento TIRS e ajustar a calibração para garantir a integridade radiométrica dos produtos. A investigação que se seguiu determinou que o TIRS havia sido afetado por um problema de *stray light*, em que a radiância fora do campo de visada estava entrando no sistema óptico e

adicionando um sinal não uniforme aos detectores (GERACE e MONTANARO, 2017). Os erros introduzidos por *stray light* podiam inicialmente atingir até 2,1 a 4,4 K para as bandas 10 e 11 respectivamente. Uma tentativa de correção foi feita em 2014 minimizando o problema (USGS, 2014), propiciando a diminuição dos erros para ± 0,87 K para a banda 10 e ± 1,67 K para a banda 11. Erros esses maiores do que o disponível para a banda 6 do Landsat 7 ETM+ (0,48 K) (MONTANARO et al., 2014)

O trabalho continuou em progresso, e um algoritmo foi desenvolvido e implementado no sistema de processamento em fevereiro de 2017 < https://landsat.usgs.gov/april-25-2017-tirs-stray-light-correction-implemented-collection-1-processing>. Nesta ocasião, os erros foram diminuídos para ± 0,52 K (banda 10) e ± 0,91 K (banda 11). Como ambos os detectores TIRS são afetados de forma diferente, um modelo específico foi gerado para corrigir cada um. Na órbita, a fonte do *stray light* de todos os locais não é conhecida, mas o algoritmo de correção em questão usa a radiância na borda da imagem como uma aproximação para o que pode estar fora do ângulo de visada. Uma vez que os resultados foram promissores, a USGS implementou o software de correção desenvolvido como parte do produto da “Landsat Collection 1”.

Conforme já mencionado, trabalhos recentes estão focando em técnicas single-channel para dados da banda 10 do Landsat 8 (JIMÉNEZ-MUÑOZ et al., 2014; WANG et al., 2015; CHEN et al., 2016; CHATTERJEE et al., 2017; CRISTÓBAL et al., 2018). Yu et al. (2014) ao compararem três métodos (método baseado na RTE, algoritmo SW (QIN et al., 2001b) e algoritmo SCG (JIMÉNEZ-MUÑOZ et al., 2014) concluíram que a maior acurácia foi atingida por meio do uso da RTE com a banda 10. Ambos os métodos que utilizam apenas uma banda demonstraram maior acurácia com uso da banda 10 quando comparados à 11.

3. MATERIAL E MÉTODOS

3.1 Área de estudo

A área de estudo é representada por uma duna transgressiva localizada litoral no norte do Rio Grande do Sul, entre os municípios de Cidreira e Tramandaí (Figura

3), com uma extensão de aproximadamente 30 km² e foi selecionada por apresentar grande estoque de areia quartzosa fina (tamanhos entre 125-250 μm), composta por 99,53 % de quartzo e 0,47 % de minerais pesados (PITTIGLIANI et al., 2017). Este alvo possui regiões de inter-dunas que, em geral, apresentam uma vegetação rasteira e abrigam corpos d'água temporários, principalmente nos períodos de inverno, devido à presença próxima do lençol freático (TOMAZELLI et al., 2008).

Em geral, o litoral norte do Rio Grande do Sul é caracterizado pelos elementos fundamentais de sua paisagem natural, que são as topografias de terras baixas (planície costeira), e o regime de ventos apropriado em velocidade e direção (TOMAZELLI e VILLWOCK, 1992), o que favorece a formação de dunas costeiras. O clima é caracterizado por uma temperatura média anual de 20 ºC, precipitação anual de 1323 mm, evaporação anual de 1134.5 mm e média de umidade de 80 % (TRAVESSAS et al., 2005).

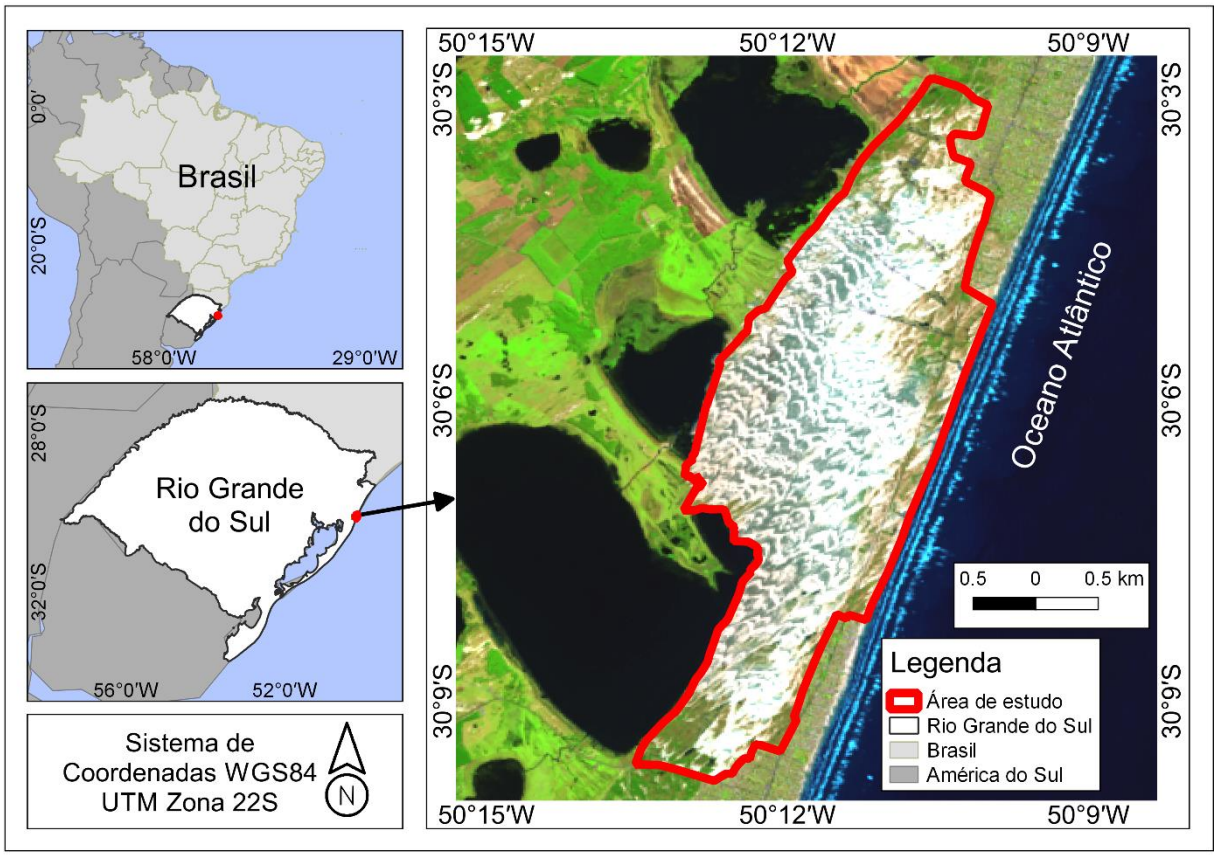

Figura 3. Localização da área de estudo no Brasil e no Rio Grande do Sul. Uma composição colorida falsa-cor RGB654 é representada na imagem.

A escolha deste local para a execução da pesquisa, está associada às suas características pseudo-invariantes, como é chamada na literatura, uma vez que apresenta poucas mudanças temporais, espaciais e de composição em sua superfície. Sendo assim, são excelentes alvos para validar dados de emissividade e temperatura a partir de dados de sensoriamento remoto orbital no TIR (HULLEY e BALDRIDGE, 2013).

3.2 Material

O material necessário para o desenvolvimento desta pesquisa consistiu em:

- ✓ Imagens orbitais Landsat 8 OLI/TIRS;
- ✓ FT-IR (Model 102);
- ✓ Desumidificador;
- ✓ 2 aparelhos de GPS;
- ✓ Termômetro infravermelho;
- ✓ Softwares específicos para processamento de dados: *WinFT, Envi* (Exelis, 2018)*, Matlab,* entre outros.

3.3 Procedimentos metodológicos

O fluxograma da Figura 4 ilustra as principais etapas metodológicas realizadas neste trabalho. A metodologia detalhada é mostrada em cada um dos dois artigos científicos elaborados neste trabalho, que constam na seção “Resultados e Discussão”. O artigo número 1 se refere à análise do efeito da emissividade na LST e o artigo número 2 se refere à análise comparativa entre os métodos de obtenção de LST. Ambos os artigos estão apresentados conforme as respectivas normas necessárias para o processo de submissão. O artigo número 1 foi submetido para a revista *IEEE Journal of Selected Topics in Applied Earth Observations and Remote Sensing* (IEEE JSTARS), enquanto que o artigo número 2 foi submetido para a *International Journal of Remote Sensing* (IJRS).

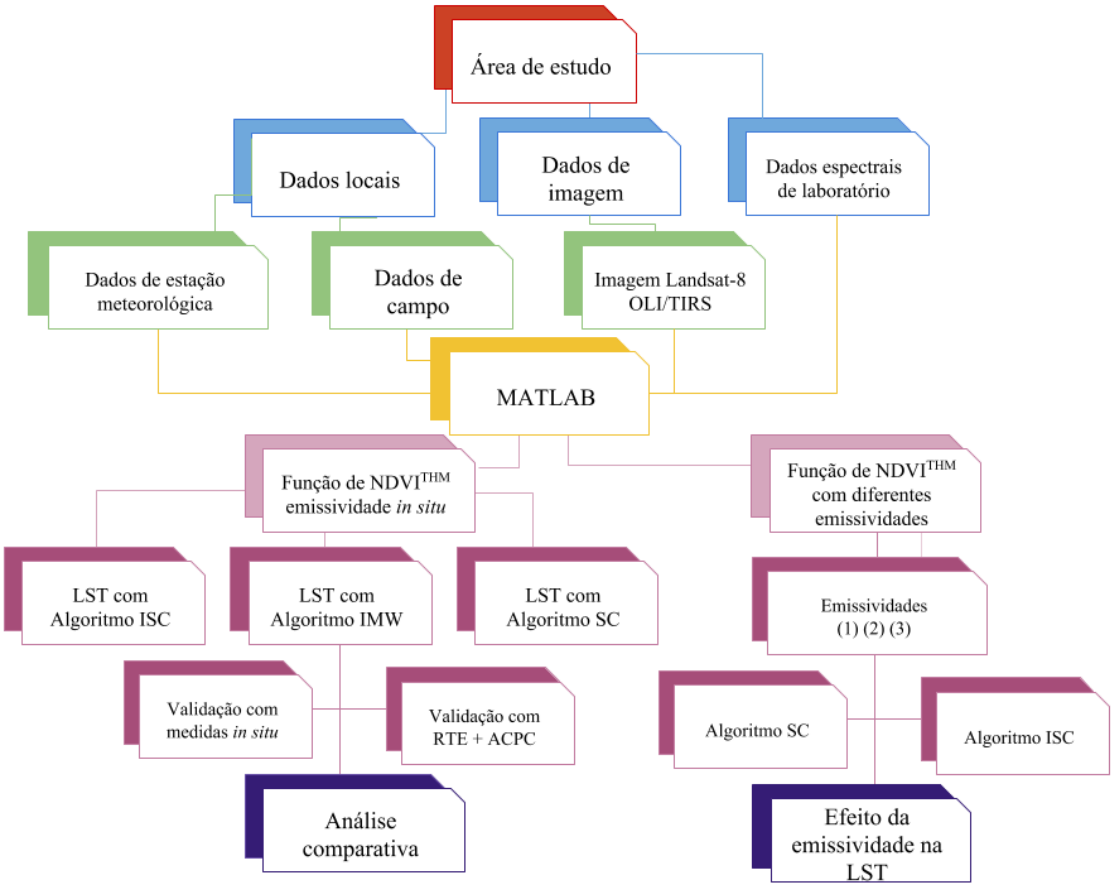

Figura 4. Fluxograma ilustrando as principais etapas do estudo.

4. RESULTADOS E DISCUSSÃO

4.1 ARTIGO 1 - Land Surface Temperature Retrieval by LANDSAT 8 Thermal Band: Applications of Laboratory and Field Measurements

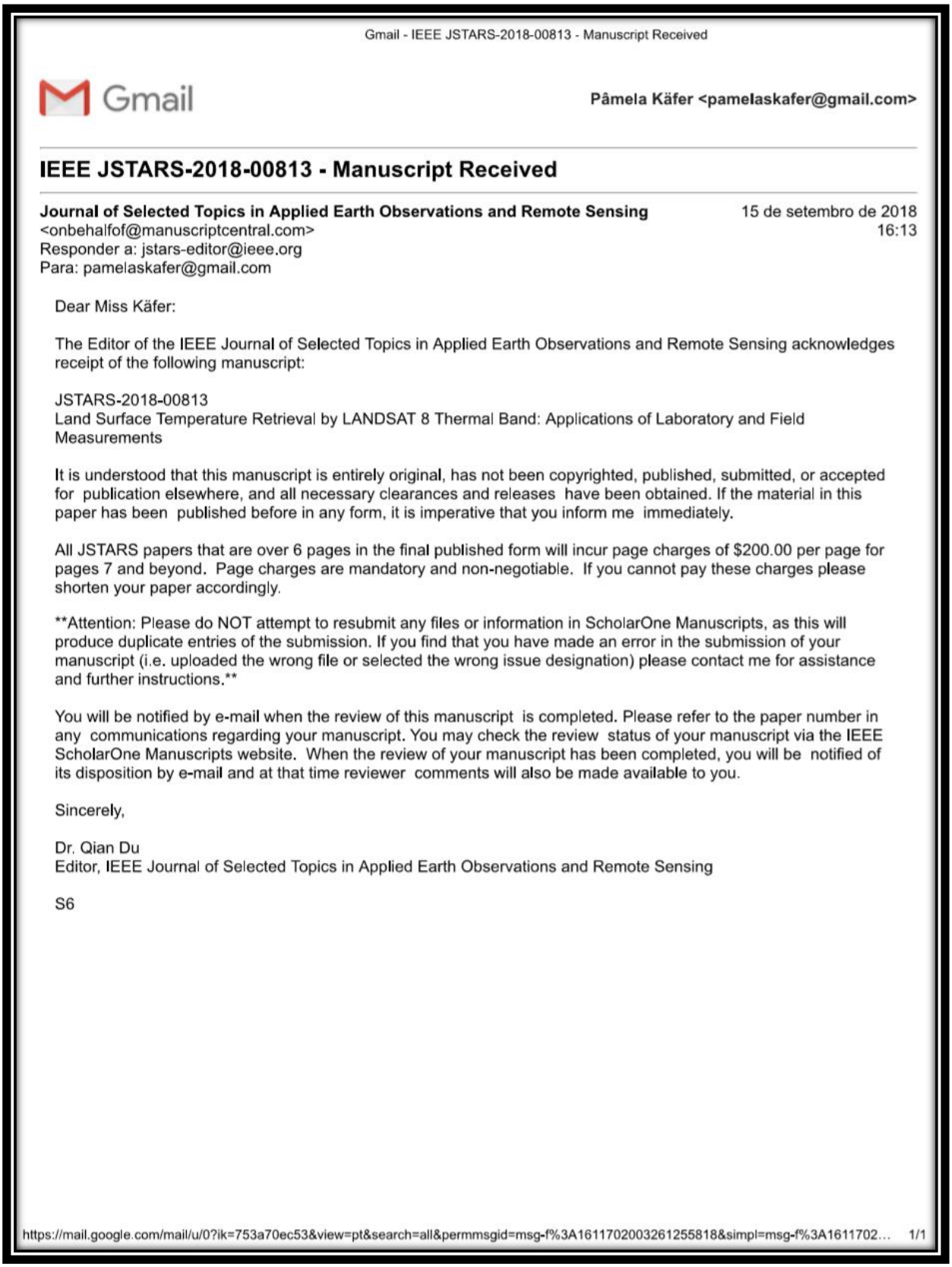

Gmail - IEEE JSTARS-2018-00813 - Manuscript Received

Gmail

Pâmela Käfer <pamelaskafer@gmail.com>

IEEE JSTARS-2018-00813 - Manuscript Received

Journal of Selected Topics in Applied Earth Observations and Remote Sensing 15 de setembro de 2018 16:13
<onbehalfof@manuscriptcentral.com>
Responder a: jstars-editor@ieee.org
Para: pamelaskafer@gmail.com

Dear Miss Käfer:

The Editor of the IEEE Journal of Selected Topics in Applied Earth Observations and Remote Sensing acknowledges receipt of the following manuscript:

JSTARS-2018-00813
Land Surface Temperature Retrieval by LANDSAT 8 Thermal Band: Applications of Laboratory and Field Measurements

It is understood that this manuscript is entirely original, has not been copyrighted, published, submitted, or accepted for publication elsewhere, and all necessary clearances and releases have been obtained. If the material in this paper has been published before in any form, it is imperative that you inform me immediately.

All JSTARS papers that are over 6 pages in the final published form will incur page charges of $200.00 per page for pages 7 and beyond. Page charges are mandatory and non-negotiable. If you cannot pay these charges please shorten your paper accordingly.

Attention: Please do NOT attempt to resubmit any files or information in ScholarOne Manuscripts, as this will produce duplicate entries of the submission. If you find that you have made an error in the submission of your manuscript (i.e. uploaded the wrong file or selected the wrong issue designation) please contact me for assistance and further instructions.

You will be notified by e-mail when the review of this manuscript is completed. Please refer to the paper number in any communications regarding your manuscript. You may check the review status of your manuscript via the IEEE ScholarOne Manuscripts website. When the review of your manuscript has been completed, you will be notified of its disposition by e-mail and at that time reviewer comments will also be made available to you.

Sincerely,

Dr. Qian Du
Editor, IEEE Journal of Selected Topics in Applied Earth Observations and Remote Sensing

S6

https://mail.google.com/mail/u/0?ik=753a70ec53&view=pt&search=all&permmsgid=msg-f%3A1611702003261255818&simpl=msg-f%3A1611702... 1/1

Land Surface Temperature Retrieval by LANDSAT 8 Thermal Band: Applications of Laboratory and Field Measurements

Pâmela Suélen Käfer, *Student member, IEEE*, Silvia Beatriz Alves Rolim, *Member, IEEE*, María Luján Iglesias, Nájila Souza da Rocha and Lucas Ribeiro Diaz

***Abstract*—Land surface temperature (LST) plays an important role in a wide variety of scientific studies. Several methodologies to retrieve LST and correct the atmospheric effects for thermal infrared satellite imagery have been developed recently and all of them require prior knowledge of the land surface emissivity (LSE). The techniques developed for LSE and LST retrieval need to be validated with field measurements. However, in-situ measurements are a challenge, hence, it is essential to investigate the particularities of each instrument to verify the best approach to collect data and validate the algorithms. Fourier Transform Infrared spectrometer (FT-IR) has been widely used to obtain emissivity of different targets and calculate temperature. The instrument may be used to validate remote sensing data. Moreover, FT-IR allows to collect both emissivity and temperature at the laboratory, thus being an alternative to field validation. We investigated the emissivity dependence of the temperature. In addition, we evaluated the possibility of replacing in-situ measurements by laboratory-controlled measurements. We have chosen two single-channel methods to calculate LST and perform the analysis in a Landsat 8 image. We also performed field measurements at the same time of the satellite overpass. FT-IR showed great potential to validate remotely sensed data. However, the instrument needs some time to acquire stability and attention in the calibration process. Laboratory measurements can replace field data producing approximately 2 % of difference in the LSE. Both single-channel methods provide good accuracy for LST retrieval. Nonetheless, ISC has superior performance for the study area conditions.**

***Index Terms*—Emissivity, LSE, LST, Quartz, Sand lands, Single channel method.**

INTRODUCTION

Land surface temperature (LST) is a parameter that plays an important role in a wide variety of scientific studies, such as climatology, hydrology, ecology, biogeology, global change studies, evapotranspiration, net radiation and air temperature modeling [1-2]. Several methodologies to retrieve LST and correct the atmospheric effects for thermal infrared satellite imagery have been developed based on a split-window method (SW), a single-channel method (SC), or a mono-window algorithm (MW), among others [3-5], and have exhibited very good results.

The Landsat project provides an opportunity for the LST retrieval because it is the most complete data continuous sequence that extends back to 1984. For much of this period, Landsat thermal data were provided through a single broadband thermal channel [6]. Even though Landsat 8 was an advance in relation to previous sensors because it includes two bands in the thermal infrared region (TIR) between 10 and 12 μm, TIRS sensor had calibration issues caused by stray light since its launch [7-8]. Only after 2017 the problem was completely solved, and SW techniques were encouraged [9].

The Landsat 8 calibration issue allowed the scientific community to focus on SC methods so that many efforts were done to develop more accurate algorithms in recent years [5-7, 10-12]. All these methods require prior knowledge of the land surface emissivity (LSE) [13]. In most studies that use SC algorithms, NDVI Threshold method ($NDVI^{THM}$) [14] is applied to obtain LSE parameter with good approximations. The method requires the emissivity values of predetermined targets [15], generally assigned based on available spectral libraries.

The estimation of LSE by remote sensing in the TIR is mainly dependent on the surface cover and viewing angle [16-18] and its accuracy affects the determination of LST. [19] highlights that an LSE error of 1.5 % will result in an LST error of approximately 1 K. [20] reported that an error of 2.5 % in LSE calculation can produce an error of 2 K in the LST retrieval. For urban areas, [13] pointed out the importance and potential impacts of LSE have been ignored in the most investigations, often because of data unavailability.

All the techniques developed for LSE and LST retrieval from remote sensing data require validation with field measurements [21-22], which is rarely done, since it is difficult to perform ground measurements comparable with satellite data [23]. Different sensor data specifications and field data can also limit the validation; therefore, in-situ measurements are a challenge. Furthermore, the observations are affected by many types of noises included in the measurement, leading the accuracy to be out of expectation [24].

It is essential to investigate the particularities of each instrument to verify the best approach to collect data in-situ. In this context, MODEL 102F is a *Fourier Transform*

Infrared spectrometer (FT-IR) that has been broadly used to collect emissivity of different targets in the spectral range of middle and thermal infrared wavelength (2~25µm) with a spectral resolution of 4, 8 or 16cm^{-1} [24-25]. The instrument may be used to validate remote sensing data because it allows to calculate LSE and LST in the field from radiance measurements. Moreover, FT-IR also allows to obtain both emissivity and temperature at a controlled environment. Hence, it can be used as an alternative to field validation, since field measurements are commonly restricted to a limited number of pixels [26].

When measurements are performed at a controlled environment by using a FT-IR spectrometer, it is required to heat the sample in order to increase the thermal contrast and the accuracy of the measurements. According to the theorical Planck's equation, the emissivity of a target, which depends on its wavelength, also depends on the target temperature [3]. But it is usually not taken into account, because for most surface materials, the emissivity dependence on the temperature is negligible [13]. We investigated the emissivity dependence of the temperature and evaluated the possibility of replacing in-situ measurements by laboratory-controlled measurements.

The paper explores the use of laboratory measurements of emissivity and temperature in the land surface variables (LSE and LST) estimation from remote sensing data in the TIR. We have chosen two single-channel methods [5,7] to calculate LST and perform the analysis by using the band 10 (10.6-11.19µm) of a Landsat 8 image. In addition, field campaign with measurements concurrently with the satellite overpass was conducted to validate the algorithms and compare the results.

METHODOLOGY

Study area

We selected one of the remaining transgressive dunes at Cidreira Beach (30 km²) as study area, located in the North Coast of Rio Grande do Sul state, Brazil (Fig. 1). The area has a large stock of fine quartz sand (125 to 250 µm), with grains varying among sub-rounded (68 %), rounded (18 %), sub-angular (14 %) and composed of quartz (99.53 %) and heavy minerals (0.47 %).

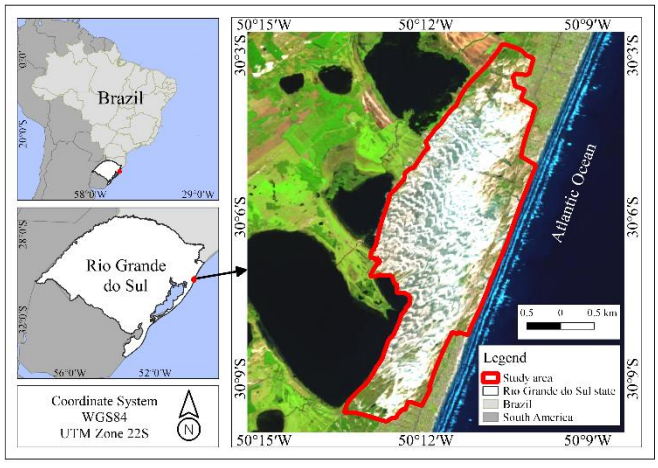

Fig. 1. Study area location in Southern Brazil. Dune field mask shown by the red line (Landsat 8 OLI - color composite RGB: 432).

The dune was chosen mostly because it is considered a pseudo-invariant target therefore suitable for the terrestrial validation of LST retrieval by remote sensing data [19].

In general, the north coast of Rio Grande do Sul state is characterized by the fundamental elements of its natural landscape, which are the lowland topographies (coastal plain), and the appropriate speed regime and direction [27], this characteristics favors the formation of coastal dunes. Its average annual temperature is 20 °C, the annual precipitation is 1323 mm, the annual evaporation is 1135 mm and the average humidity is 80 % [28].

Data acquisition and pre-processing

The flowchart (Fig. 2) illustrates the main steps of the study.

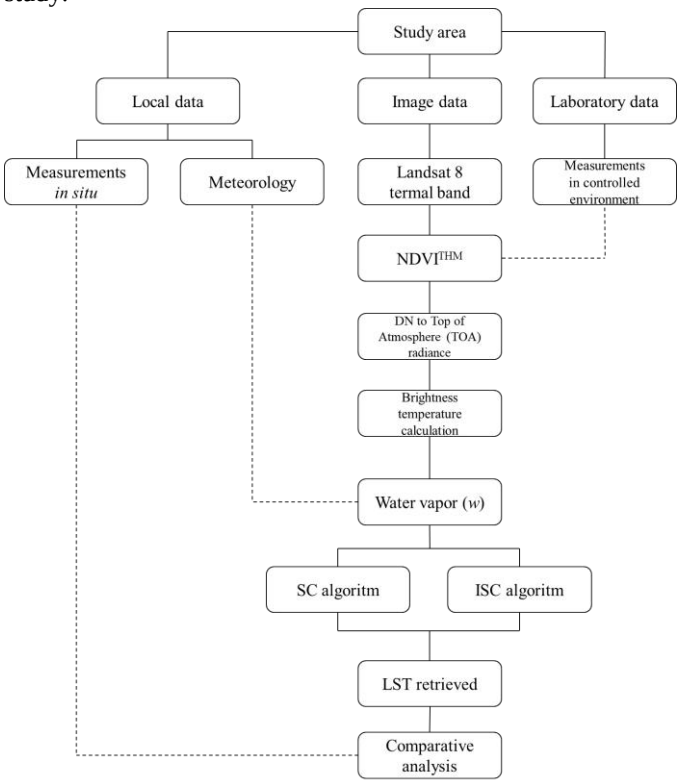

Fig. 2. Main steps of the study.

One scene of Landsat 8 OLI/TIRS was acquired covering the study area. The image was downloaded from the US Geological Survey website in level 1G product (http:// www.earthexplorer.usgs.gov/). The day was cloud free with very clear atmospheric conditions. Details of the remotely sensed data applied in this study are shown in Table I.

TABLE I LANDSAT 8 OLI/TIRS IMAGE INFORMATION.

Year	Path	Row	Acquisition	Time	Sun elevation (º)
2018	220	081	Mar, 14	13:12.22	48

Landsat 8 carries two sensors, the Operational Land Imager (OLI), which collects data at a 30 m spatial resolution with eight bands located in the visible and near-infrared and in the short-wave infrared regions of the electromagnetic spectrum, and the thermal infrared sensor (TIRS), which measures the TIR radiance at 100 m spatial resolution using two bands

(Fig. 3) located in the atmospheric window between 10 and 12 µm [29].

Although the Landsat 8 TIRS has two spectrally adjacent channels that are appropriate for the SW methods [2], it is important to emphasize that band 10 is located in a lower atmospheric absorption region (high atmospheric transmissivity values) as pointed out by [7], being preferable using it for the LST determination by SC methods.

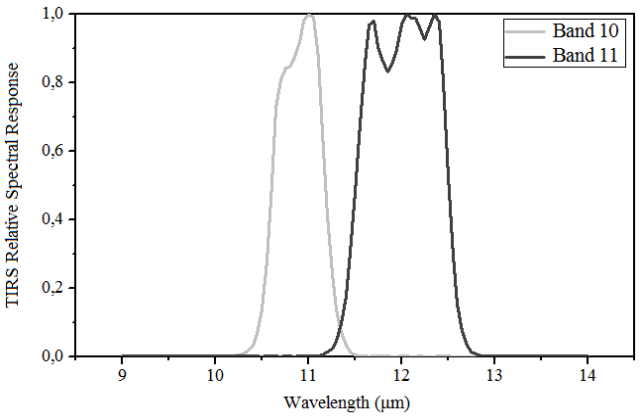

Fig. 3. Relative spectral response function of Landsat 8 TIRS bands. (Data adapted from USGS, 2018).

Image processing was automated through the development of the NDVI^{THM} function and SC algorithms in *MATLAB* environment. Since it is not necessary to perform accurate corrections to retrieve PV (vegetation proportion) [30] from a scaled NDVI, we assumed that the atmospheric contribution was corrected in the visible bands [31]. Additionally, radiometric and geometric corrections have been done to the image, considering the Universal Transverse Mercator coordinate system with the WGS-84 datum.

Emissivity

Laboratory measurements

As mentioned, the emissivity values of the targets can be taken from the bibliography [32] based on available spectral libraries. In most investigations, the emissivity is obtained through the ASTER spectral library (http://speclib.jpl.nasa.gov), which provides more than 2300 spectra in wavelengths covering from the visible to TIR. However, there is no temperature information, and different temperatures might have different emissivities for the same land-surface types.

To understand the relationship between the target emissivity and its temperature, we performed radiance measurements in controlled environment, based on temperatures using the Fourier Transform Infrared spectroscopy (FT-IR) Model 102F. The atmospheric downwelling radiance L^↓ λ was obtained by measuring a golden reference panel with an emissivity of 0.04. Afterwards, the sample spectral emissivity ε was calculated from the following equation:

$$\varepsilon_\lambda = \frac{L\lambda - B\lambda(Ts)}{B\lambda(Ts) - L^{\downarrow}\lambda} \quad (1)$$

where $L\lambda$ is the spectral radiance and $B\lambda(Ts)$ refers to Planck's equation, given as:

$$B\lambda(Ts) = \frac{C1\lambda^{-5}}{exp(C2/\lambda T)-1} \quad (2)$$

where C1 and C2 are constants (C1 = 1.191 × 108 W µm^4 sr^{-1} m^{-2}, C2 =1.439×10^4 µm K). Assuming that ε =1 between 7.5 and 8 µm, the sample temperature can be obtained by the inversion of the Eq. (2). This wavelength range was chosen because the emissivity and temperature retrieval are most accurate at the maximum emissivity value [33]. The downwelling radiance measurement was carried out before and after the sample measurements. If the amount of downwelling radiance changes between measurements, the properties determined for the material will have an associated error. Therefore, the accuracy in the downwelling radiance measurements determine the accuracy in obtaining the emissivity and temperature spectra.

We organized two sets of measurements, the first was performed in the first 30-40 minutes of instrument operation and after the first calibration against the blackbodies. The second set was done after 45 minutes and the second calibration of the instrument. In the calibration process, two temperatures are chosen, a temperature for the cold blackbody (below the ambient temperature), and another for the warm blackbody, (above the sample temperature). This leads to a more accurate calibration [34]. The calibration interval assumed was 10 to 40 ºC (283.15 to 313.15 K).

The temperature of the laboratory was about 25ºC (295 K) and the relative humid 58 %. We selected samples from the whole dune area in order to homogenize the sampling. The sand was heated up to +/- 60 ºC (333 K) and the measurements were taken. They ceased when the sample temperature achieved 26 ºC, totaling about 61 measurements for the first set, and 63 measurements for the second (1-2 measurement per minute). The calibration of the instrument was carried out twice in the whole process. Afterwards, we weighted the data by the sensor spectral response function (SRF) (Fig. 3), since it may be a potential source of uncertainties in the LSE estimation if it is not considered [13, 16].

Field measurements

The field campaign at the study area was done concurrently with Landsat 8 overpass. As this kind of validation method is restricted to a limited number of pixels [26], we selected a very homogeneous and bare site within the dune area to settle the instrument. As it had not rained in the previous days, we did not have much influence of humity in the sand, which makes the site highly homogeneous in terms of both surface temperature and emissivity, thus easing the measurements [35].

The in-situ emissivity and temperature spectra were obtained from radiance measurements with the FT-IR spectrometer as well. At the field, the instrument calibration was carried out same as at the laboratory. However, the downwelling radiance measurements were taken more often, because the radiance in the field may have more variations than in a controlled environment. The FT-IR was placed facing the surface sand at angles close to nadir. The standard input optic is 1 inch in diameter with a 4.8 degree expanding

field of view. The measurements were taken at a rate of 1-2 per minute, and the emissivity and temperature were calculated by (1) and inversion of (2), respectively.

LSE determination from remote sensing data

Accurate LST retrieval from remotely sensed data requires both, a proper characterization of atmospheric influence and an adequate knowledge of LSE [13]. In this context, different approaches have been used to estimate LSE from several sensors, which have been reviewed and discussed in detail by [3]. These methods may be categorized into three groups: (i) semi or empirical methods, (ii) multi-channel temperature/emissivity separation methods, and (iii) physically based methods [3]. However, for SC methods only the empirical ones (i) are applicable.

Some approaches for LSE estimation from remote sensing measurements use the *Normalized Difference Vegetation Index* (NDVI) [36-38], because of a relationship between the NDVI [39] and the emissivities of terrestrial materials [36]. [37] proposed a theoretical model that relates the emissivity to the NDVI. For the Landsat 8 data, a very operational way to estimate LSE is using the *NDVI Threshold Method* ($NDVI^{THM}$) [14]. The method obtains the emissivity values from the NDVI considering different cases:

(a) NDVI<NDVIs

NDVIs corresponds to the NDVI of soil; thus, the pixel is entirely composed of bare soil, and the soil emissivity (εs) is assumed. However, in this work the soil is actually considered pure quartz, therefore here we assumed the quartz emissivity (εq) and NDVI<NDVIq.

(b) NDVI>NDVIv

NDVIv corresponds to the NDVI of the fully vegetated area; thus, the pixel is fully vegetated, and the emissivity εv is assumed to be 0.99.

(c) NDVIs≤NDVI≤NDVIv

In this case, the pixels comprise a mixture of both targets, and the emissivity ε is calculated according to a simplified equation (4). The three cases can be seen below.

$$LSE \begin{cases} \varepsilon_{q\lambda} & NDVI < NDVI_q \quad (3) \\ \varepsilon_{V\lambda} P_V + \varepsilon_q (1 - P_V) + d\varepsilon\lambda & NDVI_q < NDVI < NDVI_V \quad (4) \\ \varepsilon_{V\lambda} + d\varepsilon\lambda & NDVI > NDVI_V \quad (5) \end{cases}$$

where *Pv* is the vegetation proportion obtained according to [30]:

$$P_V = \left(\frac{NDVI - NDVI_q}{NDVI_V - NDVI_q}\right)^2 \quad (6)$$

where $NDVI_v$=0.5 and $NDVI_q$=0.2. These values were proposed by [38] to apply the method under global conditions, but the values can be also extracted from the NDVI histogram [14-15]. In this study, the original values were well adapted to the study area. The term $d\varepsilon$ includes the effect of the geometrical distribution of the natural surfaces and the internal reflections ($d\varepsilon$=0 for flat surfaces). For heterogeneous and rough surfaces, it can reach a value of 2 % [17].

$$d\varepsilon = (1 - \varepsilon_S)(1 - P_V) F \varepsilon_V \quad (7)$$

where *F* is a shape factor [40] whose mean value, assuming different geometrical distributions, is 0.55.

Soil emissivity is considered a critical question in $NDVI^{THM}$ because it varies greatly with composition. As we were sure that the area was composed by more than 99.53 % of quartz, the error produced by the composition was eliminated. We defined the quartz emissivity based on the laboratory data and assumed the emissivity of vegetation as 0.99 according to the literature [41]. A meticulous analysis of the vegetation emissivity characteristics is beyond the scope of this paper. Instead, we focused on quartz temperature and emissivity response.

In order to verify the differences yelded by the emissivity values choice for quartz in the $NDVI^{THM}$ we tested some possibilities of emissivity assignment. (ε_1) was selected from the second set of measurements performed at the laboratory. The values above 1.0 were excluded. (ε_2) was obtained from Johns Hopkings University (JHU) (http://speclib.jpl.nasa.gov). The spectrum used in this case was the one with the most similar characteristics of our sample (powder, particle size, etc). As JHU spectra are provided as reflectance, emissivity values must be calculating by Kirchhoff's law [13]. (ε_3) was the in-situ emissivity. The three emissivities (Table II) were used as input $NDVI^{THM}$ function that was calculated three times.

TABLE II EMISSIVITY OF QUARTZ AND VEGETATION FOR LANDSAT 8 BAND 10. THE SRF WAS APPLIED TO THE QUARTZ VALUES.

Emissivity	Quartz	Vegetation
ε_1	0.9987	0.99
ε_2	0.9733	0.99
ε_3	0.9798	0.99

LST retrieval

[5] have developed an *Improved Single-Channel* (ISC) algorithm for Landsat 8 thermal band based on the *generalized Single-Channel* (SC) algorithm proposed by [7]. The authors added the near-surface air temperature (*Ta*) to the method, as performed by [15] for the previous Landsat satellites, in order to minimize the errors produced by the algorithms for atmospheric water vapor content (*w*) higher than 3 $g \cdot cm^{-2}$. The novel method was able to produce lower errors than models based only on *w*, but its validation was performed only in vegetation and snow land covers, which are grey bodies [42]. Both algorithms were applied in this paper. The whole methodology will be described below.

Convertion to radiance and brightness temperature

To estimate the LST from the Landsat 8 TIR data, digital number (DN) of sensors were converted to spectral radiance using the following equation:

$$L_{sen} = ML\, Q_{cal} + AL \quad (8)$$

where L_{sen} is the top of atmosphere radiance (TOA) in [W/(m².sr. μm)], *ML* is the band-specific multiplicative factor, *AL* is the band-specific additive rescaling factor, and Q_{cal} are the pixel values (DN). Then, the TIR band data was converted to brightness temperature by using:

$$T_{sen} = \frac{K_2}{ln\left(\frac{K_1}{L_{sen}} + 1\right)} \quad (9)$$

where T_{sen} is the satellite brightness temperature (K), K_1 and K_2 are the band-specific conversion constant from the metadata (K_1= 774.8853 and K_2= 1321.0789 for the Landsat 8 band 10).

SC and ISC methods

As mentioned, the generalized single-channel (SC) algorithm [7] and the improved single-channel (ISC) [5] were chosen to perform the comparison among the emissivities considered (Table II). Both algorithms retrieve LST from the following equation:

$$T_s = \gamma\left[\frac{1}{\varepsilon}(\psi_1 L_{sen} + \psi_2) + \psi_3\right] + \delta \quad (10)$$

where T_s is the land surface temperature (LST) in K; ε is the LSE, γ and δ are variables based on the Planck's function given by:

$$\gamma = \left\{\frac{c_2 L_{sen}}{T_{sen}^2}\left[\frac{\lambda^4 L_{sen}}{c_1} + \frac{1}{\lambda}\right]\right\}^{-1} \quad (11)$$

$$\delta = -\gamma L_{sen} + T_{sen} \quad (12)$$

where c_1=1.19104. 10^8 W.μm^{-2}sr^{-1} and c_2=14387.7 μm; λ is the effective wavelength in μm. The Atmospheric Functions (AFs) ψ_1, ψ_2 and ψ_3 can be obtained as functions of the total atmospheric water vapor content (w) using the following equations for SC method:

$$\psi_1 = 0.04019w^2 + 0.02916w + 1.01523, \quad (13)$$

$$\psi_2 = -0.38333w^2 - 1.50294w + 0.20324, \quad (14)$$

$$\psi_3 = 0.00918w^2 + 1.36072w - 0.27514. \quad (15)$$

For ISC method, the AFs are obtained as functions of w and Ta using (16), (17) and (18), respectively:

$$\psi_1 = -7.2122w^2 + 0.00005T_a^2 - 2.452321w - 0.026275T_a - 0.00005T_a^2 w + 0.02317T_a w + 0.04663T_a w^2 - 0.00007T_a^2 w^2 + 4.47297, \quad (16)$$

$$\psi_2 = 89.61569w^2 - 0.00038T_a^2 + 106.55093w + 0.21578T_a + 0.00141T_a^2 w - 0.78444T_a w - 0.5732T_a w^2 + 0.00091T_a^2 w^2 - 30.37028, \quad (17)$$

$$\psi_3 = -14.65955w^2 - 0.0001T_a^2 - 79.95838w + 0.04181T_a - 0.00091T_a^2 w + 0.54535T_a w + 0.09114T_a w^2 - 0.00014T_a^2 w^2 - 3.76184. \quad (18)$$

where Ta is the mean atmospheric temperature in K calculated from the near surface air temperature (To) by the equation given for mid-latitude summer [10]:

$$Ta = 16.011 + 0.9262\,To \quad (19)$$

Water vapor content (w), required to retrieve LST from the methods, was calculated by using Leckner method proposed by [43]. The input data were taken from a nearby atmospheric observation station of the Brazilian National Institute of Meteorology (INMET-http://www.inmet.gov.br/portal/) located 6 km away from the study area (station coordinates: -30.010268º; -50.135887º and 5 m a.s.l.). As a result, w in the atmospheric column up to satellite altitude is estimated as follows:

$$w = \frac{0.493\phi_r P_s}{T_o} \quad (20)$$

where φr is the relative humidity in fraction; and Ps is the partial pressure of water vapor given as:

$$P_s = exp\left(26.23 - \frac{5416}{T_o}\right) \quad (21)$$

Finally, we ran the SC and ISC algorithms three times in the same image by changing the NDVI^{THM} function according to the emissivities shown in Table II.

RESULTS

Laboratory emissivity measurements and in-situ comparison

Emissivity curves from laboratory measured at different temperatures are shown (Fig. 4a and 4b). We selected five spectra from each set to represent the variations of the temperature measured in controlled environment (303-319 K).

Fig. 4a displays the first set of measurements, in which is demonstrated the relation between emissivity and temperature, obtained at the first half hour that the instrument was turned on. As the temperature decreases, the noise is bigger and there are significantly more oscillations in the emissivity curves.

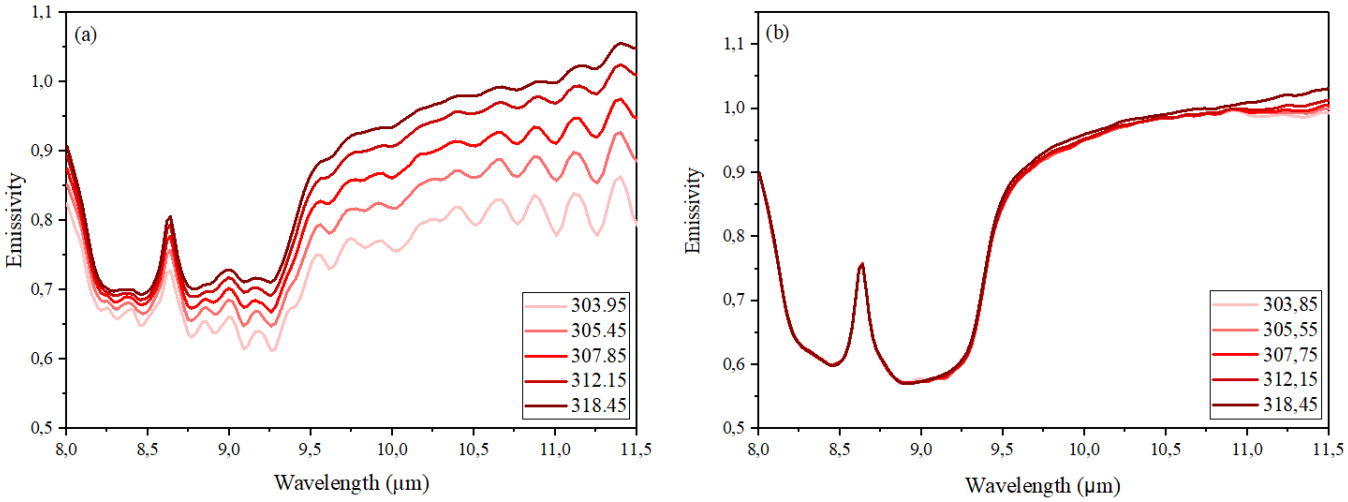

Fig. 4. Emissivity curves of quartz sand sample for five different temperatures (K). (a) refers to the set of measurements performed at the first half hour of the instrument turned on, (b) refers to measurements performed at the time after the second calibration.

The emissivity increases with the temperature and the difference among curves is greater in the longer wavelengths. Above 11 μm, the two largest temperatures (312.15 and 318.45) exceeded 1.0. However, these values are noise, since only a theoretical body has emissivity equal 1.0. Restrahlen feature that occurs at 8.5 μm for quartz and feldspar (framework silicates) [44] had an emissivity value higher than 0.7 for the highest temperatures of the set (318.45 K), and up to 0.6 for the lower temperature evaluated (303.95 K). These results showed that an error of 10 % is expected from FT-IR in the shorter wavelengths for a not accurate calibration.

Fig. 4b shows the second set of measurements, taken after the first half hour and the second calibration of the instrument. The emissivity measurements are clearly more accurate and do not vary so much with the temperature. Although the variation is minimal in the most part of the electromagnetic spectrum, the highest temperature has slightly the highest emissivity. Furthermore, noticeable variations among curves in longer wavelengths (above 9.5 μm) are observed, which become even more evident above 11 μm. Another difference is that the restrahlen feature presents a lower emissivity value (<0.6) and for all temperatures here considered there are very similar emissivity values at this wavelength.

When compared the two database sets, it is noted that the lack of calibration and instability of the instrument may induce greater differences in the emissivity measurements, related to the temperature of the material. If the first set is used to assign an emissivity value in the $NDVI^{THM}$ an error up to 18.5 % is observed, as reported in [45]. By using the second set of measurements from the database, evidently more accurate, we isolated the emissivity response *versus* temperature at the wavelength of Landsat 8 band 10 (10.6-11.19μm) (Fig. 5).

A tendency of emissivity to increase with temperature is seen. Moreover, the saturation is noticed approximately at 314 K (40.85 ºC), when the emissivity achieves 1.0, so that we can infer that an emissivity value very close to 1.0 might be assumed for temperatures higher than 314 K. The minimum emissivity value found is 0.978 corresponding to the temperature of 302.45 K (29.3 ºC). However, higher emissivity values are observed at temperatures lower than 302.45 as well. Hence, the results here showed are described as a tendency and not as absolute values. The highest difference of emissivity relative to the temperature seen is below 2.2 % for Landsat 8 band 10. This difference, according to [13, 19-20, 49] would be able to produce an error of approximately 1.5 K in the LST retrieved.

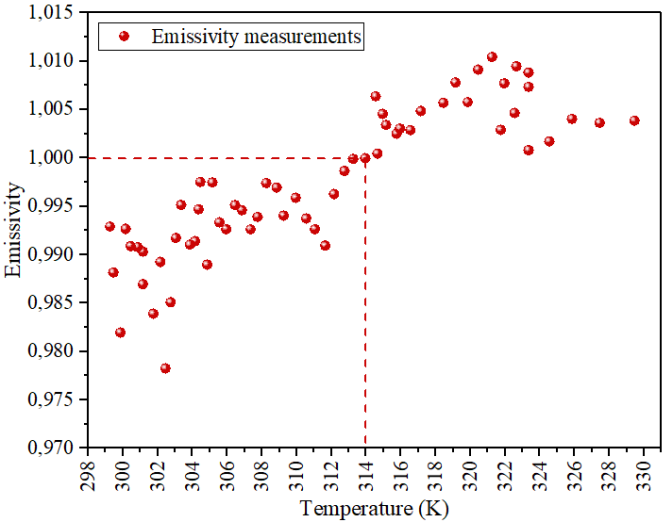

Fig. 5. Quartz emissivity versus temperature at the band 10 Landsat 8 (10.6-11.19 μm) measured at laboratory. The SRF was applied to the data.

Field work revealed that the major portion of the dune were bare, with a few pockets of undergrowth so that we could chose a spot especially bare to measure the quartz sand. Relative humid, near surface air temperature (*To*), and wind speed were about 67 %, 299.25 K (26.1 ºC) and 2 m/s, respectively, at the time of the satellite overpass. We chose a curve from the laboratory database (second and best set) to compare with another curve at the same temperature (313 K) acquired in the field (Fig. 6).

In the wavelength that comprises the restrahlen feature more noise is observed in the in-situ measurements. Moreover, it can be noted a reduction of the emissivity at some points of the feature. After 9.5 μm, the reduction is more evident relative to the laboratory curve. Considering that both curves are at the same temperature, when analysing the wavelength range of 9.5-11.5 μm, the general variations are lower than 2 %. However, an emissivity difference up to 3.2 % is verified in the wavelength of 10.05-10.08 μm.

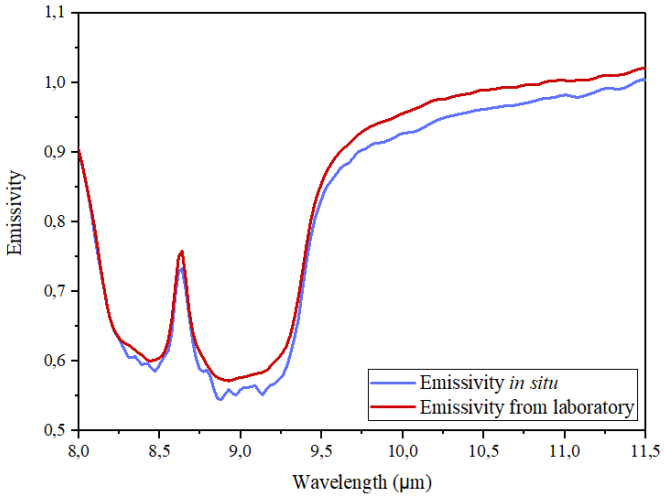

Fig. 6. Comparison between emissivities in-situ and from laboratory. Both curves chosen to perform the comparison were measured at 313 K of temperature.

LST retrieval and in-situ measurements

In the Table III, the results for the LSTs calculated are displayed. The LST in-situ used in the comparison was composed by an average of all the field measurements centered in the range of 7 minutes before and after the Landsat 8 overpass. The two methods here tested had a good agreement with the in-situ measurements. However, the ISC algorithm yelded a superior performance for LST estimation.

These results were expected because the method has been improved by adding *Ta* as input variable [5], even though ISC had not been applied to sandy surfaces until this study. Nevertheless, it is important also to take into account the spatial variability of climatic data, particularly air temperature (*To*) that is needed to find *Ta*. Meteorological variables may be directly measured, but often the station density is poor [46] so that in global scale ISC algorithm cannot be the best option.

Although ISC showed superior results, it subestimated in 0.6 K the LST relative to the in-situ measurements. On the other hand, SC method overestimated the LST with a higher difference, when compared to the field measurement it had a difference of -2.71. The biggest difference could be seen when the emissivity value of the JHU spectral library and the SC algorithm were applied jointly. In this sense, it is important to mention that the decrease of the accuracy in the SC algorithm can be attributed to the slightly high value of *w* (3.75 $g.cm^{-2}$), mainly because the method is only dependent of this parameter in addition to the LSE [5,7].

The LST retrieval using the laboratory emissivity measurement showed a difference of 1.56 and -1.79 K for ISC and SC, respectively, in relation to the LST in-situ, which is also a good performance. Therefore, it is feasible to use laboratory measurements as an alternative to field validation as long as the measures have been performed accurately. JHU-based emissivity value can be also used for similar atmospheric conditions to those presented in this work. Nevertheless, when SC algorithm is applied in a condition of humid larger than here, it is preferable to measure samples of the specific study area at the laboratory or perform field validation.

TABLE III PARAMETERS USED IN THE LST DETERMINATION BY SINGLE-CHANNEL ALGORITHMS AND RESULTS OF THE LSTS RETRIEVED.

ε	$LST_{in\ situ}$ (K)	LST_{SC} (K)	Δ (K)	LST_{ISC} (K)	Δ (K)
0.9987	314.19	315.98	-1.79	312.63	1.56
0.9733	314.19	317.23	-3.04	313.92	0.27
0.9798	314.19	316.90	-2.71	313.59	0.60

We carried out approximately 40 measurements in the field campaign concurrently with the Landsat 8 overpass. Nonetheless, we reduced the time interval within 7 min before and after the satellite overpass time so that we did not introduce too much temporal variability [35].

The Fig. 7 shows the LST changes at the time of the Landsat 8 overpass. The maximum difference observed in the LST of the sand dune during the time considered was lower than 4 K. There is a tendency for LST to increase over time, therefore larger time ranges are likely to lead to larger differences. The LST measurements in-situ performed during the whole time had an average of 314.19 K and standard deviation of 0.92 K. It demonstrates that the interval here considered can be assumed in other studies. However, the smaller the range assumed, more accurate tends to be the measurement.

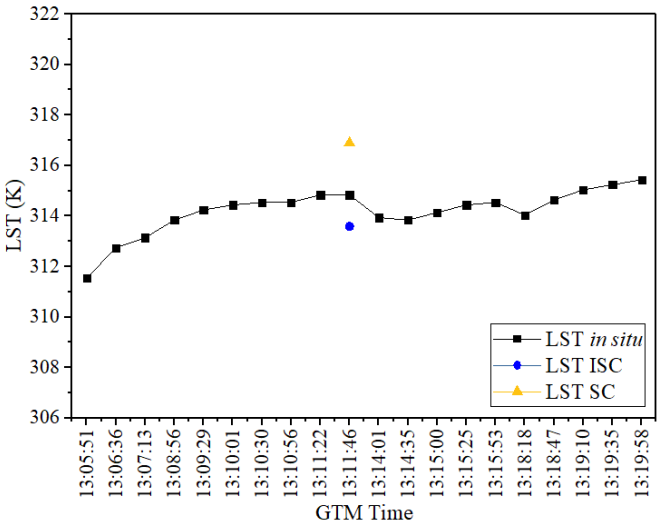

Fig. 7. LST in-situ and retrieved by TIRS sensor for the study area at the time of the Landsat 8 overpass.

DISCUSSION

As indicated above, this paper proposed investigate the use of laboratory and field measurements when retrieving LST from remote sensing data. According to the results, in order to keep a good performance of the methods presented and make the retrieval more operational, some attentions should be paid.

The first set of measurements performed at the first half hour is not accurate and can induce systematic errors, which are more significant when the sample is at lower temperature. Perhaps this result is associated with the sample spectral contrast that is dependent on the environment where the measurements were taken. A lower environment temperature will result in a low thermal contrast between the environment and the sample, especially if the sample is at a low temperature as well. It is mandatory to turn on the instrument

for at least 30 minutes before starting to take measurements to achieve thermal and mechanical equilibrium. Otherwise, the measurements will not be accurate enough.

When isolating the emissivity response *versus* temperature at the wavelength of Landsat 8 band 10, the emissivity values above 1.0 produced apparent noise effects, since a body with emissivity above 1.0 is only theorical. The temperature of the instrument is related to these results because the calibration is carried out considering the range from 10 to 40 ºC. It is worth mentioning that at very high temperatures the instrument has a tendency for reducing its accuracy, which is a limitation of the FT-IR spectrometer Model 102F, even though a bigger temperature interval is considered during the calibration process.

Field work indicated the presence of noise in the emissivity curve, especially in restrahlen feature (Fig. 6). According to [34], The calibration for field measurements deteriorates faster because the variable heat load from changing solar insolation typically causes instrument temperature drift. Therefore, for maximum accuracy, calibration measurements in the field must be repeated with each sample measurement. According to [19], the emissivity over a desert region is always overestimated compared to laboratory results. The opposite was observed in this study, where the field measurement subestimated the emissivity in 3.2 % relative to the laboratory curve.

Meteorological conditions have a great influence on the FT-IR spectrometer measurements. Solar energy influences the material temperature and therefore its self-emitted energy. Wind speed is also an important factor, as it can cool the surface layer of the material very quickly. Since the surface layer is the one that plays the major role in the TIR emission, if the wind causes quick and long changes in the field of radiance, it will affect the determination of the emissivity, mainly because the LST will change while reading the spectrum [34].

The comparison between the two methods for retrieving LST showed that both had a good agreement with the in-situ and laboratory data, although ISC was more efficient for the study area. It is known that the algorithms, particularly the ones that use only one channel in thermal infrared region, work best when the *w* is low. In very humid conditions they perform badly [47-49].

According to [13] 1 % uncertainly in LSE may cause an error of 0.5 K in LST retrieval for a moderate atmospheric condition with LST of 300 K and *w* of 2 $g.cm^{-2}$. [49] found that in a standard atmosphere with 302.55 K of LST and *w* of 1.6 $g.cm^{-2}$ an error on emissivity of 1 % may lead an error on the LST retrieval of 0.6 K. The same result was reported by [37] in temperature over a dry atmosphere condition when a single-channel algorithm was applied. Here, the study area is located close to the sea and has a characteristic of humid atmosphere so that SC method was less suitable when compared to the ISC, improved for humid atmospheres. Perhaps in a condition of less humid atmosphere the SC method would have a similar performance, as already proved in other studies [5,7,21-22,50].

The results indicate that under the study area conditions it is possible to retrieve LST by remote sensing data with an accuracy between 0.27-1.56 K, without needing emissivity measurements in the field, or only using emissivity values of available spectral libraries. However, it must be considered that an almost pure target was being analysed in this paper. The target temperature can be neglected without loss of accuracy, but the relation between emissivity and temperature should be investigated considering other land cover types, especially the ones that involve mixture of targets. Although the target emissivity variations with its temperature are small for quartz, the variation process considering other land covers can be detectable by satellite remote sensing.

CONCLUSIONS

The work presented contributes to a more operational LST retrieval of Landsat 8 imagery in sand lands. When using an FT-IR spectrometer in the laboratory, it is essential to pay attention to some factors, such as the time required for the instrument to acquire stability and the calibration process that should be carried out at least twice during a set of measurements of +/- half an hour, in order not to introduce errors in the measurements.

The variability of the targets emissivities relative to its temperature is poorly discussed in satellite-based temperature investigations that use spectral libraries, mainly because for most surface materials, the emissivity dependence on the temperature can be neglected [13]. We could note that a difference of approximately 2 % in the emissivity in comparison to the temperature is observed for almost pure quartz (99.53 %). These minimal variations do not really affect the accuracy of emissivity measurements when single-channel methods are used, because these methods normally have accuracy varying between 1-2 K.

Single-channel methods have proved to be a very good option, especially the ones developed in recent years. ISC provided superior results compared to SC, however, *Ta* is required, and the variable depends on meteorological station data, sometimes poorly represented. In this sense, for global scale the algorithm SC might be preferable, but for humid atmospheres (>3 $g.cm^{-2}$) must be carefully used.

Considering the limitations of the FT-IR, laboratory measurements can be successfully replaced for field validation in the estimation of LSE, avoiding the need of field campaign concurrently with the satellite overpass. The factors mentioned should be considered to build databases as accurate as the second set (Fig 4b.) measured after the instrument acquires stability. The relation between emissivity and temperature must be investigated for other targets. This approach can provide more reliable data, especially when there is no field experimental data and available spectral libraries are not representative. New tests are being performed to expand the use of reliable laboratory measurements in the LSE and LST retrieval for other land covers.

ACKNOWLEDGMENT

The Landsat 8 OLI/TIRS product is a courtesy of the US Geological Survey Earth Resources Observation and Science Center. This study was financed in part by the Coordenação de Aperfeiçoamento de Pessoal de Nível Superior - Brazil (CAPES), finance code 001.

REFERENCES

[1] Z. Zhang and G. He, “Generation of Landsat surface temperature product for China, 2000–2010,” *Int. J. Remote Sens.*, vol. 34, pp. 7369–7375, 2013.

[2] X. Yu, X. Guo, and Z. Wu, “Land Surface Temperature Retrieval from Landsat 8TIRS—Comparison between Radiative Transfer Equation-Based Method, Split Window Algorithm and Single Channel Method,” *Remote Sens*. vol. 6, pp. 9829-9852, 2014.

[3] Z. L. Li *et al*. “Satellite-derived land surface temperature: Current status and perspectives,” Remote Sensing of Environment, vol. 131 pp. 14–37, 2013.

[4] S. Li, and G. M. Jiang, "Land Surface Temperature Retrieval From Landsat-8 Data With the Generalized Split-Window Algorithm." *IEEE Access*, vol. 6 pp. 18149-18162, 2018.

[5] J. Cristóbal, J. C. Jiménez-Muñoz, A. Prakash, C. Mattar, D. Skokovic´, J. A. Sobrino, "An Improved Single-Channel Method to Retrieve Land Surface Temperature from the Landsat-8 Thermal Band," *Remote Sens*. vol. 10, no. 431, 2018.

[6] J. Rosas, R. Houborg, and M. F. McCabe, “Sensitivity of Landsat 8 Surface Temperature Estimates to Atmospheric Profile Data: A Study Using MODTRAN in Dryland Irrigated Systems,” *Remote Sens*., vol. 9 no. 10, pp. 988, 2017.

[7] J. C. Jiménez-Muñoz, J. A. Sobrino, D. Skokovic, C. Mattar, J. Cristóbal, “Land surface temperature retrieval methods from Landsat-8 thermal infrared sensor data.” *IEEE Geosci. Remote Sens. Lett.*, vol. 11, pp. 1840–1843, 2014.

[8] M. Montanaro, J. Barsi, A. Lunsford, S. Rohrbach and B. Markham, “Performance of the Thermal Infrared Sensor on-board Landsat 8 over the first year on-orbit,” *Proceedings of SPIE, Earth Observing Systems XIX*, pp. 9218-17, 2014.

[9] A. Gerace and M. Montanaro, "Derivation and validation of the stray light correction algorithm for the thermal infrared sensor onboard Landsat 8." *Remote Sens. of Environ.* vol 191, no. 15, pp. 246-257, 2017.

[10] F. Wang, Z. Qin , C. Song, L. Tu, A. Karnieli and S. Zhao, "An Improved Mono-Window Algorithm for Land Surface Temperature Retrieval from Landsat 8 Thermal Infrared Sensor Data," *Remote Sens*., vol. 7, pp. 4268-4289, 2015.

[11] F. Chen, S. Yang, Z. Su, B. He, “A new single-channel method for estimating land surface temperature based on the image inherent information: The Hj-1B case,” *ISPRS Journal of Photogrammetry and Remote Sens.*, vol. 101, pp. 80-88, 2015.

[12] B. Tardy, V. Rivalland, M. Huc, O. Hagolle, S. , Marcq, G. Boulet, “A Software Tool for Atmospheric Correction and Surface Temperature Estimation of Landsat Infrared Thermal Data,” *Remote Sens*, vol. 8, pp. 696, 2016.

[13] F. Chen, S. Yang, Z. Su, K. Wang, “Effect of emissivity uncertainly on surface temperature retrieval over urban areas: Investigations based on spectral libraries,” *ISPRS Journal of Photogrammetry and Remote Sensing*, vol. 114, pp. 53–66, 2016.

[14] J. A. Sobrino, J. C. Jiménez-Muñoz, G. Sòria, M. Romaguera, L. Guanter, J. Moreno, “Land Surface Emissivity Retrieval From Different VNIR and TIR Sensors,” *IEEE Transactions on Geosc. and Remote Sens.*, vol. 46, no.2 , 2008.

[15] J. Cristóbal, J. C. , Jiménez-Muñoz, J. A., , Sobrino, M. Ninyerola, and X. Pons, “Improvements in land surface temperature retrieval from the Landsat series thermal band using water vapor and air temperature,” *J Geophys Res*, vol. 114, D08 103, 2009.

[16] G. C. Hulley, S. J. Hook, and A. M. Baldridge, "Investigating the effects of soil moisture on thermal infrared land surface temperature and emissivity using satellite retrievals and laboratory measurements," *Remote Sens. of Environ.*, vol. 114, no. 7, pp. 1480-1493, 2010.

[17] Z-L. Li, e*t al*. "Land surface emissivity retrieval from satellite data," *Int. J. of Remote Sens.*, vol. 34, no. 9-10, 2013.

[18] O. Rozenstein, *et al*., "Diurnal emissivity dynamics in bare versus biocrusted sand dunes," *Science of the Total Environ*., 506-507, pp. 422-429, 2015.

[19] C. G. Hulley and, S. J. Hook, “Intercomparison of versions 4, 4.1 and 5 of the MODIS Land Surface Temperature and Emissivity products and validation with laboratory measurements of sand samples from the Namib desert, Namibia,” *Remote Sens. of Environ.*, vol. 113, pp. 1313-1318, 2009.

[20] K. Tan, Z. Liao, P. Du, and L. Wu, “Land surface temperature retrieval from Landsat 8 data and validation with geosensor network,” *Front. Earth Sci*. vol. 11, no.1, pp. 20–34, 2017.

[21] V.A. Copertino, M. D. Pierro, G. Scavone and V. Telesca, “Comparison of algorithms to retrieve Land Surface Temperature from LANDSAT-7 ETM+ IR data in the Basilicata Ionian band,” *Tethys, J. of Mediterranean Meteorology & Climatology*, vol. 9, pp. 25–34, 2012.

[22] C. Mattar, A. Santamaría-Artigas, F. Ponzoni, C. T. Pinto, C. Barrientos and G. Hulley, "Atacama Field Campaign: laboratory and in-situ measurements for remote sensing applications," *Int. J. of Digital Earth*, 2018.

[23] C. Coll, *et al.* "Ground measurements for the validation of land surface temperatures derived from AATSR and MODIS data," *Remote Sens. of Environ.* vol. 97, no. 3, pp. 288-300, 2005.

[24] K. Yan, H. Ren, R. Hu, X. Mu, Z. Liu, G. Yan, “Error analysis for emissivity measurement using FTIR spectrometer,” *IEEE Int. Geosc. and Remote Sens. Symposium*, 2013.

[25] T. E. Berry and R. E. Melton, “Multi-spectral thermal image analysis of natural backgrounds and targets,” in Defense and Security. *Int. Society for Optics and Photonics*, 2005.

[26] H. Tang, and Z.-L. Li. “Quantitative Remote Sensing in Thermal Infrared: Theory and Applications,” *Heidelberg: Springer Science & Business Media*, 2014.

[27] J. A. Villwock, , L. J. Tomazelli, E. L. Loss, E. A. Dehnhardt, F. N. O. Horn, F. A. Bachi, and B. A. Dehnhardt, “Geology of the Rio Grande do Sul Coastal Province,” *In: Rabassa, J. (ed.). Quaternary of South America and Antartic Peninsula*. Rotterdam, A. A. Balkema. pp. 79-97, 1986.

[28] F. A. Travessas, S. R. Dillenburg, and L. C. P. Clerot, “Estratigrafia e evolução da barreira holocênica do Rio Grande do Sul no trecho Tramandaí-Cidreira.” *Bol. Paranaense de Geoc.*, vol. 53 pp. 57-73, 2005.

[29] J. R. Irons, J. L. Dwyer, and J. A. Barsi, “The next Landsat satellite: The Landsat Data Continuity Mission,” *Remote Sens. of Environ.*, vol. 122, pp. 11–21, 2012.

[30] T. N. Carlson, and Ripley, D. A. “On the relation between NDVI, fractional vegetation cover, and leaf area index,” *Remote Sens. of Environ*, vol. 62 no. 3, pp. 241–252, 1997.

[31] J. C. Jiménez-Muñoz, J. Cristóbal, J. A. Sobrino, G. Sòria, M. Ninyerola, X. Pons, “Revision of the Single-Channel Algorithm for Land Surface Temperature Retrieval From Landsat Thermal-Infrared Data,” *IEEE Trans Geosci Remote Sensing*, vol. 47, pp. 339–349, 2009.

[32] E. Rubio, V. Caselles, and C. Badenas, “Emissivity measurements of several soils and vegetation types in the 8–14 mm wave band: Analysis of two field methods,” *Remote Sens. of Environ*., vol. 59, pp. 490–521, 1997.

[33] A. Korb, J. W. Salisbury, and D. M. D'Ária, “Thermal-infrared remote sensing and Kirchhoff's law 2. Field measurements,” *J. of Geophysical Research*, vol. 104, B7, pp. 339-350, 1999.

[34] A. R. Korb, P. Dybwad, W. Wadsworth and J. W. Salisbury, "Portable Fourier transform infrared spectroradiometer for field measurements of radiance and emissivity," *Applied Optics*, vol. 35, no. 10, pp. 1679-1692, 1996.

[35] C. Coll, J. M. Galve, J. M. Sanchez and V. Caselles, "Validation of Landsat-7/ETM+ Thermal-Band Calibration and Atmospheric Correction With Ground-Based Measurements." *IEEE Transactions on Geosc. and Remote Sens*. vol. 48, no. 1, 2010.

[36] A. A. Van de Griend and M. Owe, "On the relationship between thermal emissivity and the normalized difference vegetation index for natural surfaces," *Int. J. of Remote Sens.*, vol. 14 no. 6, pp. 1119–1131, 1993.

[37] E. Valor, and V. Caselles, "Mapping land surface emissivity from NDVI: Application to European, African and South American areas," *Remote Sens. of Environ.*, vol. 57, pp. 167–184, 1996.

[38] J. A. Sobrino, and N. Raissouni, "Toward remote sensing methods for land cover dynamic monitoring," *Int. J. of Remote Sens.*, vol. 21, no. 2, pp. 353-366, 2000.

[39] J. W. Rouse, R. H. Haas, J. A. Schell and D. W. Deering, "Monitoring Vegetation Systems in the Great Plains with ERTS," *Paper Presented at the Third ERTS-1 Symposium*, Washington, DC, NASA SP-351, 1 (A): pp. 309–317, 1973.

[40] J. A. Sobrino, V. Caselles, and F. Becker, "Significance of the remotely sensed thermal infrared measurements obtained over a citrus orchard," *ISPRS-J Photogramm Remote Sens*, vol. 44, pp. 343–354, 1990.

[41] J. A. Sobrino, J. C. Jiménez-Muñoz and L. Paolini "Land surface temperature retrieval from LANDSAT TM5," *Remote Sens. of Environ.* vol. 90, pp. 434–440, 2004.

[42] G. C. Hulley, and S. J. Hook, "Generating Consistent Land Surface Temperature and Emissivity Products Between ASTER and MODIS Data for Earth Science Research," *IEEE Trans. Geosc. and Remote Sens*, vol. 49 no. 4, pp. 1304-1315, 2011.

[43] M. Iqbal, "An introduction to solar radiation," *Academic Press*, New York, 1983.

[44] S. J. Hook, T. J. Cudahy, A. B. Kahle, and L. B. Whitbourn, "Synergy of active and passive airborne thermal infrared systems for surface compositional mapping," *J. Geophys. Res.*, vol. 103, B8, pp. 18,269–18,276, 1998.

[45] P. S. Käfer, *et al*, "Land surface temperature retrieval from Landsat-8 data: a comparison using a quartz spectral library based on temperatures," *IEEE Int. Geosc. and Remote Sens. Symposium*, 2018.

[46] D. Courault, B. Seguin and A. Olioso, "Review on estimation of evapotranspirationfrom remote sensing data: From empiricalto numerical modeling approaches," *Irrigation and Drainage Systems*, vol. 19, pp. 223–249, 2005.

[47] A. J. Prata, "Land surface temperature determination from satellites," *Advances in Space Research*, vol. 14, no. 3, pp.15-26, 1994.

[48] J. A. Barsi, J. R. Schott, F. D. Palluconi, S. J. Hook, "Validation of a web-based atmospheric correction tool for single thermal band instruments," Proceedings vol 5882, *Earth Observing Systems X*, 58820E, 2005.

[49] J. C. Jiménez-Muñoz, and J. A. Sobrino, "A generalized single channel method for retrieving land surface temperature from remote sensing data," *J Geophys Res*, vol. 108, 2003.

[50] Zhang *et al*. "Towards an operational method for land surface temperature retrieval from Landsat 8 data," *Remote Sens. Lett*. vol. 7, no. 3, pp. 279–288, 2016.

P. S. Käfer (M.'18) received the B.S. degree in Forestry from the Federal University of Santa Maria (UFSM), Brazil, in 2017. Currently she is working toward the M.S. degree in Remote Sensing with the Federal University of Rio Grande do Sul (UFRGS), Brazil (2019). Her research interests include radiative transfer in the atmosphere, optical radiometry, time series and remote sensing analysis.

S. B. A. Rolim (M.'18) received the B.S degree in Geology from the UFRGS in 1988, the M.Sc. degree in Remote Sensing from National Institute of Space and Research (INPE) in 1992 and Ph.D degree in Geosciences from UNICAMP, in 2001. She has a postdoctoral at Stockholm University-Sweden, in 2004. Currently, she is a Full Professor at the Institute of Geosciences of the UFRGS. Her research interests include: radiative transfer in the atmosphere, optical radiometry and geological remote sensing.

M. L. Iglesias received the B.S. in Physics from the Universidad Nacional del Sur (UNS), Argentina, in 2010, and the M.S. degree in Remote Sensing from the UFRGS, in 2013. She is currently working toward the Ph.D degree in Physics at IF-UFRGS. She collaborates in the LabSRGeo-UFRGS. Her research interests include optical radiometry in thermal infrared, nanotribology, microscopic friction and molecular dynamics simulation.

N. S. Rocha received the B.S degree in Forestry from the UFSM, in 2012 and the M.S. degree in Forestry from the same University, in 2016. She is currently working toward the Ph.D degree in Remote Sensing at Federal University of Rio Grande do Sul, Brazil. Her research interests include the remote sensing analysis and the biosphere-atmosphere-hydrosphere interactions.

L. R. Diaz is an Environmental Engineering undergraduate student at the UFRGS. Since December 2014, he has been working in a scholarship at the Geological Remote Sensing Laboratory of the State Center for Remote Sensing and Meteorology Research, UFRGS, Brazil. His current research interests include atmospheric simulations for atmospheric correction in the thermal infrared region.

4.2 ARTIGO 2 - Towards single-channel methods for land surface temperature retrieval from Landsat 8 thermal band in Southern Brazil

Gmail

Pâmela Käfer <pamelaskafer@gmail.com>

Manuscript submission to the International Journal of Remote Sensing - Manuscript ID TRES-PAP-2019-0154

1 mensagem

International Journal of Remote Sensing <onbehalfof@manuscriptcentral.com> 14 de fevereiro de 2019 17:14
Responder a: IJRS-Administrator@dundee.ac.uk
Para: pamelaskafer@gmail.com
Cc: pamelaskafer@gmail.com, silvia.rolim@ufrgs.br, luiza.v.heinz@gmail.com, lujaniglesias@gmail.com, najila.rocha@ufrgs.br

14-Feb-2019

Dear Ms. Pâmela Suélen Käfer
(cc'd to co-authors, if any)

Your manuscript entitled "Towards single-channel methods for land surface temperature retrieval from Landsat 8 thermal band in Southern Brazil" has been successfully submitted online and is presently being given full consideration for publication in International Journal of Remote Sensing.

Your manuscript ID is TRES-PAP-2019-0154.

Please mention the above manuscript ID in all future correspondence. If there are any changes in your contact details, please log in to the International Journal of Remote Sensing - ScholarOne Manuscripts site at https://mc.manuscriptcentral.com/tres and edit your user account information as appropriate.

You can also view the status of your manuscript at any time by checking the appropriate folder in your "Corresponding Author Centre" after logging in to https://mc.manuscriptcentral.com/tres.

The journal to which you are have submitted to is participating in the PEER project. This project, which is supported by the European Union EC eContentplus programme(http://ec.europa.eu/information_society/activities/econtentplus/index_en.htm), aims to monitor the effects of systematic self-archiving (author deposit in repositories) over time. If your submission is accepted, and you are based in the EU, you may be invited to deposit your accepted manuscript in a repository as part of this project. The project will develop models to illustrate how traditional publishing systems may coexist with self-archiving For further information please visit the PEER project website at http://www.peerproject.eu.

Thank you for submitting your manuscript to the International Journal of Remote Sensing.

Yours sincerely

Mrs Catherine Murray
Administrator, International Journal of Remote Sensing
IJRS-Administrator@Dundee.ac.uk

Towards single-channel methods for land surface temperature retrieval from Landsat 8 thermal band in Southern Brazil

Land surface temperature (LST) is an essential parameter in investigating environmental, ecological processes and climate change at local to global scales, and Thermal Infrared (TIR) remote sensing is recognized as a useful tool to acquire information regarding the LST. Several accurate LST retrieval methodologies have been developed or refined in recent years and they have demonstrated a great potential. Given that most methods are developed focusing on North hemisphere, operational and accurate ways of obtaining LST must be constantly investigated. In this study, an assessment of various recent LST inversion single-channel algorithms is presented. These algorithms include improved mono-window (IMW), single-channel (SC) and improved single-channel (ISC). We compared the methods using a site composed most by a pseudo-invariant target (SiO_2). Moreover, we carried out two kinds of validation: field measurements of temperature and emissivity with the satellite overpass and a comparative analysis using the web-based Atmospheric Correction Parameter Calculator (ACPC) tool (https://atmcorr.gsfc.nasa.gov/) to solve the Radiative Transfer Equation (RTE). The three methods analysed showed strong correlation with the RTE (producing R^2 between 0.998-0.999). Therefore, they can be used to retrieve LST, specially for regions such as Southern Brazil, where radiosonde points have low density. ISC algorithm demonstrated superior performance, in which a difference of 0.6 K is found when a pure pixel is analysed, and RMSE of 0.019 for average values. In future study we will investigate a larger variety of land surface types and carry out field work considering distinct periods of the year.

Keywords: thermal infrared; LST retrieval methods; quartz;

1. Introduction

Land surface temperature (LST) is an essential parameter in investigating environmental, ecological processes and climate change at local to global scales. Additionally, it is valuable in the studies of evapotranspiration, soil moisture conditions, surface energy balance, and urban heat islands (Weng et al. 2014; Yu et al. 2014; Krishnan et al. 2015).

Thermal Infrared (TIR) remote sensing is recognized as a useful way to acquire quantitative and qualitative information regarding the LST (Zhang et al. 2016; Tardy et al.

2016). The Landsat serie of satellites has been one of the major contributing factors in the development of global-scale earth systems science research, since it represents the most complete data continuous sequence that extends back to 1982 (Rosas et al. 2017; Käfer et al. 2019; Malakar et al. 2018).

A number of LST retrieval methods from remotely sensed data have been proposed in the last three decades, and these methods can be roughly grouped into three categories according to some authors as Du et al. (2015): (i) the single-channel, (ii) multi-channel and (iii) multi-time methods. As Landsat thermal sensors had only one single thermal band (Landsat 4–7) (Jiménez Muñoz et al., 2014; Malakar et al. 2018), a considerable amount of algorithms developed to retrieve LST from Landsat data belongs to the (i) group.

Three single-channel methods are widely well-known i.e. Radiative Transfer Equation (RTE) method (Tang and Li, 2014), Qin's mono-window method (Qin et al. 2001), and Jiménez-Muñoz and Sobrino's single-channel method (Jiménez-Muñoz and Sobrino 2003). All of them are able to correct the atmospheric effects on the data measured by the sensor and require the land surface emissivity (LSE) in advance.

Qin's and Jiménez-Muñoz and Sobrino's methods are both based on the RTE and were developed to avoid radiosonde dependence. Jiménez-Muñoz and Sobrino's method showed superior performance when compared to Qin's method (Sobrino et al. 2004; Copertino et al. 2012).

RTE application requires an *in-situ* radiosonde launched simultaneously with the satellite overpass. Afterwards, a radiative transfer code has to be used to generate the parameters downelling radiance ($L\downarrow$), upwelling radiance ($L\uparrow$) and atmospheric transmitance (τ). However, in the real world is not common to have radiosonde data available for specific sites (Sobrino et al. 2004; Wang et al. 2015).

If radiosonde data is unavailable, another option for Landsat serie currently is to use the freely online tool Atmospheric Correction Parameter Calculator (ACPC) (available in: https://atmcorr.gsfc.nasa.gov/) (Barsi et al. 2005) that creates interpolated vertical profiles through the National Center for Environmental Prediction (NCEP) reanalysis data (Zhang et al. 2016).

The launch of Landsat 8 in February 2013 represented an important innovation because TIRS sensor measures TIR radiance using two bands (10 and 11) located in the atmospheric window between 10-12 μm (Jiménez Muñoz et al. 2014). Nevertheless, the sensor had been affected by stray light artefacts (Yu et al. 2014; Montanaro et al. 2014; Barsi et al. 2014; Wang et al. 2015; Cristóbal et al., 2018), particularly in the band 11, so that the researchers kept focus on improving single-channel techniques for band 10 (Jiménez-Muñoz et al. 2014; Wang et al. 2015; Zhang et al. 2016; Cristóbal et al. 2018). Only in the end of 2017 the issue was completely fixed (Gerace and Montanaro 2017). As a result, several accurate methodologies have been developed or refined in recent years and they have demonstrated a great potential in the LST retrieval.

As previously mentioned, Qin et al. (2001) developed the mono-window algorithm. The model retrieves LST by using two atmospheric parameters as input: water vapor (w) and near-surface air temperature (To). The estimation of transmitance (τ) and effective mean atmospheric temperature (Ta) were proposed from local meteorological observations when the in situ atmospheric profile data were unavailable. The main limitation of this model is the range of w for which it was designed, (0-3 $g \cdot cm^{-2}$) (Cristóbal et al. 2009). Thereafter, Wang et al. (2015) expanded the methodology for Landsat 8 data. The improvement purposed was mainly in the determination of the three essential parameters required in the model. The simulations and sensitivity analysis indicated that under moderate errors in w estimation, the model may have an accuracy of 1.4 K for LST retrieval.

The single-channel technique developed by Jiménez-Muñoz et al. (2003) depends only on the *w*. The model was expanded to Landsat 8 data by Jiménez-Muñoz et al. (2014) and tested with simulated data from a robust database (Mattar et al. 2014). However, an error in *w* may produce great errors in the LST retrieved, especially at high *w* values. Similarly, Cristóbal et al. (2009) purposed an improvement by adding *Ta* parameter to the model, as performed by Qin et al. (2001), which worked very well for Landsat 4–7 data. Later, Cristóbal et al. (2018) updated the methodology for Landsat 8 thermal band and yelded lower overall errors and demonstrating good accuracy even when *w* is high. Nonetheless, the validation was carried out only in vegetation and snow land covers.

LST retrieval by remotely sensed data requires validation with field measurements, but in most places, there are not available LST field data (Copertino et al. 2012; Mattar et al. 2018), which makes the validation a challenge. To perform LST field measurements in Southern Brazil specifically, the researchers need to organize field campaigns, in days previously programmed (with clear atmospheric conditions) to obtain this kind of data. Furthermore, ordinary meteorological stations provide only the variables *To*, radiation, relative humidity, precipitation and wind speed. Hence, the methodologies to retrieve LST from satellite data should be dependent only on these parameters, in order to be as operational as possible for these regions.

Considering that most methodologies are developed and tested focusing on North hemisphere, operational and accurate ways of obtaining LST must be constantly investigated. In this study, an assessment of various recent LST inversion single-channel algorithms is presented. These algorithms include improved mono-window (IMW), single-channel (SC) and improved single-channel (ISC). We proposed to compare the methods by performing the analysis in a site composed most by a pseudo-invariant target (SiO_2), with a known composition, and small portion of vegetation. Additionally, we carried out a field campaign to measure temperature and emissivity with the satellite overpass. It is important to emphasize

that a validation more comprehensive over a larger variety of land cover types will be performed in a future study.

2. Material and Methods

2.1 Study area

The study site is a dune field located in the North Coast of Rio Grande do Sul state, Brazil (Figure. 1). The area has a large stock of fine quartz sand (125 to 250 μm), composed by quartz (99.53%) and heavy minerals (0.47%), with grains varying among sub-rounded (68%), rounded (18%), subangular (14%). The sand dune is a controlled test area, where is possible to carried out field campaigns, mostly because it is considered a pseudo-invariant target, and therefore suitable for the terrestrial validation of LST retrieval by remote sensing data (Hulley and Hook, 2009). In addition, Tramandaí Meteorological Station is located about 5 km away from the area (station coordinates: 30.010268ºS; 50.135887ºW and 5 m a.s.l.). The site has in general an average annual temperature of 20°C. The annual precipitation is 1323 mm, the annual evaporation is 1135 mm and the average humidity is 80% (Travessas et al. 2005).

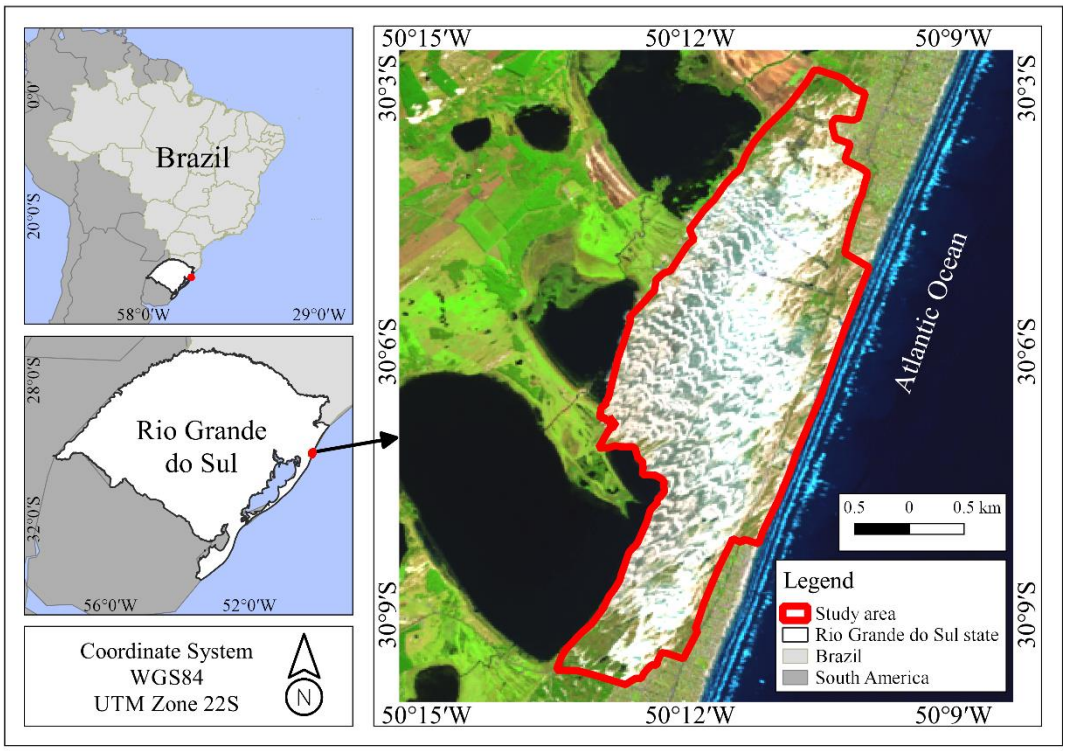

Figure 1. Location of the study site in Southern Brazil.

2.2 Data acquisition

2.2.1 Satellite data

Landsat 8 has two sensors, the Operational Land Imager (OLI) that collects data at a 30 m spatial resolution with eight bands located in the visible, near-infrared and in the short-wave infrared regions of the electromagnetic spectrum, and the thermal infrared sensor (TIRS), which measures the TIR radiance at 100 m spatial resolution using two bands located in the atmospheric window between 10-12 μm (Irons et al. 2012). To match OLI multispectral data, TIRS data at 100 m were resampled to 30 m (Duan et al. 2018).

TIRS band 10 image was downloaded over the study site from the US Geological Survey website in Level 1 product. Landsat Level 1 data are radiometric, geometric and terrain corrected (USGS, 2018). To obtain the normalized difference vegetation index (NDVI), used for the LSE derivation, Landsat 8 OLI surface reflectance product was also downloaded from the Landsat Data collection (USGS, 2018). The image chosen to perform analysis pixel by pixel in comparison to the field data was acquired in March 14, 2018 (Path: 220, Row: 081). Besides, we acquired four more cloud free scenes from the summer with very clear atmospheric conditions: December 27, 2018; February 26, 2018; March 11, 2017 and March 08, 2016 to perform quantitative analysis. Only summer images were used in order not to introduce much seasonal variation to the data due to changes in the atmospheric conditions (Rosas et al. 2017).

2.2.2 Field data

The field campaign was carried out concurrently with Landsat 8 overpass. As this kind of validation method is restricted to a limited number of pixels (Tang and Li 2014), we selected a very homogeneous and bare site within the dune area to settle the instrument. We did not have

much influence of humidity in the sand because it had not rained in the previous days. The in-situ emissivity and temperature spectra were obtained from radiance measurements by using a Fourier-transform infrared spectroscopy (FT-IR) Model 102F (Korb et al. 1999). The downwelling radiance parameter ($L^{\downarrow}\lambda$) was obtained by measuring a gold reference panel with an emissivity of 0.04. The sample spectral emissivity (ε) was calculated from the equation:

$$\varepsilon_{\lambda} = \frac{L\lambda - B\lambda(Ts)}{B\lambda(Ts) - L^{\downarrow}\lambda} \quad (1)$$

where Lλ is the spectral radiance and Bλ(Ts) refers to Planck's equation, given as:

$$B\lambda(Ts) = \frac{C1\lambda^{-5}}{exp(C2/\lambda T) - 1} \quad (2)$$

where C1 and C2 are constants (C1 = 1.191 × 10^8 W μm^4 sr^{-1} m^{-2}, C2 =1.439×10^4 μm K). Assuming that ε =1 between 7.5 and 8 μm, the sample temperature was obtained. The wavelength range was chosen because the emissivity and temperature retrieval are most accurate at the maximum emissivity value (Korb et al. 1999). The L↓ measurement is carried out before and after the sample measurement. If the amount of downwelling radiation changes between measurements, the properties determined for the material will have an associated error. Therefore, the accuracy in the L↓ measurement determines the accuracy in obtaining the emissivity and temperature spectra.

The calibration process was performed by choosing two temperatures: a temperature for the cold blackbody (below the ambient temperature), and another for the warm blackbody, (above the sample temperature). This leads to a more accurate calibration, since the instrument response between two known radiances and for each longitude is linear (Korb et al. 1996). Thus, the calibration interval assumed was 10-40 ºC (283.15 - 313.15 K).

The FT-IR was placed looking at the target at angles close to nadir. The standard input optic is 1 inch in diameter with a 4.8 degree expanding field of view. The measurements were

taken at a rate of 1-2 measurement per minute, in which around 40 measurements were done in the field. Nonetheless, we reduced the time interval within 7 minutes before and after the satellite overpass time so that we did not introduce too much temporal variability (Coll et al., 2010). The calibration of the instrument was carried out twice in the whole process. Afterwards, we weighted the data by the sensor spectral response function (SRF), since it may be a potential source of uncertainties in the LSE calculation if it is not considered (Cristóbal et al. 2009; Chen et al. 2016). The equation for the SRF is defined as:

$$\varepsilon_{(\lambda)} = \frac{\int_{\lambda S}^{\lambda E} R(\lambda)\varepsilon(\lambda)d\lambda}{\int_{\lambda S}^{\lambda E} R(\lambda)d\lambda} \quad (3)$$

where R(λ) is the SRF of the channel, given in a discrete form with a finite range, while λ_S and λ_E are the start and the end wavelengths of the channel. $\varepsilon(\lambda)$ is the emissivity spectra of the channel.

2.3 Physical basis of LST retrieval

As the land surface is not a perfect blackbody for thermal emittance, the retrieval of land surface temperature from the observed thermal radiance in space is more complex. The atmosphere and ground effects have to be considered (Li et al. 2013; Wang et al. 2015). Therefore, to retrieve LST, the radiative transfer equation (RTE) is applied to a certain sensor channel and wavelength interval according to

$$L_{sensor,\lambda} = \left[\varepsilon_\lambda B_\lambda(T_s) + (1-\varepsilon_\lambda)L_\lambda^{\downarrow}\right]\tau_\lambda + L_\lambda^{\uparrow} \quad (4)$$

where *Lsensor* is the at-sensor radiance in Wm^{-2} μm^{-1} sr^{-1}, ε is the land surface emissivity (LSE), Bλ(Ts) is the Planck's law given by Eq. (2), $L\downarrow$ is the downwelling atmospheric radiance

in Wm^{-2} μm^{-1} sr^{-1}, $L\uparrow$ is the upwelling atmospheric radiance in Wm^{-2} μm^{-1} sr^{-1}, and τ is the atmospheric transmissivity.

2.4 Land surface temperature (LST) calculation

To begin with, radiometric calibration is applied to convert the Digital Number (DN) recorded by the remote sensor into the at-atmosphere radiance (Qin et al. 2011). Afterwards, the brightness temperature is calculated as follows:

$$T_{sen} = \frac{K_2}{ln\left(\frac{K_1}{L_{sen}}+1\right)} \tag{5}$$

where T_{sen} is the satellite brightness temperature in K, K_1 and K_2 are the band-specific conversion constant from the metadata for the Landsat 8 band 10 (K_1= 774.8853 and K_2= 1321.0789).

2.4.1 Single-Channel Method (SC)

Although Landsat 8 TIRS has two spectrally adjacent channels, band 10 is preferable to be used as input instead band 11 because it is in a lower atmospheric absorption region (high atmospheric transmissivity values) (Jiménez-Muñoz et al. 2014), providing superior results (Yu et al. 2014). The general equation for the SC and ISC method is:

$$T_s = \gamma\left[\frac{1}{\varepsilon}(\psi_1 L_{sen} + \psi_2) + \psi_3\right] + \delta \tag{6}$$

where T_s is the land surface temperature (LST) in K; ε is the land surface emissivity (LSE), γ and δ are variables based on the Planck's function expressed as:

$$\gamma \approx \frac{T^2_{sen}}{b_y L_{sen}},\ \delta \approx T_{sen} - \frac{T^2_{sen}}{b_y} \tag{7}$$

where bγ is equal to 1324 for band 10 and the three Atmospheric Functions (AFs) ψ_1, ψ_2 and ψ_3 are obtained as functions of the total atmospheric water vapor content (w) using the following equations for SC method:

$$\psi_1 = 0.04019w^2 + 0.02916w + 1.01523, \quad (8)$$

$$\psi_2 = -0.38333w^2 - 1.50294w + 0.20324, \quad (9)$$

$$\psi_3 = 0.00918w^2 + 1.36072w - 0.27514. \quad (10)$$

2.4.2 Improved Single-Channel Method (ISC)

On the other hand, the three AFs for ISC method (Cristóbal et al. 2018) can be obtained as functions of w and the near-surface air temperature Ta given by:

$$\psi_1 = -7.2122w^2 + 0.00005T_a^2 - 2.452321w - 0.026275T_a - 0.00005T_a^2w + 0.02317T_aw + 0.04663T_aw^2 - 0.00007T_a^2w^2 + 4.47297, \quad (11)$$

$$\psi_2 = 89.61569w^2 - 0.00038T_a^2 + 106.55093w + 0.21578T_a + 0.00141T_a^2w - 0.78444T_aw - 0.5732T_aw^2 + 0.00091T_a^2w^2 - 30.37028, \quad (12)$$

$$\psi_3 = -14.65955w^2 - 0.0001T_a^2 - 79.95838w + 0.04181T_a - 0.00091T_a^2w + 0.54535T_aw + 0.09114T_aw^2 - 0.00014T_a^2w^2 - 3.76184. \quad (13)$$

2.4.3 Improved Mono-window (IMW)

Three essential parameters are required for LST retrieval by using the IMW algorithm (Ta, LSE and τ). As some of them are not easy to obtain (especially Ta and τ), the methodology also presents ways to determine these parameters to make it more operational. According to Wang

et al. (2015) the LST can be retrieved from Landsat TIRS band 10 using the following general equation:

$$Ts = [a10(1 - C10 - D10) + (b10(1 - C10 - D10) + C10 + D10)T10 - D10Ta]/C10 \quad (14)$$

where *Ts* is the LST retrieved; *T10* is the brightness temperature of Landsat 8 TIRS band 10 (Eq. 5); *a10* and *b10* are the constants used to approximate the derivative of the Planck radiance function for TIRS band 10 given according to a certain range of temperature, assumed as *a10*=−70.1775 and *b10*=0.4581 (Wang et al. 2015). C10 and D10 are the internal parameters for the algorithm, given as follows:

$$C10 = \tau 10 \varepsilon 10 \quad (15)$$

$$D10 = (1 - \tau 10)[1 + (1 - \varepsilon 10)\tau 10] \quad (16)$$

where τ10 is atmospheric transmittance of TIRS band 10 and ε10 is the LSE for the band. Qin et al. (2001) demonstrated that the standard atmospheric profiles for typical climatologic zones can be used to combine with local meteorological data for *Ta* estimation. Thus, the authors proposed linear relations for approximation of *Ta* from the near surface air temperature (*T0*), which were classify into three atmosphere kinds: Tropical model, Mid-latitude summer and Mid-latitude winter. In this study, the field work was carried out at summer, therefore, we assumed the equation for Mid-latitude summer:

$$Ta = 16.0110 + 0.9262\, T0 \quad (17)$$

The atmospheric water vapor (*w*) has the maximal importance in governing the change of atmospheric transmittance (τ) in the thermal range of the spectrum. Hence, the parameter τ required to retrieve LST is usually estimated through *w* (Qin et al. 2001). In order to obtain τ, Wang et al. (2015) established a function between τ and *w*. Therefore, according to the following equation, $\tau 10$ can be estimated from the known *w*:

$$\tau 10 = 1.0163 - 0.1330\, w \quad (18)$$

2.4.3 Water vapor calculation (w)

As an accurate estimation of *w* determines the accuracy of the LST retrieval, we calculated *w* by using Leckner method proposed by Iqbal (1983). The input data were taken from the nearby atmospheric observation station (Tramandaí Meteorological Station) of the Brazilian National Institute of Meteorology (INMET-http://www.inmet.gov.br/portal/) located 5 km away from the study area (station coordinates: -30.010268º; -50.135887º and 5 m a.s.l.). Therefore, *w* in the atmospheric column up to satellite altitude is estimated as:

$$w = \frac{0.493 \phi_r P_s}{T_o} \quad (19)$$

where *φr* is the relative humidity in fraction; and *Ps* is the partial pressure of water vapor given as:

$$P_s = exp\left(26.23 - \frac{5416}{T_o}\right) \quad (20)$$

2.5 Land surface emissivity (LSE) calculation

Single-channel methods prevent it from utilizing the well-known temperature/emissivity separation method (Gillespie et al. 1998) to retrieve LSE. In this context, an operational way to estimate LSE that is widely applied by scientific community, is the NDVI threshold method ($NDVI^{THM}$) (Sobrino et al. 2008; Zhang et al. 2016). This method is based on the principle that there is a relationship between the NDVI and the emissivities of terrestrial materials (Van de Griend and Owe, 1993). The first step to calculate LSE is to compute NDVI from the atmosphere red reflectance (RED) and near infra-red (NIR) reflectance from the Landsat 8 OLI data:

$$NDVI = \frac{NIR-RED}{NIR+RED} \quad (21)$$

The *Pv* is the vegetation proportion, which means the percentage of the vertical projection of vegetation canopy per unit area (Qin et al. 2011). It can be calculated according to the following equation given by Carlson and Ripley (1997):

$$P_V = \left(\frac{NDVI-NDVI_s}{NDVI_s-NDVI_s}\right)^2 \quad (22)$$

where NDVIv=0.5 and NDVIs=0.2. These values were proposed by Sobrino and Raissouni (2000) to apply the method under global conditions. $NDVI^{THM}$ obtains the emissivity values from the NDVI considering three different cases:

(a) NDVI<NDVIs

NDVIs corresponds to the NDVI of bare soil (Pv=0), thus the soil emissivity (εs) is assumed, typically 0.973. As the soil of the study site is composed most by quartz (SiO_2), we used the emissivity value of 0.978 taken at the field with the μFT-IR spectrometer.

(b) NDVI>NDVIv

NDVIv corresponds to the NDVI of the fully vegetated area, (Pv=1) and the emissivity εv has a constant value assumed to be 0.99. It was proposed by Sobrino and Rassouni (2000) and is widely adopted (Sobrino et al. 2004; Bonafoni et al. 2016).

(c) NDVIs≤NDVI≤NDVIv

In this case, the pixels comprise a mixture of both targets, and the emissivity ε is calculated according to the simplified equation:

$$\varepsilon = \varepsilon_{V\lambda}P_V + \varepsilon_s(1-P_V) + d\varepsilon\lambda \quad (23)$$

The term $d\varepsilon$ includes the effect of the geometrical distribution of the natural surfaces and the internal reflections ($d\varepsilon$=0 for flat surfaces). For heterogeneous and rough surfaces, it can reach a value of 2% (Li et al. 2013).

$$d\varepsilon = (1-\varepsilon_S)(1-P_V)F\varepsilon_V \quad (24)$$

where F is a shape factor whose mean value, assuming different geometrical distributions, is 0.55.

2.6 Analysis, data processing and validation

The image processing was automated through the development of the algorithms in *Matlab* environment. We assumed that the atmospheric contribution was corrected in the visible bands, since it is not necessary to perform accurate corrections to obtain the vegetation proportion (PV) (Carlson and Ripley, 1997) from a scaled NDVI (Jiménez-Muñoz et al. 2009). The same vector from the whole dune area (Figure 1) was used to clip all the scenes. We analysed the data generated using two different methods of validation.

The first one was an analysis of a pure SiO_2 pixel between LST estimated by the image and measured in situ with the satellite overpass. In this case, the emissivity was obtained from an average of field measurements and assumed in the $NDVI^{THM}$ for all methods. The second validation analysis was carried out by using five scenes, in which we applied the web-based ACPC tool (https://atmcorr.gsfc.nasa.gov/) to generate the atmospheric parameters $L\downarrow$, $L\uparrow$ and τ, and solve RTE (Eq. 4). Thus, RTE was assumed as ground truth.

The ACPC tool takes the National Centers for Environmental Prediction modeled atmospheric profiles as input to the MODTRAN radiative transfer code (Barsi et al. 2005) for a given site and date (Coll et al., 2010). In addition, it is very useful for the atmospheric correction of Landsat thermal infrared data (Zhang et al., 2016). The ACPC validation demonstrated in several studies that it can achieve satisfactory results in the LST retrieval from Landsat data (Barsi et al. 2005; Jiménez-Muñoz et al., 2010; Zhang et al., 2016).

The atmospheric parameters used as input to the ACPC to generate $L\downarrow$, $L\uparrow$ and τ were taken from the Tramandaí Meteorological Station. The application of single-channel algorithms always requires the LSE and these values can be taken from the bibliography (Rubio et al. 1997)

based on available spectral libraries. Therefore, the emissivity assumed in $NDVI^{THM}$ in the second validation analysis was based on the ASTER spectral library (http://speclib.jpl.nasa.gov), which provides more than 2300 spectra in wavelengths covering from the visible to TIR region and is used in most land surface investigations. Afterwards, the emissivity data from the spectral library was weighted by using SRF (Eq. 3).

A linear function was applied to fit the data. To evaluate the performance of the functions, the coefficient of determination (R^2) at 95% probability was used. An evaluation was also made by the determination of RMSE (Root Mean Square Error), which accounts for the total error of measurement for a given model, defined by the square root of the sum of the variances (Käfer et al. 2018). Ultimately, we applied the one-way analysis of variance (ANOVA) and t test (Miller, 1997; Lee and Wang, 2013; Yu et al. 2014) for all the methods in order to identify if the results presented statistical significance.

3. Results and discussion

3.1 Validation with in situ measured LST

The field campaign revealed that the major portion of the dune area was exposed, with only a few pockets of undergrowth. In general, the site has a feature of homogeneous LST distribution. A bare spot was chosen to measure the quartz (SiO_2) at the time of the Landsat 8 overpass. A total of 40 measurements were performed, thereafter, the range of time was reduced to 20 measurements, in order do not introduce too much temporal variability (Coll et al. 2010). Table 1 displays the LST and ε measured in situ using FT-IR spectrometer, the LST retrieved from the three algorithms, and the differences among the methods and the measures in situ.

The dune has very high LST in the summer season, usually above 308.15K (≥35 °C). The average of the measurements carried out in the field campaign resulted in an LST of 314.19

K (41.04 ºC). The pure pixel analysis demonstrated that ISC algorithm had the best agreement, producing 0.6 K of difference when compared to the in situ LST. Cristóbal et al. (2018) reported variations between -1~1.19 for snow and vegetation land covers. The authors also compared ISC against the two single-channel methods here tested and found that ISC is able to yield superior results of RMSE.

The SC algorithm overestimated the LST, producing a difference of -2.71 K. Jiménez-Muñoz et al. (2014) reported that testing results indicated that the SC algorithm provides about a -1.5 K LST retrieval error with atmospheric profiles with *w* less than 3 g·cm^{-2} and more than -4 K when *w* is higher than 3 g·cm^{-2}. On the other hand, Wang et al. (2015) found RMSE values between -2.86 and 1.05 K when evaluating the same algorithm. In this study, the calculation of *w* presented higher values than 3 g·cm^{-2} for the five scenes analysed. This limitation of the method may have influenced the final LST derivation.

In the pure pixel analysis, the IMW was the one that generated the worst agreement, once it subestimated the LST, yielding 3.6 K of difference. Wang et al. (2015) pointed out that IMW is able to produce an accuracy of 1.4 K under moderate errors in both water vapor content and ground emissivity estimations. In this case, the authors considered in its sensitivity analysis an error of ±0.3 g·cm^2 in *w* and ±0.006 in LSE estimation. However, the authors did not perform validation with in situ data for real world conditions when the algorithm was proposed.

Table 1. Comparison of a pure pixel of SiO_2 among the LST retrieval methods applied in the March, 14 Landsat TIRS band 10 image and the FT-IR field data. An average of the $\varepsilon_{in\ situ}$ measured is assumed in the NDVI^{THM} and applied for all the methods.

Method	$\varepsilon_{in\ situ}$	*LST (K)*	$\boldsymbol{LST_{difference}}$
$\boldsymbol{LST_{in\ situ}}$	0.9798	314.19	0
$\boldsymbol{LST_{ISC}}$	0.9798	313.59	0.60
$\boldsymbol{LST_{SC}}$	0.9798	316.90	-2.71
$\boldsymbol{LST_{IMN}}$	0.9798	310.58	3.61

The Figure 2 shows the changes in the LST measures taken concurrently with the Landsat 8 overpass. There is a tendency for LST to increase over time, therefore larger time ranges are likely to lead to larger differences. The difference found in the LST measurements performed at the field was up to 3.9 K, between 13:05 and 13:19 GTM time. We decided to work with the average values in this range, nevertheless, the smaller the time interval is, more accurate tends to be the measures. In this context, Rosas et al. (2017) highlighted that accurately determining of a LST absolute value is challenging, given that it varies considerably throughout the diurnal cycle as a function of the surface radiative balance, as well as expressing a broad range of spatial and temporal variations due to changing land surface and atmospheric condition.

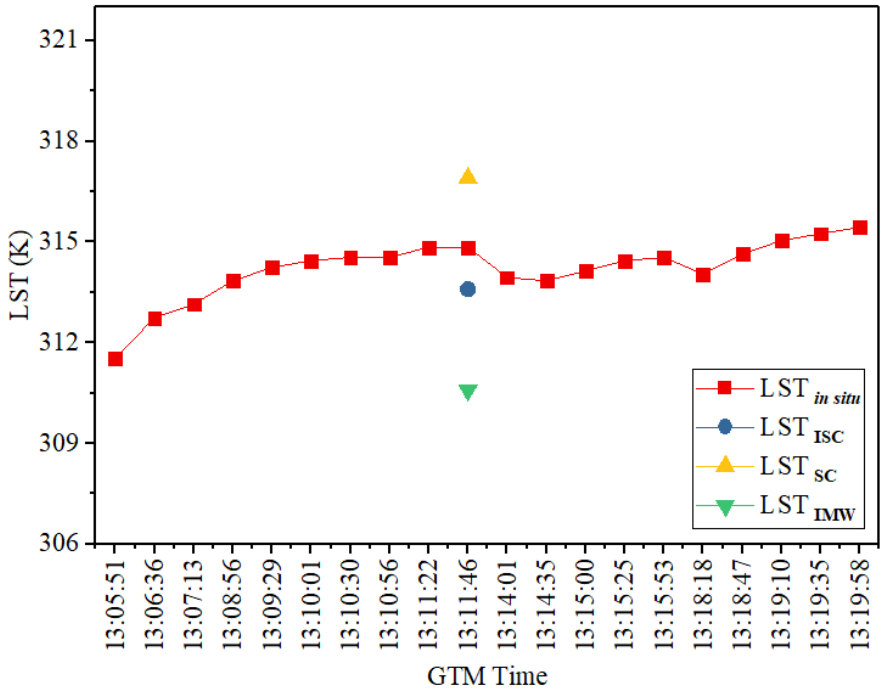

Figure 2. LST measures in situ by FT-IR spectrometer at the time of the Landsat 8 overpass and retrieved by the algorithms. ISC is the improved single-channel, SC is the single-channel, and IMW is the improved mono-window.

3.2 Validation with the ACPC results

Five Landsat scenes were used to validate the results assuming RTE with the parameters $L\downarrow$, $L\uparrow$ and τ generated by ACPC (Barsi et al. 2005) as ground truth. To compare the LSTs estimated and the RTE solved, we employed the coefficient of determination (R^2) and the root mean square error (RMSE) for all dates.

All the correlations among the LSTs retrieved and the ACPC results were strong, with coefficients of determination (R^2) ranging between 0.998-0.999 (Table 2). These results were expected, since we were working with a very homogeneous site and almost pure target. Zhang et al. (2016) also reported a strong correlation of 0.995 when evaluating SC algorithm using RTE as ground truth. However, the authors found higher values of RMSE (varying between 0.61 and 1.24 K), which is certainly related to the larger variety of land surface types analysed. Uncertainties in LSE may be a source of errors in the LST retrieval (Chen et al. 2016), and variations in the landscape can leads to LSE estimation errors because $NDVI^{THM}$ only considered soil and vegetation (Yu et al. 2014).

Table 2. Comparison of the Coefficient of determination (R^2) and the root mean square error (RMSE) for all scenes evaluated.

Method	*Data*	R^2	*RMSE*
ISC	March 14, 2018	0.99957	0.02400
	March 08, 2016	0.99998	0.00410
	March 11, 2017	0.99998	0.00880
	February 26, 2018	0.99971	0.02628
	December 27, 2018	0.99967	0.03203
Mean		**0.99978**	**0.01904**
SC	March 14, 2018	0.99958	0.02383
	March 08, 2016	0.99998	0.00410
	March 11, 2017	0.99999	0.00575
	February 26, 2018	0.99958	0.03141
	December 27, 2018	0.99953	0.03782
Mean		**0.99973**	**0.02058**
IMW	March 14, 2018	0.99849	0.05302
	March 08, 2016	0.99998	0.00515
	March 11, 2017	0.99968	0.03881
	February 26, 2018	0.99998	0.00886
	December 27, 2018	0.99997	0.01199

Mean	**0.99962**	**0.02357**

Table 3 displays the averages and standard deviations (σ) of LST retrieved from the dune area. In comparison to the RTE, there is an overall overestimation for almost all methods and scenes analysed. The only exception was the IMW algorithm, in which we found a slightly underestimation for the scenes of February 26, 2018; March 11, 2017 and March 8, 2016. The underestimation of IMW was also noted when performed the pixel pure analysis. However, those results had showed more significant difference. The R^2 and RMSE demonstrated mean results of 0.9996 and 0.0235 respectively. Although the average values were the closest to the RTE, the regression analysis characterized the worst fit.

SC algorithm was the one that produced LST average results farther from the RTE. However, the values of R^2 and RMSE (0.9997 and 0.021, respectively) were slightly superior compared to the IMW. The method demonstrated a tendency for overestimating the LST in the first validation method applied, which also ocurred in the average values (Table 3), since it is sensitive to *w* in the atmosphere. Nonetheless, the linear regression results showed that the algorithm is able to fit better than IMW.

ISC algorithm had slightly higher average values of LST when compared to the RTE, even so it demonstrated good agreement with the highest R^2 (0.9998) and lowest RMSE (0.019). Hence, the method displays superior performance in relation SC algorithm, indicating that the inclusion of *Ta* together with *w* in the method improves LST retrieval and yields superior performance than models based only on *w*, as reported in Cristóbal et al. (2018). We observed that ISC algorithm was able to provide good results in the two methods of validation considered in this work.

Table 3. Comparison among the LSTs retrieved by the methods and the ACPC results.

Date	LST_{ISC}	$LST_{ISC}\sigma$	LST_{SC}	$LST_{SC}\sigma$	LST_{IMW}	$LST_{IMW}\sigma$
March 14, 2018	311.99	1.79	315.31	1.79	308.73	2.18
March 08, 2016	305.96	1.02	308.32	1.03	302.78	1.21
March 11, 2017	301.43	1.17	304.27	1.16	297.12	1.36
February 26, 2018	311.33	1.54	314.22	1.55	308.35	1.87
December 27, 2018	311.90	1.74	314.80	1.75	309.06	2.13

The standard deviation (σ) values indicated that when the LST is lower, the variations among pixels are less significant. The averages of the five images generated using IMW produced the highest values of σ. It is important to highlight that IMW considers more approximations and is based on more relations to obtain the atmospheric parameters, which might influence the results. In contrast, the ISC and SC showed lower and similar values of σ, once both algorithms present the same mathematical structure, only the AFs based on *w* vary.

According to Coll et al. (2012), the accuracy of the single-channel algorithms depends mostly on how well the atmospheric parameters represent the conditions of the atmosphere over the study area. Barsi et al. (2005) reported that a limitation of the ACPC is that the calculator generates parameters for a single point and, in some cases, this can be inadequate to describe the atmosphere across a whole scene. The study site is not a large area, nevertheless, the nearest continuous launch radiosonde is about 80 km (Costa et al. 2018), which can easily make the atmosphere conditions to vary in this range. Considering the operationality, ACPC tool provides a good approximation and does not require much effort to obtain input parameters, being therefore useful in the cases when there are no radiosonde data available.

Finally, ANOVA was applied for all methods and showed a f-value and p-value of 1.77 and 0.19 respectively, which indicates that at the 0.5 level the population means are not significant. It consolidates the comparison of RMSE and R^2 as mentioned by Yu et al. (2014). The box plot of the estimated LSTs is shown in Figure 3.

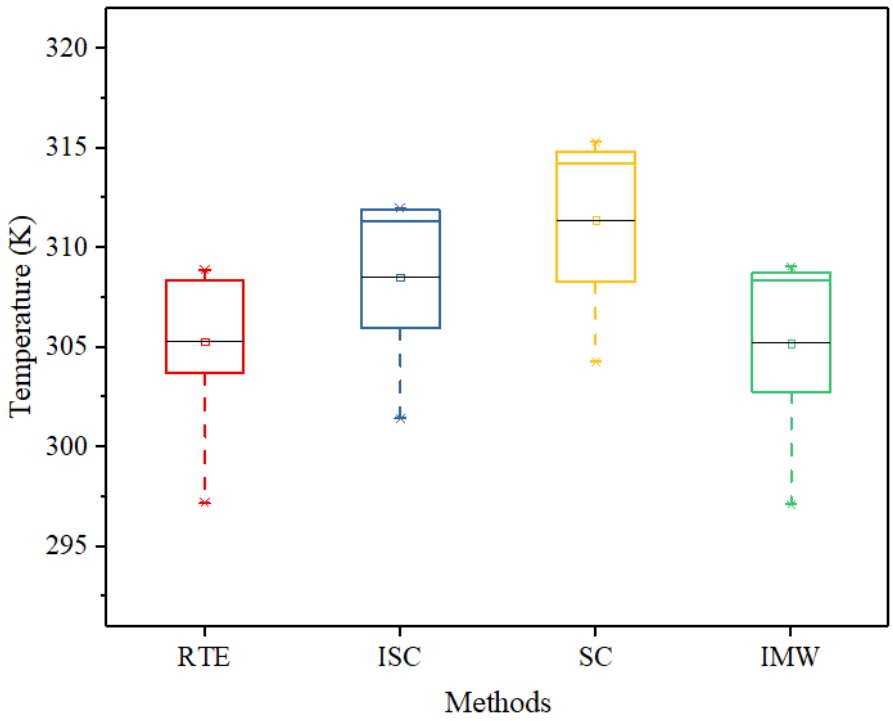

Figure 3. Box plot of the three LST retrieval methods (ISC, SC, IMW) and RTE using Landsat 8 band 10 with the parameters L↓, L↑ and τ generated by ACPC.

Additionally, the t test from the RTE with ACPC parameters and the three methods provided p-value results of 0.33, 0.08 and 0.98 for ISC, SC and IMW, respectively (also larger than 0.05), which testifies that the results from the three algorithms are not significant. These values suggest that we can obtain an acceptable accuracy for LST retrieval by applying the three algorithms in our region. However, ISC demonstrated good performance in the two methods of validation, being a preferable choice for sandy lands.

4. Conclusions

This paper details three operational methodologies for retrieving LST from the Landsat 8 thermal band developed in recent years. In addition, two methods of LST data validation are presented and discussed. A very homogeneous site (99.53% of quartz) was selected in the North Coast of Rio Grande do Sul state in Brazil.

The three methods for retrieving LST analysed were able to yield strong correlation when the RTE along with ACPC tool is assumed as the truth, with coefficients of determination

(R^2) ranging between 0.998-0.999. Hence, they have acceptable accuracy and can be used to obtain LST data, especially for regions such as Southern Brazil, where radiosonde points have low density.

ISC algorithm is the most suitable method, demonstrating superior performance related to SC and IMW. A difference of 0.6 K is found when a pure pixel is analysed, and RMSE of 0.019 for average values.

In future study we intend to investigate a larger variety of land surface types and carry out field work with FT-IR spectrometer in distinct periods of the year, so that we improve even more the validation process.

Acknowledgment

The Landsat 8 OLI/TIRS product are a courtesy of the US Geological Survey Earth Resources Observation and Science Center. This study was financed in part by the Coordenação de Aperfeiçoamento de Pessoal de Nível Superior - Brazil (CAPES), finance code 001.

Conflicts of Interest

The authors declare no conflict of interest.

5. References

Barsi, J. A.; Schott, J. R.; Palluconi, F. D.; Hook, S. J. "Validation of a web-based atmospheric correction tool for single thermal band instruments," Proceedings vol 5882, Earth Observing Systems X, 58820E, 2005.

Barsi, J.A.; Schott, J.R.; Hook, S.J.; Raqueno, N.G.; Markham, B.L.; Radocinski, R.G. Landsat-8 Thermal Infrared Sensor (TIRS) vicarious radiometric calibration. Remote Sens. 2014, 6, 11607–11626.

Bonafoni, S., Anniballe, R., Gioli, B. and Toscano, P. Downscaling Landsat Land Surface Temperatureover the urban area of Florence. European Journal of Remote Sensing, 49: 553-569, 2016. doi: 10.5721/EuJRS20164929.

Chen, F.; Yang, S.; Su, Z.; Wang, K. “Effect of emissivity uncertainly on surface temperature retrieval over urban areas: Investigations based on spectral libraries,” ISPRS Journal of Photogrammetry and Remote Sensing, vol. 114, pp. 53–66, 2016.

Carlson, T. N. and Ripley, D. A. “On the relation between NDVI, fractional vegetation cover, and leaf area index,” Remote Sens. of Environ, vol. 62 no. 3, pp. 241–252, 1997.

Coll, C.; Galve, J. M.; Sanchez, J. M.; and Caselles, V. "Validation of Landsat-7/ETM+ Thermal-Band Calibration and Atmospheric Correction With Ground-Based Measurements." IEEE Transactions on Geosc. and Remote Sens. vol. 48, no. 1, 2010.

Coll, C.; Caselles, V.; Valor, E.; Niclòs, R. Comparison between different sources of atmospheric profiles for land surface temperature retrieval from single channel thermal infrared data. Remote Sensing of Environment, 117, 199–210, 2012. doi:10.1016/j.rse.2011.09.018

Copertino, V.A., Pierro, M. D., Scavone, G. and Telesca, V. “Comparison of algorithms to retrieve Land Surface Temperature from LANDSAT-7 ETM+ IR data in the Basilicata Ionian band,” Tethys, J. of Mediterranean Meteorology & Climatology, vol. 9, pp. 25–34, 2012.

Costa, B. S. C. ; Rocha, N. S. ; Silva, S. C. S. ; Molmann Junior, R. A. ; Munchow, G. B.; Silveira, V. C. ; Rolim, S. B. A. ; Alves, R. C. M. ; Kafer, P. ; Diaz, L. R. . The use of the Weather Research and Forecasting Model to estimate the vertical profile of meteorological data. In: International Geoscience and Remote Sensing Symposium, IGARSS 2018, the 38th annual symposium of the IEEE Geoscience and Remote Sensing Society (GRSS), 2018, Valencia. Proceedings Books of the RAQRS 2017 of IGARSS, 2018. v. 1. p. 1-4.

Cristóbal, J.; Jiménez-Muñoz, J. C.; Sobrino, J. A. Ninyerola, M. and Pons, X. “Improvements in land surface temperature retrieval from the Landsat series thermal band using water vapor and air temperature,” J Geophys Res, vol. 114, D08 103, 2009.

Cristóbal, J.; Jiménez-Muñoz, J. C.; Prakash, A.; Mattar, C.; Skokovic, D.; Sobrino, J. A. An Improved Single-Channel Method to Retrieve Land Surface Temperature from the Landsat-8 Thermal Band. Remote Sensing, v. 10, n. 431, pp. 1-14, 2018.

Du, C.; Ren, H.; Qin, Q.; Meng, J.; Zhao, S. A Practical Split-Window Algorithm for Estimating Land Surface Temperature from Landsat 8 Data. Remote sensing. v. 7, n. 1, 2015, p. 647-665.

Duan, S-B., Li, Z-L., Wang, C., Zhang, S., Tang, B-H., Leng, P., Gao, M-F. Land-surface temperature retrieval from Landsat 8 single-channel thermal infrared data in combination with NCEP reanalysis data and ASTER GED product. *International Journal of Remote Sensing*, 2018 https://doi.org/10.1080/01431161.2018.1460513

Gerace A., and Montanaro, M. "Derivation and validation of the stray light correction algorithm for the thermal infrared sensor onboard Landsat 8." Remote Sens. of Environ. vol 191, no. 15, pp. 246-257, 2017.

Gillespie, A., S. Rokugawa, T. Matsunaga, J. S. Cothern, S. Hook, and A. B. Kahle. 1998. “A Temperature and Emissivity Separation Algorithm for Advanced Spaceborne Thermal

Emission and Reflection Radiometer (ASTER) Images." IEEE Transactions on Geoscience and Remote Sensing 36: 1113–1126. doi:10.1109/36.700995.

Hulley, C. G.; and Hook, S. J. "Intercomparison of versions 4, 4.1 and 5 of the MODIS Land Surface Temperature and Emissivity products and validation with laboratory measurements of sand samples from the Namib desert, Namibia," Remote Sens. of Environ., vol. 113, pp. 1313-1318, 2009.

M. Iqbal, "An introduction to solar radiation," Academic Press, New York, 1983.

Irons, J. R.; Dwyer, J. L. and Barsi, J. A. "The next Landsat satellite: The Landsat Data Continuity Mission," Remote Sens. of Environ., vol. 122, pp. 11–21, 2012.

Jiménez-Muñoz, J. C. and Sobrino, J. A. "A generalized single channel method for retrieving land surface temperature from remote sensing data," J Geophys Res, vol. 108, 2003.

Jiménez-Muñoz, J. C.; Cristóbal, J.; Sobrino, J. A.; Sòria, G.; Ninyerola, M.; Pons, X. "Revision of the Single-Channel Algorithm for Land Surface Temperature Retrieval From Landsat Thermal-Infrared Data," IEEE Trans Geosci Remote Sensing, vol. 47, pp. 339–349, 2009.

Jiménez-Muñoz, J. C., J. A. Sobrino, C. Mattar, and B. Franch. 2010. "Atmospheric Correction of Optical Imagery from MODIS and Reanalysis Atmospheric Products." Remote Sensing of Environment 114: 2195–2210. doi:10.1016/j.rse.2010.04.022.

Jiménez-Muñoz, J. C.; Sobrino, J. A.; Skokovic, D.; Mattar, C.; Cristóbal, J. "Land surface temperature retrieval methods from Landsat-8 thermal infrared sensor data." IEEE Geosci. Remote Sens. Lett., vol. 11, pp. 1840–1843, 2014.

Käfer, P. S.; Rex, F. E.; Breunig, F. M.; Balbinot, R. ModelingPinus elliottiigrowth with multitemporal Landsat data: a study case in Southern brazil. Bulletin of Geodetic Sciences, v. 24, 3, pp. 286-299, 2018. doi: 10.1590/s1982-21702018000300019.

Korb, A. R.; Dybwad, P.; Wadsworth, W.; and Salisbury, J. W. "Portable Fourier transform infrared spectroradiometer for field measurements of radiance and emissivity," Applied Optics, vol. 35, no. 10, pp. 1679-1692, 1996.

Korb, A. R.; Salisbury, J. W.; and D'Ária, D. M. "Thermal-infrared remote sensing and Kirchhoff's law 2. Field measurements" J. of Geophysical Research, vol. 104, B7, pp. 339-350, 1999.

Krishnan, P.; Kochendorfer, J.; Dumas, E. J.; Guillevic, P. C.; Baker, C. B.; Meyers, T.P.; Martos, B. Comparison of in-situ, aircraft, and satellite land surface temperature measurements over a NOAA Climate Reference Network site, *Remote Sensing of Environment*, v. 165, p. 249-264, 2015.

Lee, E.T.; Wang, J.W. Statistical Methods for Survival Data Analysis; John Wiley & Sons: Hoboken, NJ, USA, 2013.

Li, Z.-L. et al. "Satellite-derived land surface temperature: Current status and perspectives," Remote Sensing of Environment, vol. 131 pp. 14–37, 2013.

Malakar, N. K., Hulley, G. C., Hook, S. J., Laraby, K., Cook, M., Schott, J. R. An Operational Land Surface TemperatureProduct for Landsat Thermal Data: Methodology and Validation. *IEEE Transactions on Geoscience and Remote Sensing*. 2018. 10.1109/TGRS.2018.2824828

Mattar, C., Durán-Alarcón, C., Jiménez-Muñoz, J. C., Santamaria-Artigas, A.; Oliveira-Guerra, L., Sobrino, J. A. Global Atmospheric Profiles from Reanalysis Information (GAPRI): a new database for earth surface temperature retrieval. International Journal of Remote Sensing, 2015. doi:10.1080/01431161.2015.1054965.

Mattar, C., Santamaría-Artigas, A., Ponzoni, F., Pinto, C. T., Barrientos C. and Hulley, G. "Atacama Field Campaign: laboratory and in-situ measurements for remote sensing applications," *International Journal of Digital Earth*, 2018.

Miller, R.G., Jr. Beyond Anova: Basics of Applied Statistics; CRC Press: Boca Raton, FL, USA, 1997.

Montanaro, M.; Barsi, J.; Lunsford, A.; Rohrbach S. and Markham, B. "Performance of the Thermal Infrared Sensor on-board Landsat 8 over the first year on-orbit," Proceedings of SPIE, Earth Observing Systems XIX, pp. 9218-17, 2014.

Montanaro, M.; Gerace, A.; Lunsford, A.; Reuter, D. Stray light artifacts in imagery from the Landsat 8 Thermal Infrared Sensor. Remote Sens. 2014, 6, 10435–10456.

Qin, Q.; Zhang, N.; Nan, P.; Chai, L. Geothermal area detection using Landsat ETM+ thermal infrared data and its mechanistic analysis—A case study in Tengchong, China. Journal International Journal of Applied Earth Observation and Geoinformation. n.13, 2011, pp. 552–559.

Rosas, J.; Houborg R., Mccabe M. F. Sensitivity of Landsat 8 Surface Temperature Estimates to Atmospheric Profile Data: A Study Using MODTRAN in Dryland Irrigated Systems. *Remote Sensing*, v. 9, n. 10, 2017 p. 988.

Sobrino, J. A. and Raissouni, N. "Toward remote sensing methods for land cover dynamic monitoring," Int. J. of Remote Sens., vol. 21, no. 2, pp. 353-366, 2000.

Sobrino, J. A.; Jiménez-Muñoz, J. C. and Paolini, L. "Land surface temperature retrieval from LANDSAT TM5," Remote Sens. of Environ. vol. 90, pp. 434–440, 2004, doi:10.1016/j.rse.2004.02.003.

Sobrino, J. A., Jiménez-Muñoz, J. C., Sòria, G., Romaguera, M.; Guanter, L., Moreno, J., Plaza, A. and Martínez, P. 2008. "Land Surface Emissivity Retrieval from Different VNIR and TIR Sensors." IEEE Transactions on Geoscience and Remote Sensing 46 (2): 316–327. doi:10.1109/TGRS.2007.904834.

Tang, H.; and Li. Z.-L. "Quantitative Remote Sensing in Thermal Infrared: Theory and Applications," Heidelberg: Springer Science & Business Media, 2014.

Tardy, B., Rivalland, V., Huc, M., Hagolle, O., Marcq, S., and Boulet, G. A Software Tool for Atmospheric Correction and Surface Temperature Estimation of Landsat Infrared Thermal Data. *Remote Sensing*. 2016, 8, 696; doi:10.3390/rs8090696.

Travessas, F. A.; Dillenburg, S. R. and Clerot, L. C. P. “Estratigrafia e evolução da barreira holocênica do Rio Grande do Sul no trecho Tramandaí-Cidreira.” Bol. Paranaense de Geoc., vol. 53 pp. 57-73, 2005.

USGS. 2018. “Landsat OLI/TIRS Data.” Accessed 03 November, 2018. https://earthexplorer.usgs.gov/.

Van de Griend, A. A. and Owe, M. “On the relationship between thermal emissivity and the normalized difference vegetation index for natural surfaces,” Int. J. of Remote Sens., vol. 14 no. 6, pp. 1119–1131, 1993.

Wang, F.; Qin, Z.; Song, C.; Tu, L.; Karnieli, A.; Zhao. S. An Improved Mono-Window Algorithm for Land Surface Temperature Retrieval from Landsat 8 Thermal Infrared Sensor Data. Remote Sens. v. 7, n. 4, 2015, p. 4268-4289.

Weng, Q.; Fu, P.; Gao, F. Generating daily land surface temperature at Landsat resolution by fusing Landsat and MODIS data. *Remote Sensing of Environment*, 145, p. 55–67, 2014.

Yu, X., Guo, X., and Wu, Z. “Land Surface Temperature Retrieval from Landsat 8TIRS—Comparison between Radiative Transfer Equation-Based Method, Split Window Algorithm and Single Channel Method,” *Remote Sensing*. vol. 6, pp. 9829-9852, 2014.

Zhang, Z., He, G., Wang, M., Long, T., Wang, G., Zhang, X., and Jiao, W. “Towards an operational method for land surface temperature retrieval from Landsat 8 data.” *Remote Sensing Letters*, 2016 v. 7, no. 3, pp. 279–288 http://dx.doi.org/10.1080/2150704X.2015.1130877.

5. CONSIDERAÇÕES FINAIS

O trabalho apresentado se propôs a investigar as particularidades do uso do sensoriamento remoto na região do infravermelho termal (*Thermal Infrared* - TIR) para a recuperação da temperatura de superfície terrestre (*Land surface temperature* - LST) de dados do satélite Landsat 8 OLI/TIRS em regiões de clima subtropical do hemisfério sul.

Foram exploradas por meio de experimentos, as aplicações de medidas de laboratório e de campo, bem como avaliados equipamentos (radiômetro *Fourier Transform Infrared* – FT-IR) e formas de validar adequadamente estes dados. Ademais, três metodologias single-channel (SC) operacionais foram descritas detalhadamente, avaliadas e comparadas entre si.

Uma duna costeira com grande estoque de areia fina (SiO_2) e pequena porção de vegetação foi escolhida como área de estudo principalmente por ser considerada um alvo pseudo-invariante e, desse modo, adequada para a validação terrestre de recuperação de LST por dados de sensoriamento remoto.

Conforme mencionado no decorrer desta pesquisa, a LST é um parâmetro chave na física dos processos de superfície terrestre em diversas escalas, sendo uma variável fundamental para estudos nas mais diversas áreas do conhecimento. Por este fato, muitos esforços têm sido dedicados nos últimos anos para a estabelecer algoritmos para obter a LST a partir de dados de sensoriamento remoto orbital.

No entanto, é preciso ressaltar que a estimativa direta de LST a partir de medidas de radiância no TIR é uma tarefa desafiadora, uma vez que as radiâncias medidas pelos satélites são influenciadas pelos efeitos de superfície e atmosféricos.

Além disso, a validação destas metodologias usando medidas de campo é complexa, uma vez que seu sucesso depende da acurácia dessas medidas e do quão bem elas representam a LST na escala de pixel do satélite. É neste contexto que formas alternativas de melhorar a precisão da recuperação de LST por satélite devem ser constantemente estudadas.

Visando avaliar a hipótese de dependência da emissividade da temperatura, e a possibilidade de substituição de validação de campo por medidas de laboratório, um experimento de laboratório foi realizado e dois conjuntos de dados com diferentes abordagens de calibração foram gerados.

Foi observado que ao utilizar o FT-IR para obtenção de radiância e posterior cálculo de emissividade e temperatura, o conjunto de medidas feito na primeira meia hora de operação do equipamento não resulta em dados precisos e pode induzir, inclusive, a erros sistemáticos, que são mais significativos quando houver menos contraste entre a temperatura da amostra e o ambiente.

Além disso, o processo de calibração contra os corpos negros deve ser realizado pelo menos duas vezes durante um período de, no mínimo, 40 minutos de medições, se for realizado somente uma vez, ocorre defasagem e a acurácia das medidas é prejudicada. Este tempo necessário para o instrumento adquirir estabilidade é essencial para a realização de medidas com boa acurácia.

Superada a limitação do período inicial que o FT-IR leva para atingir a estabilidade, o equipamento é capaz de produzir dados com boa acurácia adequados para a validação de dados de sensoriamento remoto. Em laboratório, caso o mesmo alvo seja medido em diferentes temperaturas, esta temperatura não influencia significativamente nos dados de emissividade e, portanto, não introduz erros significativos na obtenção da LST (uma vez que a emissividade é um parâmetro para se obter a LST).

Em contrapartida, acima da temperatura assumida durante o processo de calibração do FT-IR (que deve ficar entre 10-40ºC), o instrumento tende a perder a acurácia. Isso foi visto neste trabalho quando a resposta da emissividade *versus* a temperatura foi isolada no comprimento de onda da banda 10 do Landsat 8, em que valores de emissividade acima de 1,0 foram produzidos. Porém, valores desta magnitude não são possíveis e podem ser considerados ruído, uma vez que um corpo com emissividade acima de 1,0 seria apenas um corpo negro teórico.

Considerando as limitações do FT-IR e executando corretamente os procedimentos mencionados, as medições laboratoriais podem ser substituídas com sucesso pela validação de campo, evitando a necessidade de campanha de campo no momento da passagem do satélite. Ainda, bibliotecas espectrais com dados de emissividade disponíveis também podem ser aplicadas produzindo boa acurácia quando um alvo puro como o quartzo (99.53%) for avaliado.

A variabilidade das emissividades dos alvos em relação à sua temperatura é pouco discutida na literatura, principalmente porque, para a maioria dos materiais de superfície, a dependência entre a emissividade e a temperatura pode ser desprezada.

Neste estudo, foi encontrada uma diferença de aproximadamente 2% na emissividade em comparação com a temperatura foi observada.

Assim, pode-se inferir que estas variações mínimas não afetam consideravelmente a precisão das medidas de emissividade quando métodos single-channel são usados, pois esses métodos normalmente apresentam acurácias variando entre 1-2 K.

Quando comparado o algoritmo *single-channel* (SC) (Jiménez-Muñoz, et al., 2014) com o *improved single-channel* (ISC) (Cristóbal et al., 2018), que é uma versão melhorada do primeiro método, o ISC forneceu resultados levemente superiores. No entanto, a inclusão da variável temperatura média atmosférica (*Ta*) é necessária nesse algoritmo, e a mesma depende de dados medidos na área ou obtidos por estações meteorológica.

Portanto, deve-se considerar que muitos locais não apresentam boa densidade de estações meteorológicas, neste sentido, para se obter LST em escala global, o algoritmo SC pode ser preferível, mas os usuários devem atentar para o vapor de água presente na atmosfera (*w*), pois em atmosferas úmidas ($w > 3$ g.cm^{-2}) o método deve ser usado com cautela.

A comparação das metodologias SC mais atuais presentes na literatura demonstrou que os três métodos avaliados neste trabalho foram capazes de produzir forte correlação com a equação de transferência radiativa (RTE). Neste caso, a mesma foi utilizada como sendo a verdade de campo, juntamente com o uso da calculadora de parâmetros de correção atmosférica (ACPC), ferramenta amplamente utilizada nos dias atuais para corrigir atmosfericamente imagens Landsat na região do TIR. Coeficientes de determinação (R^2) variando entre 0,998-0,999 foram produzidos.

Nesta perspectiva, conclui-se que os três algoritmos têm uma acurácia aceitável e podem ser usados para obter dados LST. O algoritmo ISC, entretanto, mostrou-se como o método mais adequado em todas as análises, tendo desempenho levemente superior em comparação aos demais. Quando um pixel puro foi comparado com medidas obtidas em campo no momento da passagem do satélite Landsat 8 com o FT-IR, uma diferença de somente 0,6 K foi encontrada.

É importante ressaltar que o ISC é um algoritmo proposto recentemente e sua validação com dados de campo havia sido realizada somente em dois tipos de cobertura da terra (neve e vegetação). Nesse sentido, as descobertas deste estudo quanto as áreas de dunas compostas por quartzo apresentam relevância científica,

principalmente considerando seu melhor acordo em comparação com um método que é amplamente utilizado (SC) pela comunidade científica para obter LST por sensoriamento remoto.

Ademais, outro fato que deve ser enfatizado é que a maior parte das metodologias de obtenção de LST são desenvolvidas e validadas no hemisfério norte. Desta maneira, estudos no hemisfério sul com resultados de validação são essenciais, principalmente tendo em vista que cada região apresenta particularidades. Alguns autores comentam que pelo fato de uma única imagem de sensoriamento remoto conter elementos diferentes, como solo, rocha e vegetação. A validação completa da recuperação da LST é limitada.

Além disso, de modo geral, a área observada pela instrumentação terrestre não é necessariamente representativa da área observada pelo satélite e as geometrias de visualização associadas aos sensores são raramente idênticas. A LST além de variar com o espaço, também varia temporalmente, deste modo, em estudos futuros deve ser investigada uma maior variedade de tipos de superfície terrestre.

A realização de campanhas de campo com o radiômetro FT-IR em períodos distintos do ano pode ser fundamental para aprimorar o processo de validação e se obter uma caracterização do comportamento da LST no hemisfério sul. Por fim, o uso combinado de técnicas de aquisição de dados no TIR pode melhorar a acurácia da obtenção da LST, podendo assim ser fortemente recomendado como uma continuidade deste estudo.

6. REFERÊNCIAS

BALDRIDGE, A. M.; HOOK, S. J.; GROVE, C. L.; RIVERA, G. The ASTER spectral library version 2.0. **Remote Sensing of Environment**. v. 113, p. 711–715, 2009.

BARSI, J. A.; SCHOTT, J. R.; PALLUCONI, F. D.; HOOK, S. J. Validation of a Web-Based Atmospheric Correction Tool for Single Thermal Band Instruments. Earth Observing Systems X, edited by James J. Butler, **Proceedings of SPIE,** v. 5882 (SPIE, Bellingham, WA, 2005) 0277-786X/05/$15 · doi: 10.1117/12.619990.

BARSI, J. A.; SCHOTT, J. R.; HOOK, S. J.; RAQUENO, N. G.; MARKHAM, B. L.; RADOCINSKI, R. G. Landsat-8 Thermal Infrared Sensor (TIRS) vicarious radiometric calibration. **Remote Sensing**. 6, p. 11607–11626, 2014.

BECKER, F.; LI, Z.-L.(a) Towards a local split window method over land surfaces. **International Journal of Remote Sensing**, v. 11, p. 369-393, 1990.

BECKER, F.; LI, Z.-L.(b) Temperature-independent spectral indexes in thermal infrared bands. **Remote Sensing of Environment**. v. 32, p. 17–33, 1990.

BECKER, F.; LI, Z-L. Surface temperture and emissivity at various scales: Definition, measurements and related problems. **Remote Sensing** v. 12, p. 225-253, 1995.

CHATTERJEE, R. S.; SINGH, N.; THAPA, S.; SHARMA, D.; KUMAR, D. Retrieval of land surface temperature (LST) from Landsat TM6 and TIRS data by single channel radiative transfer alforithm using sattelite and ground-based inputs. **International Journal of Applied Earth Observation and Geoinformation** v. 58, p. 264–277, 2017.

CHEN, F.; YANG, S.; SU, Z.; WANG, K. Effect of emissivity unvertainly on surface temperature retrieval over urban areas: Investigations based on spectrala libraries. **ISPRS Journal of Photogrammetry and Remote Sensing,** v. 114, p. 53–66, 2016.

COLL, C.; CASELLES, V.; SOBRINO, J.A.; VALOR, E. On the atmospheric dependence of the split-window equation for land surface temperature. **International Journal of Remote Sensing**, v. 15, p. 105–122, 1994.

COLL, C.; GALVE, J. M.; SÁNCHEZ, J. M. CASELLES, V. Validation of Landsat-7/ETM+ Thermal-Band Calibration and Atmospheric Correction With Ground-Based Measurements**. IEEE Transactions on Geoscience and Remote Sensing**, v. 48, n. 1, 2010.

COPERTINO, V.A.; PIERRO, M. D.; SCAVONE, G. and TELESCA, V. “Comparison of algorithms to retrieve Land Surface Temperature from LANDSAT-7 ETM+ IR data in the Basilicata Ionian band,” Tethys, **Journal of Mediterranean Meteorology & Climatology**, v. 9, p. 25–34, 2012.

CRISTÓBAL, J.; JIMÉNEZ-MUÑOZ, J. C.; SOBRINO, J. A.; NINYEROLA, M.; PONS, X. Improvements in land surface temperature retrieval from the Landsat series thermal band using water vapor and air temperature, **Journal of Geophysical Research**, v. 114, D08 103, 2009.

CRISTÓBAL, J.; JIMÉNEZ-MUÑOZ, J. C.; PRAKASH, A.; MATTAR, C.; SKOKOVIC, D.; SOBRINO, J. A. An Improved Single-Channel Method to Retrieve Land Surface Temperature from the Landsat-8 Thermal Band. **Remote Sensing**, v. 10, n. 431, p. 1-14, 2018.

CUDAHY, T. J. CACCETTA, M.; LAU, L.; RODGER, A.; LAUKAMP, C.; ONG, C. Satellite ASTER geoscience Map of Australia, **Data collection, CSIRO**, 2012.

DASH, P.; GÖTTSCHE, F.-M.; OLESEN, F.-S.; FISCHER, H. Land Surface Temperature and Emissivity Estimation from Passive Sensor Data: Theory and Practice-Current Trends **International Journal of Remote Sensing**. v. 23, p. 2563–2594, 2002.

DU, C.; REN, H.; QIN, Q.; MENG, J.; ZHAO, S. A Practical Split-Window Algorithm for Estimating Land Surface Temperature from Landsat 8 Data. **Remote sensing**. v. 7, n. 1, p. 647-665, 2015.

EISELE, A.; CHABRILLAT, S.; HECKER, C.; HEWSON, R.; LAU, I. C.; ROGASS, C. SEGL, K.; CUDAHY, T. J.; UDELHOVEN, T.; HOSTERT, P.; KAUFMANN, H. Advantages using the thermal infrared (TIR) to detect and quantify semi-arid soil properties. **Remote Sensing of Environment**, 163, p. 296–311, 2015.

GERACE, A.; MONTANARO, M. Derivation and validation of the stray light correction algorithm for the thermal infrared sensor onboard Landsat 8, **Remote Sensing of Environment**, v. 191, n. 15, p. 246-257, 2017.

GILLESPIE, A.; ROKUGAWA, S.; MATSUNAGA, T.; COTHERN, J. S.; HOOK, S.; K AHLE, A. B. A Temperature and Emissivity Separation Algorithm for Advanced Spaceborne Thermal Emission and Reflection Radiometer (ASTER) Images. **IEEE Transactions on Geoscience and Remote Sensing**, v. 36, n. 4, p. 1113-1126, 1998.

GRONDONA, A. Estimativa da temperatura-emissividade de alvos com base em regressões de dados de sensoriamento remoto proximal. (UFRGS-00097097). Tese (**Doutorado em Sensoriamento Remoto**) - Universidade Federal do Rio Grande do Sul, p. 208, 2015.

HOOK, S.J.; GABELL, A.R.; GREEN, A.A.; KEALY, P.S. A comparison of techniques for extracting emissivity information from thermal infrared data for geologic studies. **Remote Sensing of Environment**, v. 42, p. 123-135, 1992.

HOOK, S., J.; DMOCHOWSKI, J., E.; HOWARD, K., A., ROWAN, L., C.; KARLSTRO M, K., E.; STOCK, J., M.: Mapping variations in weight percent silica measured from multispectral thermal infrared imagery - Examples from the Hiller Mountains, Nevada, USA and Tres Virgenes-La Reforma, Baja California Sur, Mexico. **Remote Sensing of Environment**, v. 95, p. 273-289, 2005.

HULLEY C. G; HOOK, S. J. Intercomparison of versions 4, 4.1 and 5 of the MODIS Land Surface Temperature and Emissivity products and validation with laboratory measurements of sand samples from the Namib desert, Namibia. **Remote Sensing of Environment**, v. 113, p. 1313-1318, 2009.

HULLEY C. G; HOOK, S. J. Generating Consistent Land Surface Temperature and Emissivity Products Between ASTER and MODIS Data for Earth Science Research. **IEEE Transitions on Geoscience and Remote Sensing**. v. 49, n. 4, p. 1304-1315, 2011.

HULLEY, G. AND BALDRIDGE, A. Validation of Thermal Infrared (TIR) Emissivity Spectral Using Pseudo- invariant sand dunes sites. Kuenzer, C and Dech, S (eds.), Thermal Infrared Remote Sensing: Sensors, Methods, Applications, **Remote Sensing and Digital Image Processing**. p. 515-527, 2013.

HULLEY, G.; VERAVERBEKE, S.; HOOK, S. Thermal-based techniques for land cover change detection using a new dynamics MODIS multispectral emissivity product (MOD21). **Remote Sensing of Environment**, 140, p. 755-765, 2014.

HUNT, G. R. AND SALISBURY, J. W. Visible and Near-Infrared Spectra of Minerals and Rocks. I. Silicate Minerals. **Modern Geology**, 1, p. 283-300, 1970.

IRONS, J. R.; DWYER, J. L.; BARSI J. A. The next Landsat satellite: The Landsat Data Continuity Mission, **Remote Sensing of Environment**, v. 122, p. 11–21, 2012.

JENSEN, J. **Sensoriamento remoto do ambiente: uma perspectiva em recursos terrestres**. Tradução José Carlos Epiphanio et al., São José dos Campos, SP: Parêntese, p. 598, 2009.

JIMÉNEZ-MUÑOZ, J. C.; SOBRINO, J. A., A generalized single channel method for retrieving land surface temperature from remote sensing data. **Journal of Geophysical Research**, v. 108, n. D22, p. 2-9, 2003.

JIMÉNEZ-MUÑOZ, J. C.; SOBRINO, J. A. Split-window coefficients for land surface temperature retrieval from low-resolution thermal infrared sensors. **IEEE Geosci. Remote Sens. Lett**., v. 5, n. 4, p. 806–809, 2008.

JIMÉNEZ-MUÑOZ, J. C.; CRISTÓBAL, J.; SOBRINO, J. A.; SÒRIA, G.; NINYEROLA, M.; PONS, X. Revision of the Single-Channel Algorithm for Land Surface Temperature Retrieval from Landsat Thermal-Infrared Data. **IEEE Transitions on Geoscience and Remote Sensing**, 47, 2009, p. 339–349.

JIMÉNEZ-MUÑOZ, J. C.; SOBRINO, J.A.; SKOKOVIC, D.; MATTAR, C.; CRISTÓBAL, J. Land surface temperature retrieval methods from Landsat-8 thermal infrared sensor data. **IEEE Geoscience and Remote Sensing Letters**, 11, p. 1840–1843, 2014.

KEALY, P. S.; HOOK, S. J. Separating temperature and emissivity in thermal infrared multispectral scanner data: Implications for recovering land surface temperatures. **IEEE Transactions on Geoscience and Remote Sensing**. v. 31, p. 1155-1164, 1993.

KERR, Y. H.; LAGOUARDE, J. P. Imbernon Accurate land surface temperature retrieval from AVHRR data with use of an improved split window algorithm. **Remote Sens Environ**, v. 41, p. 197-209, 1992.

LI, J.; LI, J.; WISZ, E.; ZHOU, D. Physical retrieval of surface emissivity spectrum from hyperspectral infrared radiances. **Geophysical Research Letters**. v. 34, n. 16. 2007.

LI, Z. L.; WU, H.; WANG, N.; QIU, S.; SOBRINO, J. A.; WAN, Z.; TANG, B. H.; YAN, G. (a) Land surface emissivity retrieval from satellite data. **International Journal of Remote Sensing**. v. 34, p. 3084–3127, 2013.

LI, Z. L.; TANG, B. H.; WU, H.; REN, H.; YAN, G.; WAN, Z.; TRIGO, I. F.; SOBRINO, J. A.; (b) Satellite-derived land surface temperature: Current status and perspectives. **Remote Sensing of Environment**, 131, p.14–37, 2013.

RIBEIRO da LUZ, B.; CROWLEY, J. K. Spectral reflectance and emissivity features of broad leaf plants: Prospects for remote sensing in the thermal infrared (8.0-14.0 μm). **Remote Sensing of Environment**. v. 109, n. 4. 2007.

RONDÓN, A. C. B. Análise comparativa de métodos de recuperação de emissividade com dados do Infravermelho Termal do sensor ASTER. Dissertação. (**Mestrado em Sensoriamento Remoto**), Universidade Federal do Rio Grande do Sul, Porto Alegre, p. 61, 2017.

MALAKAR, N. K., HULLEY, G. C., HOOK, S. J., LARABY, K., COOK, M., SCHOTT, J. R. An Operational Land Surface TemperatureProduct for Landsat Thermal Data: Methodology and Validation. **IEEE Transactions on Geoscience and Remote Sensing**. 2018.

MALLICK, J.; SINGH, C. K.; SHASHTRI, S.; RAHMAN, A.; MUKHERJEE, S. M. Land surface emissivity retrieval based on moisture index from LANDSAT TM satellite data over heterogeneous surfaces of Delphi city**. International Journal of Applied Earth Observation and Geoinformation**, v. 19, p. 348–358, 2012.

MATTAR, C.; DURÁN-ALARCÓN,; JIMÉNEZ-MUÑOZ, J. C.; SOBRINO, J. A. Global Atmospheric Profiles from Reanalysis Information (GAPRI): A new dataset for forward simulations in the thermal infrared region. **IEEE Transactions on Geoscience and Remote Sensing**, 2014.

MATTAR, C.; SANTAMARÍA-ARTIGAS, A.; PONZONI, F.; PINTO, C. T.; BARRIENTOS C. and HULLEY, G. Atacama Field Campaign: laboratory and in-situ measurements for remote sensing applications. **International Journal of Digital Earth**, 2018.

MOMENI M.; SARADJIAN, M. R. Evaluating NDVI-based emissivities of MODIS bands 31 and 32 using emissivities derived by day/night LST algorithm. **Remote Sensing of Environment**, v. 106, n. 2, p. 190–198, 2007.

MONTANARO, M.; GERACE, A.; LUNSFORD, A.; REUTER, D. Stray light artifacts in imagery from the Landsat 8 Thermal Infrared Sensor. **Remote Sensing**, v. 6, p.10435–10456, 2014.

NOTESCO, G.; OGEN, Y.; BEN-DOR, E. Mineral Classification of Makhtesh Ramon in Israel Using Hyperspectral Longwave Infrared (LWIR) Remote-Sensing Data. **Remote Sensing**, 7, 9, p. 12282-12296, 2015.

NOVO, E. M. L. de M. **Sensoriamento remote: Princípios e aplicações**. 4ª ed. São Paulo: Blucher, 387 p. 2010.

OLSEN, R.C. Remote sensing from air and space. 1st ed. USA, Bellingham. **SPIE Press**, 253 p, 2007.

PITTIGLIANI, G.H. ROLIM, S. B. A. Biblioteca espectral do Laboratório de Sensoriamento Remoto Geológico (LabSRGeo): criando uma base de dados para os Sistemas Laguna-Barreira do Rio Grande do Sul. In: XXIX Salão de Iniciação Científica da UFRGS, 2017, Porto alegre. **Anais do XXVIII Salão de Iniciação Científica da UFRGS**. Porto Alegre: UFRGS, 2017. v. 1. p. 1-1.

POZO VAZQUEZ, D.; OLMO REYES, F.J.; ALADOS ARBOLEDAS L. A comparative study of algorithms for estimating land surface temperature from AVHRR data. **Remote Sensing of Environment**, v. 62, n. 3, p. 215-222, 1997.

PRICE, J. C. Estimating surface temperatures from satellite thermal infrared data — A simple formulation for the atmospheric effect. **Remote Sensing of Environment**, v. 13, p. 353-361, 1983.

QIN, Z.; KARNIELI, A.; BERLINER, P., A monowindow algorithm for retrieving land surface temperature from Landsat TM data and its application to the Israel-Egypt border region, **International Journal of Remote Sensing**, v.22, p. 3719–3746, 2001.

QIN, Z.; DALL'OLMO, G.; KARNIELI, A.; BERLINER, P. Derivation of split window algorithm and its sensitivity analysis for retrieving land surface temperature from

NOAA-advanced very high-resolution radiometer data. **Journal of Geophysical Research: Atmospheres.** v. 106, p. 22655–22670, 2001.

RIBEIRO DA LUZ, B.; J. K. CROWLEY. Spectral Reflectance and Emissivity Features of Broad Leaf Plants: Prospects for Remote Sensing in the Thermal Infrared (8.0–14.0 μm). **Remote Sensing of Environment**, v. 109, 2007, p. 393–405.

ROSAS, J.; HOUBORG R., MCCABE M. F. Sensitivity of Landsat 8 Surface Temperature Estimates to Atmospheric Profile Data: A Study Using MODTRAN in Dryland Irrigated Systems. **Remote Sensing**, v. 9, n. 10, p. 988, 2017.

ROUSE, J. W. HAAS, R. H. SCHELL, J. A. DEERING, D. W. Monitoring Vegetation Systems in the Great Plains with ERTS. **Paper Presented at the Third ERTS-1 Symposium**, Washington, DC, NASA SP-351, v. 1 n. A, p. 309–317, 1973.

ROZENSTEIN, O.; QIN, Z.; DERIMIAN, Y.; KARNIELI, A. Derivation of Land Surface Temperature for Landsat-8 TIRSUsing a Split Window Algorithm. **Sensors**. v. 14, p. 5768-5780, 2014.

SALISBURY J. W.; D'ARIA D. M. Emissivity of terrestrial materials in the 8–14 μm atmospheric window**. Remote Sensing of Environment.** v.42, n. 2, p. 83-106, 1992.

SOBRINO, J. A.; RAISSOUNI, N. Toward remote sensing methods for land cover dynamic monitoring. **International Journal of Remote Sensing**, v. 21, n. 2, p. 353-366, 2000.

SOBRINO, J. A.; RAISSOUNI, N.; LI, Z.-L. A comparative study of land surface emissivity retrieval from NOAA data. **Remote Sensing of Environment**, v. 75, n. 2, p. 256–266, 2001.

SOBRINO, J. A.; KHARRAZ, J. EL; LI, Z.-L. Surface temperature and water vapour retrieval from MODIS data. **International Journal of Remote Sensing**, v. 24, n. 24, p. 5161–5182, 2003.

SOBRINO, J. A.; JIMÉNEZ-MUÑOZ, J. C.; PAOLINI L. Land surface temperature retrieval from LANDSAT TM5. **Remote Sensing of Environment**, v. 90, p. 434–440, 2004.

SOBRINO, J. A.; JIMÉNEZ-MUÑOZ, J. C.; SÒRIA, G.; ROMAGUERA, M.; GUANTER, L.; MORENO, J. Land Surface Emissivity Retrieval from Different VNIR and TIR Sensors. **IEEE Transactions on Geoscience and Remote Rensing**, v. 46, n. 2, 2008.

SNYDER, W. C.; WAN, Z.; ZHANG, Y.; FENG, Y.-Z. Classification-Based Emissivity for Land Surface Temperature Measurement from Space. **International Journal of Remote Sensing**, v. 19, p. 2753–2774, 1998.

SUSSKIND, J. ROSENFIELD, D. REUTER, M.T. Chahine Remote sensing of weather and climate parameters from HIRS2/MSU on TIROS-N **Journal of Geophysical Research**, v. 89, p. 4677-4697, 1984.

TAN, K.; LIAO, Z.; DU, P.; and WU. L. Land surface temperature retrieval from Landsat 8 data and validation with geosensor network, **Frontiers in Earth Sciensce**, p. 20–34, 2017.

TANG, H.; LI, Z.-L. Quantitative Remote Sensing in Thermal Infrared: Theory and Applications, 1st ed**.; Springer-Verlag: Berlin/Heidelberg**, Germany, 2014.

TARDY, B.; RIVALLAND, V.; HUC, M.; HAGOLLE, O.; MARCQ, S.; AND BOULET, G. A Software Tool for Atmospheric Correction and Surface Temperature Estimation of Landsat Infrared Thermal Data. **Remote Sensing**. v. 8, n. 696, 2016.

TRAVESSAS, F. A.; DILLENBURG, S. R.; CLEROT, L. C. P. Estratigrafia e evolução da barreira holocênica do Rio Grande do Sul no trecho Tramandaí-Cidreira. **Boletim Paranaense de Geociências**, v. 53, p. 57-73, 2005.

TOMAZELLI, L. J.; VILLWOCK, J. A. Considerações sobre o ambiente praial e a deriva litorânea de sedimentos ao longo do Litoral Norte do Rio Grande do Sul, Brasil. **Pesquisas**, v. 19, n. 1, p. 3-12, 1992.

TOMAZELLI, L., DILLENBURG, S., GUIMARÃES, E., CORREA, M. Geomorfologia e potencial de preservação dos campos de dunas transgressivos de Cidreira e Itaipeva, Litoral Norte do Rio Grande do Sul. **Pesquisas em Geociências**, Instituto de Geociências da UFRGS, Porto Alegre, v. 32, n. 2, p. 47-55, 2008.

TONOOKA H. An atmospheric correction algorithm for thermal infrared multispectral data over land — A water-vapor scaling method. **IEEE Transactions on Geoscience and Remote Sensing**, v. 39, p. 682-692, 2001.

VALOR, E. and CASELLES, V. Mapping land surface emissivity from NDVI: Application to European, African and South American areas. **Remote Sensing of Environment**, v. 57, p. 167–184, 1996.

VAN DE GRIEND, A. A. and OWE, M. On the relationship between thermal emissivity and the normalized difference vegetation index for natural surfaces. **International Journal of Remote Sensing,** v. 14, n. 6, p. 1119–1131, 1993.

VICENTE, L. E.; SOUZA FILHO, C. R. Detecção de quartzo e argilominerais para o monitoramento de degradação de terras a partir de dados do infravermelho termal do sensor Aster. **Revista Brasileira de Geofísica** v. 28 n. 2, 2010.

VISUAL INFORMATION SOLUTIONS, 2014, **Exelis Vis. ENVI – IDL - v. 5.1.** Boulder CO. Disponível em: http:/www.exelisvis.com/envi/, Acesso: 10 Dez. 2018.

YU, X.; GUO, X.; WU, Z. Land Surface Temperature Retrieval from Landsat 8 TIRS—Comparison between Radiative Transfer Equation-Based Method, Split Window Algorithm and Single Channel Method. **Remote Sensing***,* p. 9829-9852, 2014.

UNITED STATES GEOLOGICAL SURVEY. **Landsat 8 Operational Land Imager and Thermal Infrared Sensor calibration notices**. Disponível em: http://landsat.usgs.gov/calibration_notices.php. Acesso: 03 Jan. 2018.

UNITED STATES GEOLOGICAL SURVEY. **Landsat 8 Operational Land Imager and Thermal Infrared Sensor calibration notices**. Disponível em: https://landsat.usgs.gov/april-25-2017-tirs-stray-light-correction-implemented-collection-1-processing. Acesso: 04 Jan. 2018.

WANG, F.; QIN, Z.; SONG, C.; TU, L.; KARNIELI, A.; ZHAO. S. An Improved Mono-Window Algorithm for Land Surface Temperature Retrieval from Landsat 8 Thermal Infrared Sensor Data. **Remote Sensing**, v. 7, n. 4, p. 4268-4289, 2015.

WAN, Z.; DOZIER, J. A generalized split-window algorithm for retrieving land-surface temperature from space. **IEEE Transactions on Geoscience and Remote Sensing**, v. 34, p. 892-905, 1996.

WAN, Z.; LI, Z.-L. A physics-based algorithm for retrieving land-surface emissivity and temperature from EOS/MODIS data, **IEEE Transactions on Geoscience and Remote Sensing**, v.35, p. 980-996, 1997.

WATSON, K. Two-temperature method for measuring emissivity **Remote Sensing of Environment**, v. 42, p. 117–121, 1992.

WENG, Q.; FU, P.; GAO, F. Generating daily land surface temperature at Landsat resolution by fusing Landsat and MODIS data. **Remote Sensing of Environment**, 145, p. 55–67, 2014.

WILBER, A. C. KRATZ; D. P.; GUPTA, S. K. **Surface Emissivity Maps for Use in Retrievals of Longwave Radiation**. 1999. Tech. Rep. NASA/TP-1999-209362. 30p. <https://eosweb.larc.nasa.gov/sites/default/files/project/calipso/Wilber.NASATchNote99.pdf>

ZHANG, Z.; HE, G. Generation of Landsat surface temperature product for China, 2000–2010. **International Journal of Remote Sensing**, v. 34, p. 7369–7375, 2013.

ZHANG, Z., HE, G., WANG, M., LONG, T., WANG, G., ZHANG, X., AND JIAO, W. Towards an operational method for land surface temperature retrieval from Landsat 8 data. **Remote Sensing Letters**, v. 7, n. 3, pp. 279–288, 2016.

ZHANG, R-H.; SU, H-B.; TIAN, J.; MI, S-J.; LI, Z-L. Non-Contact Measurement of the Spectral Emissivity through Active/Passive Synergy of CO2 Laser at 10.6 μm and 102F FTIR (Fourier Transform Infrared) Spectrometer. **Sensors**, v. 16, n. 970, p. 1-14, 2016.

7. APÊNDICES

PROXIMAL REMOTE SENSING: POTENTIAL AND LIMITATIONS OF FT-IR SPECTROMETER FOR VALIDATION OF SATELLITE MEASUREMENTS

Pâmela Suélen Käfer[1], Silvia Beatriz Alves Rolim[1], María Luján Iglesias[1], Nájila Souza da Rocha[1], Lucas Ribeiro Diaz[1], Eduardo André Kaiser[1], Atilio Efrain Bica Grondona[2], Suzianny Salazar da Silva[1], Franciel Eduardo Rex[3]

[1]Federal University of Rio Grande do Sul (UFRGS) - State Research Center for Remote Sensing and Meteorology, Porto Alegre, RS. [2]University of Vale dos Sinos (UNISINOS) - Graduate program in Civil Engineering, São Leopoldo, RS. [3]Federal University of Paraná (UFPR) - Forestry departament, Curitiba, PR, Brazil. (contact: pamelaskafer@gmail.com)

ABSTRACT

There are several methodologies to retrieve land surface temperature (LST) from thermal infrared (TIR) remote sensing data. All of them require validation with field measurements. However, it is difficult to perform ground measurements with the satellite overpass. We investigated the potential and limitations of FT-IR spectrometer for the validation of orbital remote sensing data in the thermal infrared region (TIR). Results indicated that laboratory measurements can be successfully replaced for field validation in the estimation of land surface emissivity (LSE) of quartz sand, avoiding the need of field campaign. In this case, it is essential to pay attention to some factors in the laboratory, such as the time required for the instrument to acquire stability and the calibration process.

***Keywords*—**Emissivity, Sand lands, LST, Field measurements, Laboratory measurements.

1. INTRODUCTION

Land surface temperature (LST) is an essential parameter in investigating environmental, ecological processes and climate change at various scales. Moreover, it is important in the studies of evapotranspiration, soil moisture conditions, surface energy balance, and urban heat islands [1-2]. In this context, many methodologies have been developed to retrieve this variable from satellite imagery measurements and correct the atmospheric effects for thermal infrared (TIR) [3], which are very significant when working in this spectral region.

The methods used to obtain LST from orbital remote sensing require as prior knowledge the land surface emissivity (LSE) and the data need to be validated with field measurements [4]. Nevertheless, this is not an easy task, once ground measurements must be performed concurrently with the satellite overpass in order to be comparable [5]. Furthermore, the measurements might be limited by different sensor data specifications and field data, which makes these measurements a challenge.

Proximal remote sensing is the employment of sensors on a ground level, in contrast to the remote deployment of sensors using aerial or satellite platforms [6]. To identify best approach to collect data on the ground level with a good accuracy, it is crucial to investigate the particularities of each instrument.

MODEL 102F is a *Fourier Transform Infrared Spectrometer* (FT-IR) that has been widely used to collect emissivity of different targets in the spectral range of middle and thermal infrared wavelength (2~25µm) with a spectral resolution of 4, 8 or 16cm-1 [7]. The instrument can be suitable to validate remote orbital sensing data, since it allows to calculate LSE and LST in the field from radiance measurements.

Field measurements are a challenge, in addition, they are restricted to a limited number of pixels [8], an alternative to the ground validation is to use measurements performed at the laboratory. There are several spectral libraries available to obtain emissivity from different targets of the surface and retrieve LST [9], but sometimes they are not representatives from the area evaluated.

The paper evaluates the potential and limitations of FT-IR spectrometer for the validation of orbital remote sensing data in the TIR. We focus on investigating the differences between field and laboratory measurements, in order to evaluate the particularities of the instrument in the field and the possibility of replacing field validation by laboratory measurements.

2. MATERIAL AND METHODS

2.1. Laboratory measurements

When retrieving LST, the emissivity is needed, and the values of the targets can be taken from the bibliography based on available spectral libraries. In the most investigations, the emissivity is obtained through the ASTER JPL spectral library (http://speclib.jpl.nasa.gov), which provides more than 2300 spectra in wavelengths covering from the visible to TIR region. However, if the values are not representatives from the area evaluated, errors may be introduced [9]. In addition, the available spectral libraries do not have temperature information, and different temperatures might have different emissivities for the same land-surface types [3].

We performed emissivity measurements in controlled environment, based on temperatures by using the

Fourier-transform infrared spectroscopy (FT-IR) Model 102F. The atmospheric downward radiance L^↓ λ is obtained by measuring a golden reference panel with an emissivity of 0.04. The sample spectral emissivity ε is calculated from the following equation:

$$\varepsilon_\lambda = \frac{L\lambda - B\lambda(Ts)}{B\lambda(Ts) - L^{\downarrow}\lambda} \quad (1)$$

where $L\lambda$ is the spectral radiance and $B\lambda(Ts)$ refers to Planck's equation, given as:

$$B\lambda(Ts) = \frac{C1\lambda^{-5}}{exp(C2/\lambda T) - 1} \quad (2)$$

where C1 and C2 are constants (C1 = 1.191 × 108 W μm4 sr−1 m−2, C2 =1.439×104 μm K). Assuming that ε =1 between 7.5 and 8μm, the sample temperature can be obtained. The downelling radiance measurement is carried out before and after the sample measurement. If the amount of downelling radiation changes between measurements, the properties determined for the material will have an associated error. Therefore, the accuracy in the downelling radiance measurement determines the accuracy of the emissivity and temperature spectra obtained.

We organized two sets of measurements, the first was performed in the first 30-40 minutes of instrument operation and after the first calibration against the blackbodies. The second set was done after 45 minutes and the second calibration of the instrument. In the calibration process, two temperatures were chosen, a temperature for the cold blackbody (below the ambient temperature), and another for the warm blackbody, (above the sample temperature). This leads to a more accurate calibration, since the instrument response between two known radiances and for each longitude is linear [10]. Thus, the calibration interval assumed was 10-40 ºC (283-313 K).

The temperature of the laboratory was about 25ºC (295 K) and the relative humid 58%. A sample from the sand dune was heated up to +/- 60ºC (333 K) and the measurements were taken. They were ceased when the sample temperature reached 26ºC, totaling about 61 measurements for the first set, and 63 measurements for the second (1-2 measurement per minute). The calibration of the instrument was carried out twice in the whole process.

2.2 Field measurements

We selected one of the remaining transgressive dunes of Cidreira beach (30 km²) as study area, located in the North Coast of Rio Grande do Sul state, Brazil. The area has a large stock of fine quartz sand (125 to 250 μm), with grains varying among sub-rounded (68%), rounded (18%), sub-angular (14%) and composed of quartz (99.53%) and heavy minerals (0.47%). The dune was chosen mostly because it is considered a pseudo-invariant target therefore appropriate for the terrestrial validation of LST by remote sensing data [11].

For field measurements, clear sky conditions are preferable, because downelling radiance is easier to determine and varies more smoothly. Besides, the LST retrieval of passive orbital remote sensors also requires clear sky [12]. We selected a very homogeneous and bare site within the dune area to settle the instrument. As it had not rained in the previous days, we did not have much influence of humity in the sand, which makes the site highly homogeneous in terms of both surface temperature and emissivity, thus easing the measurements [13].

The ground emissivity and temperature spectra were obtained from radiance measurements with the FT-IR spectrometer as well. At the field, the instrument calibration was carried out same as at the laboratory. However, the downeling radiance measurements were taken more often, since the radiance in the field may have more variations than in a controlled environment. The FT-IR was placed looking at the surface at angles close to nadir. The standard input optic is 1 inch in diameter with a 4.8 degree expanding field of view. The measurements were taken at a rate of 1-2 per minute, and the emissivity and temperature were calculated by (1) and (2).

3. RESULTS

3.1 Laboratory emissivity measurements

Emissivity curves from laboratory measured at different temperatures are shown (Fig. 1a and 1b). We chose five spectra from each set to represent the variations of the temperature measured (303-318 K). Fig. 1a displays the first set of measurements, in which it can be seen the relation between emissivity and temperature, obtained at the first half hour that the instrument was turned on. As the temperature decreases, the noise is bigger and there are more oscillations in the emissivity curves. Besides, the emissivity increases with the temperature and the difference among curves became greater above 10μm.

Restrahlen feature that occurs at 8.5 μm for quartz and feldspar (framework silicates) [14] had an emissivity value bigger than 0.7 for the highest temperatures of the set (318.45 K), and about 0.6 for the lower temperature evaluated (303.95 K). Fig. 1b shows the second set of, taken after the first half hour and the second calibration of the instrument. The emissivity measurements are clearly more accurate and do not vary so much with the temperature.

Although the variation is minimal in the most part of the spectrum, the highest temperature presents also the highest emissivity. Furthermore, noticeable variations among curves after 9.5μm are observed, which becomes more evident after 11μm. Another difference is that the restrahlen feature presents a lower emissivity value (<0.6), and for all temperatures here considered, there are very similar emissivity values at this wavelength.

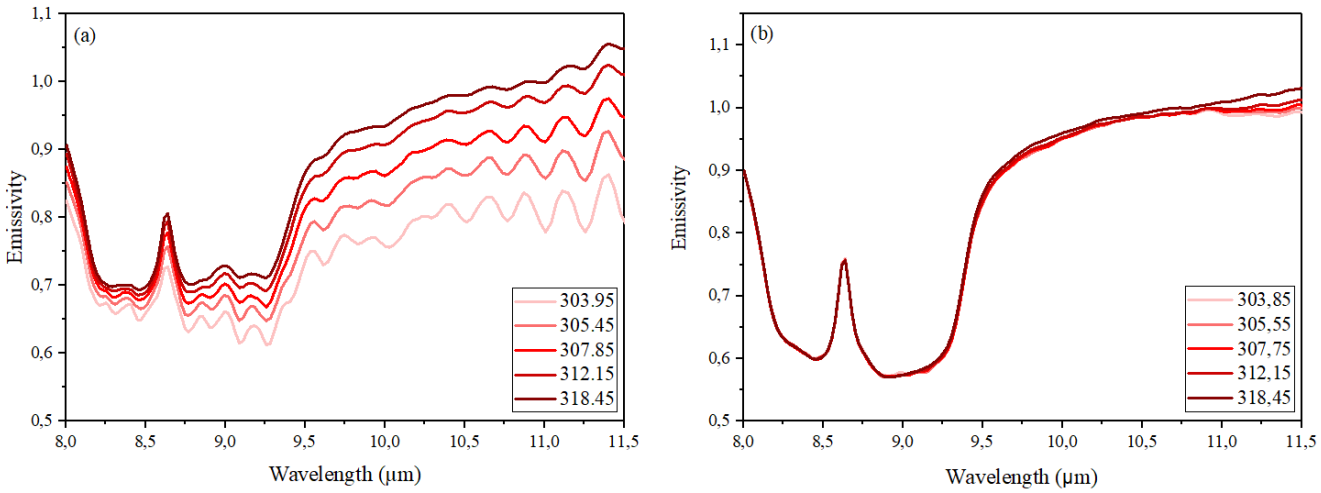

Fig. 1. Emissivity curves of quartz sand sample for five different temperatures (K). (a) refers to the set of measurements performed at the first half hour of the instrument turned on, (b) refers to measurements performed at the time after the second calibration.

When compared the two database sets, it is noted that the lack of calibration and instability of the instrument may induce greater differences in the emissivity measurements. If the first set is used to assign an emissivity value in the methods that estimate LSE as prior knowledge to retrieve LST, bigger errors are observed.

3.2 Laboratory and field measurements comparison

Ground campaign showed that the major portion of the dune were bare, with a few pockets of undergrowth so that we could chose a spot especially bare to measure the quartz sand. Relative humid, near surface air temperature (To), and wind speed were about 67%, 299.25 K (26.1 ºC) and 2 m/s, respectively, at the time of the measurements.

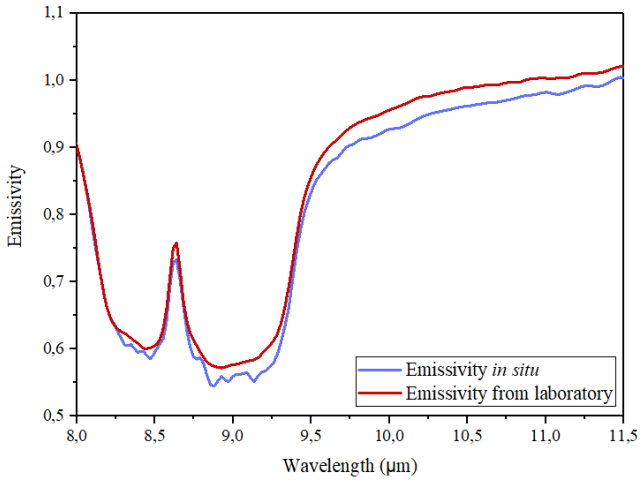

Fig. 2. Comparison between emissivities in the field and laboratory. Both curves chosen to perform the comparison were at exactly 313 K of temperature.

We chose a curve from the database (second set) to compare with another one at the same temperature (313 K) acquired in the field (Fig. 2). In the wavelength that comprises the restrahlen feature more noise is observed in the field measurements than in the laboratory. Moreover, it can be seen a reduction of the emissivity at some points of the feature. After 9.5 µm, the reduction is more evident. Considering that both curves are at the same temperature, when analyzing the wavelength range of 9.5-11.5 µm, an emissivity difference up to 3.25% is verified. However, the most variations are about 2%.

4. DISCUSSION

The first set of measurements performed at the first half hour is not that accurate and can induce systematic errors, which are more significant if the sample is at lower temperatures. This result is probably associated with the sample spectral contrast that is dependent on the environment where the measurements were taken. A lower environment temperature will result in a low thermal contrast between the environment and the sample, if the sample is at a low temperature as well. It is mandatory to turn on the instrument for at least 30 minutes before starting to take measurements in laboratory to reach thermal and mechanical equilibrium. Otherwise, the measurements taken will not be accurate enough.

The emissivity values above 1.0 presented apparent noise effects, since emissivity cannot be greater than 1.0. The temperature of the instrument influenced, since the calibration is carried out in the range from 10 to 40 ºC. It is worth mentioning that at very high temperatures the instrument has a tendency for reducing its accuracy, even if bigger temperature intervals are considered, which is a limitation of the FT-IR spectrometer.

Field measurements indicated the presence of noise in the emissivity curve, especially in restrahlen feature (Fig.

2). According to [10], the calibration for field measurements deteriorates more quickly because the variable heat load from changing solar insolation typically causes instrument temperature drift. Therefore, for maximum accuracy, calibration measurements in the field must be repeated with each sample measurement. [11] evaluated MODIS product V5 found that the emissivity over a desert region is always overestimated compared to laboratory results. The same was observed here, in which we had a difference up to 3.25% in the emissivity comparing a laboratory and field measurement. Furthermore, meteorological conditions have a great influence on the FT-IR spectrometer measurements.

According to [9] 1% uncertainly in LSE may cause an error of 0.5 K in the LST for a moderate atmospheric condition. [17] found in a standard atmosphere with 302.55 K that an error on emissivity of 1% may lead a LST error of 0.6 K. Solar energy influences the material temperature and therefore its self-emitted energy. Wind speed is also an important factor, as it can cool the surface layer of the material very quickly. Since the surface layer is the one that plays the major role in the TIR emission, if the wind causes quick and long changes in the field of radiance, it will affect the determination of the emissivity, mainly because the LST will change while reading the spectrum.

5. CONCLUSIONS

When using an FT-IR spectrometer in the laboratory, it is essential to pay attention to some factors, such as the time required for the instrument to acquire stability and the calibration process, in order not to introduce errors in the measurements. A difference about 2.2% in the emissivity in relation to the temperature was observed for almost the whole spectrum whenn analyzing almost pure quartz (99.53%). Considering the limitations of the instrument, laboratory measurements can be successfully replaced for field validation in the estimation of LSE, avoiding the need of field campaign concurrently with the satellite overpass. In this case, the factors mentioned should be considered. New tests are being performed using the emissivities obtained in the field and laboratory as *input* in LST algoritmhs from orbital remote sensing data.

6. REFERENCES

[1] Weng, Q.; Fu, P.; Gao, F. “Generating daily land surface temperature at Landsat resolution by fusing Landsat and MODIS data,” *Remote Sensing of Environment*, v. 145, pp. 55–67, 2014.

[2] Yu, X.; Guo, X. Wu, Z. “Land Surface Temperature Retrieval from Landsat 8TIRS—Comparison between Radiative Transfer Equation-Based Method, Split Window Algorithm and Single Channel Method,” *Remote Sensing*. vol. 6, pp. 9829-9852, 2014.

[3] Li, Z.-L.; et al. “Satellite-derived land surface temperature: Current status and perspectives,” *Remote Sensing of Environment*, v. 131 pp. 14–37, 2013.

[4] Mattar, C.; Santamaría-Artigas, A.; Ponzoni, F.; Pinto, C.T.; Barrientos, C.; Hulley, G. "Atacama Field Campaign: laboratory and in-situ measurements for remote sensing applications," *Int. J. of Digital Earth*, 2018.

[5] Coll, C et al. "Ground measurements for the validation of land surface temperatures derived from AATSR and MODIS data," *Remote Sens. of Environ*. vol. 97, no. 3, pp. 288-300, 2005.

[6] Deery, D.; Jimenez-Berni, J.; Jones, H.; Sirault X.; Furbank, R. "Proximal Remote Sensing Buggies and Potential Applications for Field-Based Phenotyping," *Agronomy*, v. 4, n.3, pp. 349-379, 2014.

[7] Yan, K.; Ren, H.; Hu, R.; Mu, X.; Liu, Z.; Yan, G. “Error analysis for emissivity measurement using FTIR spectrometer,” *IEEE Int. Geosc. and Remote Sens. Symposium*, 2013.

[8] Tang, H.; Li. Z.-L. “Quantitative Remote Sensing in Thermal Infrared: Theory and Applications,” *Heidelberg: Springer Science & Business Media*, 2014.

[9] Chen, F.; Yang, S.; Su, Z.; Wang, K. “Effect of emissivity uncertainly on surface temperature retrieval over urban areas: Investigations based on spectral libraries,” *ISPRS Journal of Photogrammetry and Remote Sensing*, v. 114, pp. 53–66, 2016.

[10] Korb, A. R.; Dybwad, P.; Wadsworth, W.; Salisbury, J. W. "Portable Fourier transform infrared spectroradiometer for field measurements of radiance and emissivity," *Applied Optics*, vol. 35, no. 10, pp. 1679-1692, 1996.

[11] Hulley, C.G.; Hook, S.J. “Intercomparison of versions 4, 4.1 and 5 of the MODIS Land Surface Temperature and Emissivity products and validation with laboratory measurements of sand samples from the Namib desert, Namibia,” *Remote Sens. of Environ*., v. 113, pp. 1313-1318, 2009.

[12] Masiello, G.; Serio, C.; Venafra, S.; Liuzzi, G.; Poutier, L.; Göttsche, F-M. “Physical Retrieval of Land Surface Emissivity Spectra from Hyper-Spectral Infrared Observations and Validation with In Situ Measurements,” *Remote Sens*, v. 10, n. 6, pp. 976, 2018.

[13] Coll, C.; Galve, J.M.; Sanchez, J.M.; Caselles, V. "Validation of Landsat-7/ETM+ Thermal-Band Calibration and Atmospheric Correction With Ground-Based Measurements," *IEEE Transactions on Geosc. and Remote Sens*. v. 48, n. 1, 2010.

[14] Hook, S.J.; Cudahy, T.J.; Kahle, A.B.; Whitbourn, L.B. “Synergy of active and passive airborne thermal infrared systems for surface compositional mapping,” *J. Geophys. Res*., v. 103, B8, pp. 18,269–18,276, 1998.

[15] Jiménez-Muñoz, J.C.; Sobrino, J.C. “A generalized single channel method for retrieving land surface temperature from remote sensing data,” *J Geophys Res*, v. 108, 2003.

LAND SURFACE TEMPERATURE RETRIEVAL FROM LANDSAT-8 DATA: A COMPARISON USING A QUARTZ SPECTRAL LIBRARY BASED ON TEMPERATURES

Pâmela Suélen Käfer[1]; Silvia Beatriz Alves Rolim[1]; María Luján Iglesias[2]; Luíza Vargas de Oliveira Heinz[1]; Nájila Souza da Rocha[1]; Adriana Coromoto Becerra Rondón[1]; Bibiana Salvador Cabral da Costa[1]; Suzianny Cristia Salazar da Silva[1].

Federal University of Rio Grande do Sul (UFRGS) - [1] State Research Center for Remote Sensing and Meteorology, [2] Institute of Physics. Av Bento Gonçalves, 9500, Campus do Vale, 91501-970, Porto Alegre, RS, Brazil. [Contact: pamelaskafer@gmail.com]

ABSTRACT

Land surface emissivity (LSE) is a parameter that must be known to retrieve land surface temperature (LST). Thus, this work presents the application of NDVI Threshold Method ($NDVI^{THM}$) in a field of coastal dunes with partial vegetation cover in Southern Brazil. We used a spectral library of quartz samples measured at different temperatures to minimize the error of the initial emissivity value in the method. Finally, we calculated LST through the improved single-channel (ISC) algorithm by using the band 10 (10,6-11,19µm) of a Landsat-8 image. The quartz emissivity was tested at two temperatures: (1) the emissivity value corresponding to the higher brightness temperature obtained from the image; (2) the emissivity value based on the saturation point of the spectral library. We verified that this approach is indispensable to acquire more reliable data. The ISC algorithm may produce an error up to 10K in the LST retrieval if the quartz emissivity is not correctly calibrated.

Index Terms— Quartz, emissivity, NDVI, Landsat-8, single channel method

1. INTRODUCTION

Land surface temperature (LST) is a parameter that plays an important role in a wide variety of scientific studies, such as ecology, hydrology and global change studies [1]. In the same way, the land surface emissivity (LSE) is considered a critical variable that must be known in order to retrieve LST. For instance, an error of 0.025 on the LSE retrieval can yield an error of 2 K on the LST calculation [2]. As LSE changes substantially with land cover and over short distances, it is important to estimate its value for every pixel before applying the LST retrieval methods [3].

The Landsat project provides an opportunity for the LST retrieval [1], being one of the most complete data continuous sequence that extends back to 1984. For much of this period, Landsat thermal data were provided through a single broadband thermal channel [4]. Despite having two TIR bands, Landsat-8 [5] has calibration problems caused by stray light since its launch (http://landsat.usgs.gov/calibration_notices.php). In this sense, it is not recommended that band 11 (11,5-12,51 µm) be used for the split-window (SW) technique. A number of single infrared channel methods (SC) have been developed during the past decades [6] [7] and they are the most appropriate for Landsat-8 band 10 [8].

There are several LSE retrieval methods [9] and some of them have used Normalized Difference Vegetation Index ($NDVI$) values [10] [11] [12] [13], due to a relationship between the $NDVI$ and the emissivities of terrestrial materials. In this paper, NDVI Threshold Method ($NDVI^{THM}$) was chosen because it has a reasonable accuracy for LSE retrieval from Landsat imagery and it has been widely used by the scientific community [13].

$NDVI^{THM}$ requires the emissivity values of predetermined targets [14], originally, vegetation and soil. A typical emissivity value for vegetation is generally assigned, once it is considered a grey body [15]. However, the choice of a typical value for soil is a critical question, due to the high variability of its emissivity values [13]. In this study we applied the $NDVI^{THM}$ in a field of coastal dunes (99.53% of SiO_2) with partial vegetation cover, located in Southern Brazil, because quartz has a characteristic spectral signature in the thermal infrared region. The quartz emissivity values were obtained through a temperature based spectral library (LabSRGeo).

According to Plank's equation [9], the emissivity value of a target depends on its temperature and wavelength. Nevertheless, spectral libraries hardly ever contain temperature information. Thus, we used a spectral library of quartz samples measured at different temperatures as an alternative to minimize the error of the initial emissivity value in the $NDVI^{THM}$. While the emissivity is a parameter in the LST derivation, emissivity itself varies with temperature. Therefore, a correct temperature-based emissivity calibration is required for a more accurate LST estimation. Ultimately, we calculated LST through the improved single-channel (ISC) algorithm [8] by using the band 10 (10,6-11,19µm) of a Landsat-8 image in which the quartz emissivity was tested at two temperatures: the first was the emissivity value corresponding to the higher brightness temperature obtained from the image; the second was based on the saturation point of the spectral library.

2. STUDY AREA

The study area is represented by one of the remaining transgressive dunes of Cidreira beach, with an extension of approximately 30 km², located in the North Coast of Rio Grande do Sul, Brazil (Figure 1). This area has inter-dune regions that present undergrowth and temporary water bodies, mainly in the winter periods. The dunes are characterized by fine sand, with grains varying between sub-rounded (68%), rounded (18%), and sub-angular (14%) and composed of quartz (99.53%) and heavy minerals (0.47%), with sizes ranging from 125 to 250μm.

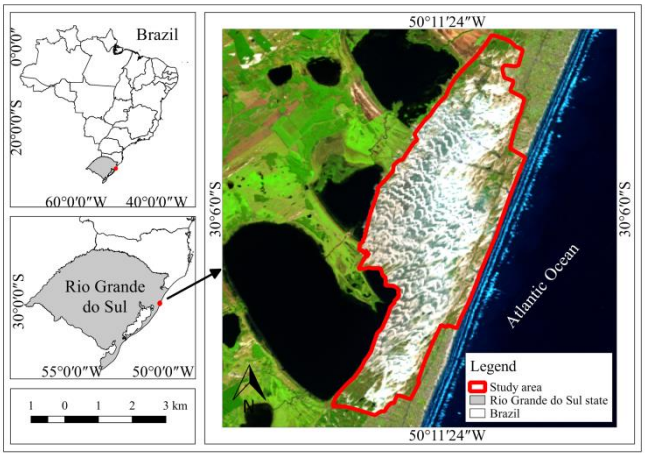

Figure 1. Study area location in Southern Brazil (Data adapted from USGS, 2017).

The average annual temperature of the area is 20°C, the annual precipitation rate is 1322.9mm, the annual evaporation rate is 1134.5mm and the average humidity is 83% [16].

3. METHODOLOGY

3.1. Data acquisition and pre-processing

One scene of Landsat 8 OLI/TIRS (level 1G) was acquired covering the study area under clear atmospheric conditions (Table 1).

Table 1. Landsat-8 OLI/TIRS image information

Year	Path	Row	Acquisition	Sun elevation (º)
2017	220	81	March 11th	48

Landsat-8 carries two sensors; the Operational Land Imager (OLI), which collects data at a 30m spatial resolution with eight bands located in the visible, near-infrared and short-wave infrared regions of the electromagnetic spectrum, and the thermal infrared sensor (TIRS), which measures the TIR radiance at 100m spatial resolution using two bands (Figure 2) [17]. In this context, it is important to emphasize that band 10 is located in a lower atmospheric absorption region (high atmospheric transmissivity values), therefore it is preferable to use it [5].

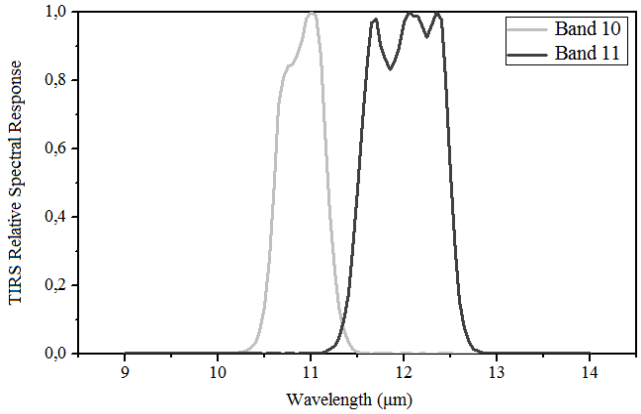

Figure 2. Relative spectral response of the TIRS thermal infrared bands of the Landsat-8.

The image processing was automated through the development of the $NDVI^{THM}$ and SC algorithms in *Matlab* environment. It was assumed that the atmospheric contribution was corrected in the visible bands, since it is not necessary to perform accurate corrections to retrieve PV (vegetation proportion) [19] from a scaled $NDVI$ [7].

3.2. Determination of LSE

According to [13], $NDVI^{THM}$ considers the land surface is soil when the $NDVI$ value is below 0.2 ($NDVI_S$) and vegetation when it is over 0.5 ($NDVI_V$). For those pixels composed of soil and vegetation ($NDVI_S \leq NDVI \leq NDVI_V$), the method uses a simplified equation. $NDVI_S$ and $NDVI_V$ can be also extracted from the $NDVI$ histogram. However, as soil and quartz have similar reflectance behavior in the $NDVI$, the original values worked well for the study area.

The vegetation ($\boldsymbol{\varepsilon_v}$) and quartz ($\boldsymbol{\varepsilon_q}$) emissivity values corresponding to the $NDVI$ ranges can be taken from the bibliography [14]. In this study, we assumed the typical emissivity vegetation value of 0.99. For the quartz, we used two emissivity values of the LabSRGeo spectral library weighted according to filter function band 10 (Figure 2). The first emissivity value corresponded to the higher brightness temperature of 26ºC taken from the image ($\boldsymbol{\varepsilon_{q1}}$) according to [20]. The second one was based on the saturation point of the spectral library ($\boldsymbol{\varepsilon_{q2}}$). The final values used in the $NDVI^{THM}$ are displayed in Table 2.

The spectral library was built by using a Fourier-transform infrared spectroscopy (FT-IR) Model 102F. A sample from the dune was heated up to 90ºC and the measurements were performed in controlled environment. The measurements were ceased when the sample temperature stabilized at 30ºC.

Table 2. Emissivity of quartz, vegetation and mixture-pixel values applied in the $NDVI^{THM}$

T (ºC)	ε_q	ε_v	$\varepsilon_{mixture}$
30.8	**0.8147** (ε_{q1})	0.99	$0.0744\ P_V + 0.9156$
45.0	**1.0** (ε_{q2})	0.99	$-0.0010\ P_V + 1$

3.3. Determination of LST

The improved single-channel algorithm (ISC) [8] was chosen to perform the comparison between both emissivities ($\varepsilon_q 1$) and ($\varepsilon_q 2$), because it has been proved to be the most accurate and recent one available on the literature and it only needs two parameters for LST inversion: LSE and water vapor content (w) [1]. The water vapor content (w) was calculated by applying the method developed by [20]. The required variables were acquired from the field meteorological station of the Brazilian National Institute of Meteorology (INMET - http://www.inmet.gov.br/portal/) located 5 km away from the study area (station coordinates: -30.010268º; -50.135887º and 5 m a.s.l.).

Finally, the ISC algorithm was carried out twice in the same image by changing the $NDVI^{THM}$ function, considering the two emissivities showed in Table 2. All equations and coefficients used in this study were performed according to [8].

4. RESULTS AND DISCUSSION

4.1. Spectral library and LSE retrieval

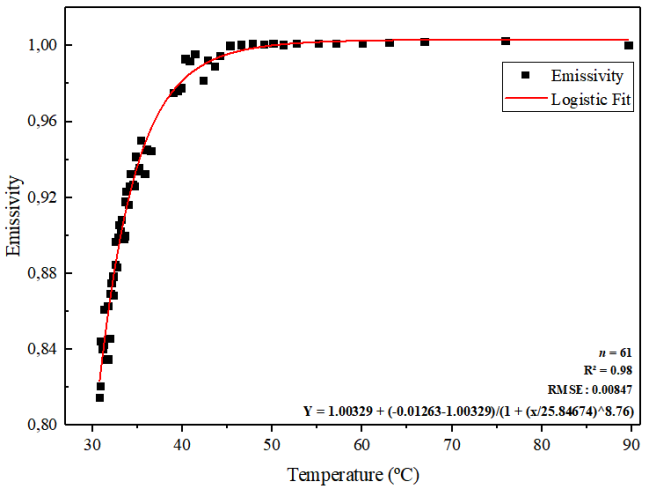

Figure 3. Quartz emissivity *versus* temperature at the band 10/Landsat-8 (10.6-11.19µm). The sensor filter function was applied to the data.

A theoretical logistic mathematical function was applied to fit the emissivity experimental data. To evaluate the performance of the function, the determination coefficient (R^2) at 95% probability and the Root Mean Square Error (RMSE) were used. The graphic presented in Figure 3 shows the emissivity response *versus* temperature in band 10. For modeling we found a determination coefficient of 0.98 and RMSE of 0.008. The adjustment curve demonstrates a saturation point when the emissivity reaches 1.0, which corresponds to +/-45°C. Before reaching the saturation point, it is possible to observe an exponential behavior of the emissivity variable related to the temperature, in which one variable increases depending on the other. It suggests the target temperature must be considered when assigning the emissivity in $NDVI^{THM}$, since it varies significantly in the temperature range from 30ºC to 45ºC.

4.2. LST retrieval

After running the ISC algorithm twice, we found that both emissivities tested may produce a maximum difference up to 10ºC (10K) in LST retrieval (Figure 4) and the differences are bigger for higher temperatures. Therefore, it is evident that the target temperature should be considered when choosing the emissivity in $NDVI^{THM}$ for quartz, since neglecting it can produce a considerable error.

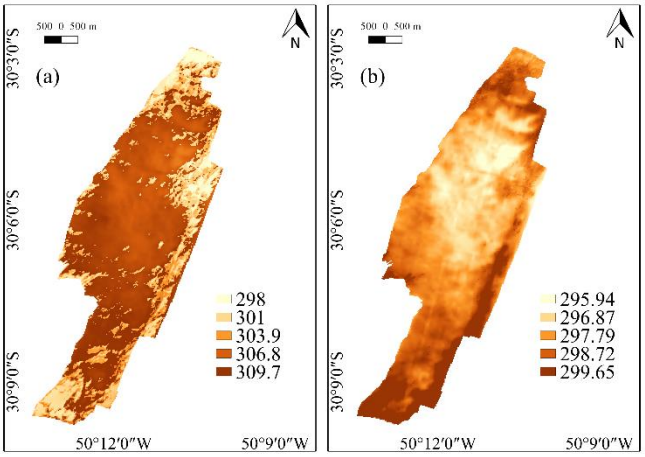

Figure 4. Map of LST retrieval for both emissivites tested. (a) refers to ε_{q1} and (b) refers to ε_{q2}.

Results suggest the only case that it would be possible to use the quartz emissivity value of 1.0 (saturation point), would be when the biggest value of brightness temperature at the image could reach 35ºC.

5. CONCLUSIONS

In this study we verified the performance of a spectral library (LabSRGeo) based on quartz at different temperatures in the LSE and LST estimations. This approach is indispensable to acquire more reliable data, especially when there is no field experimental data available. The quartz emissivity at the band 10/Landsat-8 (10.6-11.19µm) increases exponentially as the temperature increases, up to 45°C, when it reaches the unity (saturation point).

The improved single-channel (ISC) algorithm might produce a difference up to 10K in the LST retrieval for the

temperature range from 30 to 45°C if the quartz emissivity is not correctly calibrated according to its temperature.

6. ACKNOWLEDGMENTS

The authors would like to thank the Laboratory of Geologic Remote Sensing (LabSRGeo) at the Federal University of Rio Grande do Sul (UFRGS) for supporting this study, the FAPERGS research foundation for financing the Project: 2275-2551/14-1 and CAPES research foundation for the scholarships.

7. REFERENCES

[1] X. Yu, X. Guo and Z. Wu, “Land Surface Temperature Retrieval from Landsat 8 TIRS—Comparison between Radiative Transfer Equation-Based Method, Split Window Algorithm and Single Channel Method,” *Remote Sens.*, pp. 9829-9852, 2014.

[2] K. Tan, Z. Liao, P. Du and L. Wu, “Land surface temperature retrieval from Landsat 8 data and validation with geosensor network,” *Front. Earth. Sci.*, pp. 20–34, 2017.

[3] O. Rozenstein, Z. Qin, Y. Derimian and A. Karnieli, "Derivation of Land Surface Temperature for Landsat-8 TIRS Using a Split Window Algorithm," *Sensors*, pp. 5768-5780, 2014.

[4] J. Rosas, R. Houborg and M.F. McCabe, "Sensitivity of Landsat 8 Surface Temperature Estimates to Atmospheric Profile Data: A Study Using MODTRAN in Dryland Irrigated Systems," *Remote Sens.*, vol. 9, no. 10, pp. 988, 2017.

[5] J.C. Jiménez-Muñoz, J.A. Sobrino, D. Skokovic, C. Mattar and J. Cristóbal, "Land surface temperature retrieval methods from Landsat-8 thermal infrared sensor data," *IEEE Geosci. Remote Sens. Lett.*, pp. 1840–1843, 2014.

[6] Z. Qin, A. Karnieli and P. Berliner, "A monowindow algorithm for retrieving land surface temperature from Landsat TM data and its application to the Israel-Egypt border region,” *Int. J. Remote Sens.*, pp. 3719–3746, 2001.

[7] J.C. Jiménez-Muñoz, J. Cristóbal, J.A. Sobrino, G. Sòria, M. Ninyerola and X. Pons, "Revision of the Single-Channel Algorithm for Land Surface Temperature Retrieval From Landsat Thermal-Infrared Data," *IEEE Trans. Geosci. Remote Sens.*, pp. 339–349, 2009.

[8] J. Cristóbal, J.C. Jiménez-Muñoz, A. Prakash, C. Mattar, D. Skovic, J.S. Sobrino. “An Improved Single-Channel Method to Retrieve Land Surface Temperature from the Landsat-8 Thermal Band,” *Remote Sens.*, 10, 431, 2018.

[9] Z.L. Li, B.H. Tang, H. Wu, H. Ren, G. Yan, Z. Wan, I.F. Trigo and J.A. Sobrino, "Satellite-derived land surface temperature: Current status and perspectives," *Remote Sens. Environ.*, pp. 14–37, 2013.

[10] A.A. Van de Griend and M. Owe, “On the relationship between thermal emissivity and the normalized difference vegetation index for natural surfaces,” *Int. J. Remote Sens.*, pp. 1119–1131, 1993.

[11] E. Valor and V. Casseles, "Mapping land surface emissivity from NDVI: Application to European, African and South American areas," *Remote Sens. Environ.*, pp. 167–184, 1996.

[12] J.A. Sobrino and N. Raissouni, "Toward remote sensing methods for land cover dynamic monitoring," *Int. J. Remote Sens.*, vol. 21, no. 2, pp. 353-366, 2000.

[13] J.A. Sobrino, J.C. Jiménez-Muñoz, and L. Paolini, "Land surface temperature retrieval from LANDSAT TM5," *Remote Sens. Environ.*, pp. 434–440, 2004.

[14] J. Cristóbal, J.C. Jiménez-Muñoz, J.A. Sobrino, M. Ninyerola and X. Pons, "Improvements in land surface temperature retrieval from the Landsat series thermal band using water vapor and air temperature," *J. Geophys. Res.*, pp. D08103, 2009.

[15] G.C. Hulley, S.J. Hook, “Generating Consistent Land Surface Temperature and Emissivity Products Between ASTER and MODIS Data for Earth Science Research,” *IEEE Trans. Geosc. and Remote Sens.*, vol. 49, no. 4, pp. 1304-1315, 2011.

[16] F.A. Travessas, S.R. Dillenburg and L.C.P. Clerot, "Estratigrafia e evolução da barreira holocênica do Rio Grande do Sul no trecho Tramandaí-Cidreira," *Boletim Paran. de Geoc.*, pp. 57-73, 2005.

[17] J.R. Irons, J.L. Dwyer and J.A. Barsi, “The next Landsat satellite: The Landsat Data Continuity Mission,” *Remote Sens. Environ.*, pp. 11–21, 2012.

[18] Visual Information Solutions, 2014, “Exelis Vis. ENVI – IDL - v. 5.1.” *Boulder CO*. Available at: http:/www.exelisvis.com/envi/, Access: 10 Dez. 2017.

[19] T.N. Carlson, and D.A. Ripley, "On the relation between NDVI, fractional vegetation cover, and leaf area index," *Remote Sens. Environ.*, pp. 241–252, .1997.

[20] M. Pivovarník, S.J.S. Khalsa, J.C. Jiménez-Muñoz, F. Zemek, "Improved Temperature and Emissivity Separation Algorithm for Multispectral and Hyperspectral Sensors," *IEEE Trans. Geosc. and Remote Sens*, pp. 1-10, 2016.

[21] F. Wang, Z. Qin, C. Song, L. Tu, A. Karnieli, S. Zhao. "An Improved Mono-Window Algorithm for Land Surface Temperature Retrieval from Landsat 8 Thermal Infrared Sensor Data," *Remote Sens.*, 7, pp. 4268-4289, 2015.

Nesta seção foram exibidos dois resumos expandidos submetidos e/ou publicados em eventos científicos. O primeiro trabalho foi submetido e aceito no Simpósio Brasileiro de Sensoriamento Remoto – SBSR (2019) e o segundo foi apresentado no International Geoscience and Remote Sensing Symposium - IGARSS em setembro de 2018, Valência – Espanha (doi: 10.1109/IGARSS.2018.8518135).